Characterization of Glioblastoma and T Cell Migration in Brain Tissue

A DISSERTATION
SUBMITTED TO THE FACULTY OF THE
UNIVERSITY OF MINNESOTA
BY

Sarah Marie Anderson

IN PARTIAL FULFILLMENT OF THE REQUIREMENTS
FOR THE DEGREE OF
DOCTOR OF PHILOSOPHY

Advisor: David J. Odde

July 2023

Acknowledgements

I first want to thank my advisor, David Odde, for his guidance and support over the last almost 6 years. I am grateful for him helping me navigate the challenging aspects of graduate school while also making it a fun and supportive environment. Through his guidance, I have been able to develop the skills to become and independent scientist and mentor. We also had to work together to navigate continuing research through a pandemic, and Dave advocated for us to have a safe working environment, whether it was at home while the lab was shut down or developing protocols to return to lab amidst the pandemic. I also want to thank the members of the Odde laboratory, particularly Ghaidan Shamsan, Louis Prahl, and Chao Liu who trained me when I joined lab and never hesitated to answer any of my many questions. When the lab was shut down for the pandemic, Ghaidan, Riley Manning and I met almost daily. While we were supposed to be using that time to talk about science, it usually turned into an hour or two of socializing and chatting. I am thankful that we had this time to maintain friendships and connections during an isolating time. Finally, I want to thank my family and friends who supported me through the last 6 years, listening to my frustrations about experiments not working, microscopes breaking, or MATLAB codes not doing what I wanted them to do, but also celebrating with me when an experiment finally clicked or I had new, exciting results.

Research reported in this dissertation was supported by grants U54CA210190, P01CA254849, and U54CA268069. The content of this work is solely the responsibility of the authors and does not necessarily represent the official views of the NIH.

Abstract

Glioblastoma (GBM) is an aggressive malignant brain tumor with extremely low 5-year survival rates. One key characteristic of the disease is the ability of glioblastoma cells to migrate rapidly and spread throughout healthy brain tissue. To develop treatments that effectively target cell migration, it is important to understand the fundamental mechanism driving cell migration in brain tissue. In the first part of this dissertation, we utilized confocal imaging to measure traction dynamics and migration speeds of glioblastoma cells in mouse organotypic brain slices to identify that the cells are using a motor-clutch mode of migration. In addition, both integrins and CD44, as well as myosin motors, were found to play an important role in constituting the adhesive clutch. In developing a treatment that targets migration of glioblastoma cells, it is critical to take into account how this could impact T cell migration and the resulting ability of T cells to kill cancer cells. A hallmark of glioblastoma is the suppression of the immune response, allowing the tumor to grow and spread faster, and infiltration of cytotoxic CD8+ T cells into the tumor has been shown to be an important indicator of disease progression and survival. In the second part of this dissertation, we use mouse organotypic brain slices co-cultured with CD8+ T cells to image migrating CD8+ T cells in healthy brain tissue in response to cell migration targeting drugs and antibodies. We find an increase in migration speed in response to targeting CD44, which is a critical deviation between cancer cell and T cell phenotype, implicating CD44 as a potential target for improving glioma outcomes by slowing cancer cell migration and speeding up CD8+ T cells.

Table of Contents

List of Figures

List of Tables

1. Chapter 1: Introduction

1.1. Cancer

The hallmarks of cancer, the uncontrolled growth of abnormal cells, describe unique capabilities the cells acquire, including the ability to divide despite mechanisms preventing cell growth, inducing angiogenesis to maintain blood supply to the tumor, and activating invasive and metastatic behaviors[1]. At its core, cancer is a genetic disease that initially can arise from a genetic mutation in any of the many oncogenes[2]. These mutations give the cell a unique ability, such as being more likely to divide, to ignore signals that prevent uncontrolled cell growth, to acquire new genetic mutations, and to avoid repair mechanisms when a cell does acquire a genetic mutation[3]. As the cell grows into a population of cells, the cells with the most potent mutations will grow faster and ultimately dominate the tumor that will continue to mutate over time[4]. Eventually, in invasive cancers, the cells on the periphery of the tumor undergo an epithelial-to-mesenchymal transition in which the cells that were previously round and bound to neighboring cells become fibroblast-like, reduce intercellular adhesions, and become migratory[5].

1.2. Cell Migration in Cancer

Migratory cells in cancer are highly invasive. They exit the primary tumor and disseminate into the surrounding healthy tissue. Furthermore, they can even remodel the surrounding environment to create pathways for more cells to migrate out of the tumor[6]. If the cells encounter a blood vessel, it can enter the blood stream, ultimately

exit at a new site, and begin to divide and form a new tumor in a process called metastasis[7].

1.3. Glioblastoma and cell migration

Glioblastoma (GBM), or grade IV astrocytoma, is the most aggressive brain tumor. It initially arises via a genetic mutation in an astrocyte, a type of glial cell and the most common cell type in the brain [8], [9]. There are a few common genetic mutations that occur in GBM. One example is an increase in expression of epidermal growth factor receptor (EGFR), which leads to increased cell growth[10]. Another example is a mutation in p53, which will cause the cell to continue through the cell cycle even if it has acquired a genetic mutation[11]. The current standard of care treatments for glioblastoma are surgery to remove the tumor, radiation, and temozolomide chemotherapy[12]. Radiation induces significant genetic mutations in cells in a localized area. As the cancer cells have lost the ability to repair genetic mutations, they are more likely to die while the healthy cells repair the damage. Temozolomide is a drug that deposits methyl groups on DNA[13]. While healthy cells are able to repair this to an extent, the cancer cells are not and will ultimately undergo apoptosis. Despite these treatments, 2-year survival rates for glioblastoma are remarkably low at 6.7% and reports of 5-year survival are sporadic. Developments of new drugs and treatments have failed to show any significant improvement in survival[14].

Glioblastoma is a particularly invasive tumor, meaning the cells are extremely efficient at migrating away from the primary tumor into the surrounding healthy tissue. While surgery is used to remove the primary tumor and radiation and temozolomide are

initially effective, the cells that have migrated into healthy tissue remain and eventually become resistant to treatment[9]. Although the bulk of research into glioblastoma treatments has focused on killing and slowing the growth of tumor cells, treating GBM by slowing cell migration is relatively unexplored area and presents an opportunity to potentially slow disease progression.

1.4. Role of the immune system in cancer and glioblastoma

Tumors are highly complex environments, containing many cell types and components other than the cancer cells including extracellular matrix proteins, fibroblasts, and immune cells [15]–[17]. The immune cells play a key role in cancer development. In the early stages of cancer development, as a single cell first acquires a mutation, the immune system will almost always find and kill these mutated cells[18]. Mutated cells express molecules (antigens) that antigen presenting cells (APC), such as a dendritic cell (DC), can recognize as foreign and present to a CD8+ T cell, or cytotoxic T cell. The antigen is presented to the T cell via major histocompatibility complex (MHC) proteins on the surface of APC, which are complexed with the specific antigen and bind to the receptor on the T cell. The activated CD8+ T cell will then migrate and search for a cell expressing the specific antigen. When it binds to a cell expressing the antigen, it kills it[19]. In order for a tumor to develop, the cells must find a way to avoid this immune surveillance[16]. Regulatory T cells (Treg) are a cell type that works to maintain immune homeostasis by preventing excessive immune responses to infection, injury, etc. Tumor cells can release chemokines such as CCR4, CCR8, CCR10, and CXCR3 that that attract Tregs into the tumor which in turn suppress anti-tumor immune function

through a variety of methods including CTLA-4-mediated suppression of APCs, consumption of activating IL-2, releasing immunosuppressive cytokines such as TGF-B and IL-10, and killing of effector T cells and APC [20], [21]. Similarly, two types of macrophages which are typically associated with wound healing are attracted to the tumor. M1 macrophages secrete pro inflammatory cytokines such as IL-6, IL12, and TNF-α, attracting more immune cells to the tumor, and can present antigens to T cells, promoting killing of cancer cells. M2 macrophages, on the other hand, secrete the immunosuppressive cytokine IL-10 and vascular growth factor VEGF, which improve the blood supply to the tumor, thereby supporting tumor growth[17], [22]. Ultimately, the highly active immune cells in the tumor mean that a tumor behaves like a chronically wounded site with a balance between both pro-tumor and anti-tumor immune cells that ultimately results in the tumor continuing to grow[23]. Tumors can be either immunologically “cold”, meaning the pro-tumor immune cells dominate or the immune system is barely activated and there is minimal T cell killing, or immunologically “hot”, meaning anti-tumor immune cells are very active. Immunotherapies are able to hijack the ability of the immune cells to kill cancer cells by either activating the anti-tumor immune cells or inhibiting the pro-tumor immune cells thereby activating the anti-tumor immune cells[24].

Immune infiltration is a very important indicator of disease progression and survival in GBM[24]. A clinical study by Yang et al. found that patients with higher levels of intratumoral CD8+ T cell infiltration, measured by histological tumor samples, were more likely to survive longer (>403 days)[25]. This finding has continued to be

supported by further research[26], [27]. Two subtypes of GBM, mesenchymal and proneural, are known to have differing levels of immune invasion, with mesenchymal tumors being more migratory but immunologically “hot” and proneural tumors being less migratory but immunologically “cold”. Shamsan et al. induced GBMs in mice meant to mimic two known subtypes, mesenchymal and proneural. While the mesenchymal tumors had more migratory cells, the mice actually survived longer due to higher levels of CD8+ T cell infiltration and killing in the tumor[28]. Therefore, in developing a treatment that slows migration of cancer cells, it is imperative to consider the impact this would have on T cells. If slowing down cancer cells also inhibits T cell migration, this could make outcomes worse.

1.5. Cell migration models

It is not definitively known how T cells or cancer cells migrate *in vivo*. Several hypothesis have been proposed, as articulated below.

1.5.1. Motor-Clutch Model

The prevalent model of cell migration is a motor-clutch mechanism of force transmission, shown in Figure 1.1. In this model, forces in the cell are generated through non-muscle myosin II, which pulls F-actin filaments inwards towards the center of the cell as actin subunits polymerize at the leading edge of the cell and de-polymerize at center of the cell in a process known as “treadmilling”[29]. Adhesion proteins, or molecular “clutches”, connect the F-actin network to its substrate, the extracellular matrix (ECM), so the inward movement of F-actin pulls on the ECM. Ultimately, the

clutch-ECM bonds at the trailing edge break, allowing the cell to pull itself forward[30], [31].

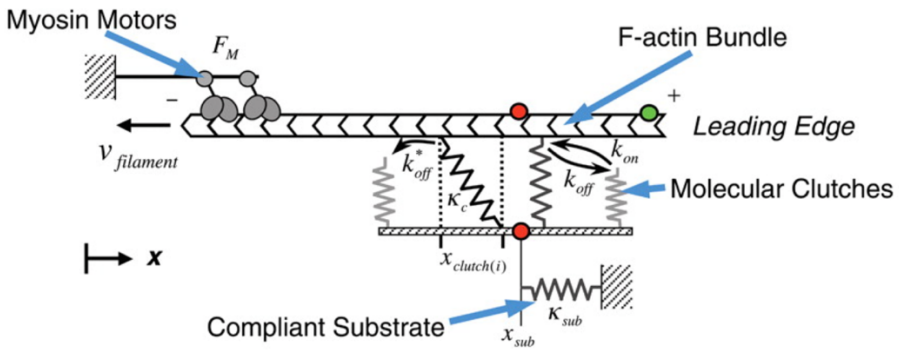

Figure 1.1 Motor Clutch Model
Schematic of the motor clutch model of cell migration, from Chan & Odde, Science, 2008

There are a few key predictions of the motor clutch model. Primarily, cell migration will exhibit a biphasic response to variations in motors and clutches in which optimal cell migration occurs when the motors and clutches are balanced[30]–[32]. If a migrating cell has too many motors relative to the number of clutches, the force from the motors will break the clutch bonds before sufficient force can build up. If a cell has too many clutches relative to the number of motors, clutches will stay bound and force will be transmitted to pull on the environment, but each clutch experiences too little force to ever break, preventing the trailing edge of the cell from detaching and preventing the cell from moving. When motors and clutches are balanced, sufficient traction force can be generated to pull the cell forward as the clutch bonds at the trailing edge break. Similarly, the stiffness of the substrate spring impacts cell migration, with optimal cell migration occurring at intermediate stiffnesses. At high stiffnesses, force on the clutches builds up quickly, causing rapid breakage. At low stiffnesses, insignificant force builds to

generate large enough traction forces. Another unique prediction of the motor clutch model is how the cell will interact with and deform its environment. At the leading edge of the cell, as F-actin polymerization is pushing the membrane forward, pushing deformations may be observed. Otherwise, the cell pulls on the environment to gain traction and pull itself forward. At the trailing edge, the cell pulls on the environment until the bonds break and the environment is released[31], [32].

1.5.2. Osmotic Engine Model

An alternate model of cell migration that has been proposed is the osmotic engine model [33], [34], in which cell migration is driven by a spatial gradient of ion/osmolyte pumps in the plasma membrane that lead to directed water fluxes throughout the cell, shown in Figure 1.2. In this model, migration does not depend on adhesion to the environment. Instead, the cell establishes a spatial gradient of ion pumps that creates a net influx of ions at the leading edge and net outflux of ions at the trailing edge. This creates an electro-osmotic gradient across the cell cytoplasm, driving water to permeate into the cell at the leading edge and out of the cell at the trailing edge, leading to net movement of the cell forward[34].

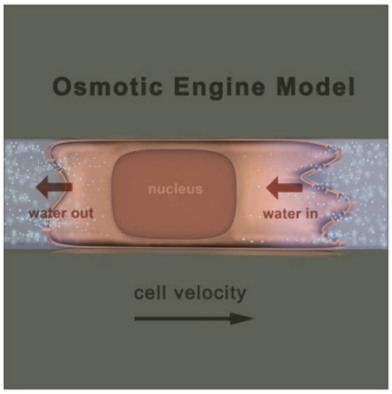

Figure 1.2.Osmotic Engine Model

Schematic of the osmotic engine model, from Stroka et al., Cell, 2014.

A few predictions arise from this model, most notably that cell migration should be sensitive to changes in Na+/H+ exchanges, changes in aquaporin water channels, and osmotic shock. Stroka et al. found cell migration sensitive to each of these, but their experiments were conducted in confined microchannels, and whether this mode of migration occurs in physiological relevant environments, such as for glioblastoma cells in brain tissue, is an open question. A cell migrating under this mechanism could still maintain adhesion to the environment, so as the osmotic forces propel the cell forward adhesions would presumably exert a frictional force resisting the motion, and so blocking adhesions would result in an increased cell migration speed. In addition, the cell would push the environment away from the leading edge.

1.5.3. Bleb-Based Motility

Another mechanism of cell migration that has been proposed is bleb-based motility[35]–[38]. A bleb is a local transient loss of plasma membrane to F-actin cortex cohesion that causes a plasma membrane protrusion to rapidly extend from the cell, appearing like boiling water on the cell wall[39], [40]. Blebbing enables the plasma membrane to rapidly advance, faster than F-actin can polymerize. Subsequently, the actin-myosin cortex reforms under the plasma membrane, adhesions can form, and the intracellular forces can be transmitted to the environment. In order for the cell to migrate following the rapid extension of the plasma membrane, adhesions must form at the leading edge and engage the cell's motor-clutch modules, pulling the cell forward before

the bleb can be retracted. In this description, bleb-based motility can be regarded as a form of motor-clutch-mediated migration, where the plasma membrane advances by blebbing rather than F-actin self-assembly, as in the original motor-clutch model. Even so, during bleb extension, this model predicts that the extracellular environment will be exclusively pushed away from the leading edge and pulling events would not occur, whereas the F-actin assembly-based motor-clutch model predicts both pulling and potentially pushing forces at the leading edge.

1.6. Mathematical modeling of cell migration

1.6.1. Motor-Clutch Model

The motor-clutch model was developed to stochastically simulate the behavior of a single motor-clutch module in a cell. The model regards the F-actin network as a rigid rod. The rod moves with a velocity v_f, described in Equation 1, which is calculated by a balance of motor force pulling the rod and the clutch force resisting this movement given by

$$v_f = v_u \left(1 - \frac{F_{sub}}{n_m F_m}\right) \quad (1)$$

where v_u is the unloaded actin velocity, F_{sub} is the force on the substrate, which is equal to the total force on the clutches. n_m is the number of motors and F_m is the force per motor. If the force from the motors is equal to the force from the clutches, the actin will not move, i.e. it is in a “stalled” state. If there is no force from the clutches, the rod will move at the unloaded velocity v_u; i.e. it is in a “free-flowing” state. The clutches are modeled as linear Hookean springs in parallel. Each bound clutch can unbind at a

frequency k_{off} dependent on force such that clutches experiencing high forces are more likely to unbind, as shown in Equation 2. Clutches fail at rate k_{off}, given by

$$k_{off} = k_{off}^{*} e^{F_c / F_b} \quad (2)$$

where koff* is the unloaded off-rate constant, F_c is the current force on the clutch, and F_b is the constant characteristic clutch bond rupture force. Following unbinding, they can re-bind with a rate k_{on}. The total force from the clutches is transmitted to a single linear Hookean substrate spring[30], [31], although more recently the model has been adapted to describe the substrate/environment as a viscoelastic material via a standard linear solid model[41].

1.6.2. Cell Migration Simulator

The cell migration simulator (CMS) connects multiple motor clutch modules by a spring at the cell body to stochastically simulate whole-cell migration, shown in Figure 1.3. The CMS specifies the number of modules and each module is assigned a number of motors and clutches from a pool of free clutches. This method imbalances the motors and clutches between the modules, leading to an element of bias towards one module, which will ultimately become the leading edge. Each module contains a cell spring with a spring constant $k_{cell.}$ The force on each module F_j is shown in Equation 3 and is calculated using a force balance on the total clutches in that module and is described by

$$F_j = k_{cell} x_{cell,j} = k_c \sum_{i=1}^{n_{c,cell}} x_{c,i} \quad (3)$$

where k_c is the stiffness of each clutch and $x_{c,i}$ is the displacement of the i^{th} clutch. The total forces across all modules is then balanced[32].

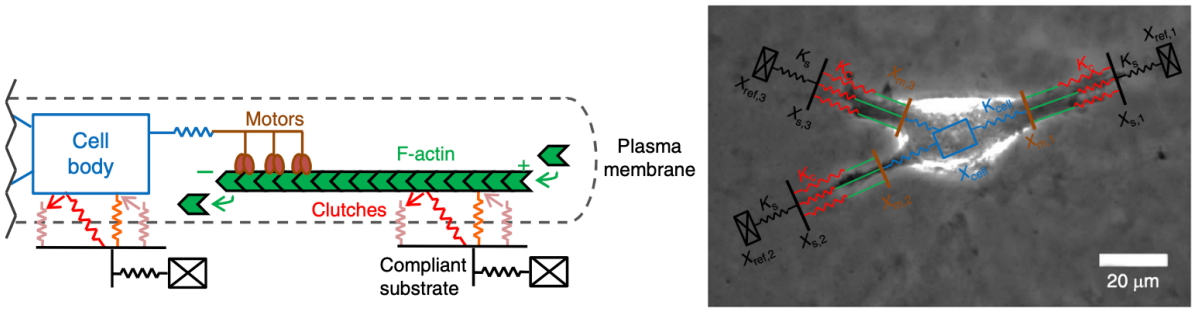

Figure 1.3 Cell Migration Simulator

a) Diagram of individual CMS modules. b) Diagram of CMS modules overlayed on an image of a cell. Images are from Bangasser et al., Nat. Comms, 2017.

While the motor clutch model informs on traction dynamics and F-actin flow rates, the cell migration simulator can make predictions on how cell migration speed is impacted by various factors including numbers of motors and clutches, substrate stiffness, clutch binding and unbinding rates, and F-actin polymerization. It also simulates traction dynamics and F-actin retrograde flow during migration. The CMS was used to develop and understand the key predictions of motor-clutch-based migration, including the optimality of cell migration at intermediate stiffnesses and balanced numbers of motors and clutches, as described in Chapter 1.5.1. These predictions have been supported by experimental findings on polyacrylamide gels of varying stiffnesses[32].

1.7. Methods of studying cell migration

1.7.1. *In vitro* systems for investigating cell migration

A variety of experimental systems have been used to study migrating cells, and in particular *in vitro* assays have been used to answer many questions about how cells migrate. Cells have been imaged on 2D glass, 2D glass coated in ECM proteins, and

2D polyacrylamide gels coated in ECM proteins[42]. These methods are used because they are relatively easy to make and cells can be imaged at very high spatial-temporal resolution. Under these methods, cancer cells have been found to migrate via a motor-clutch mode of migration[32], [43], [44]. Both actin retrograde flow and traction forces can be quantified on these surfaces and match predictions from the motor clutch model[30], [43]. Microchannels and nanopatterned surfaces (2.5D) can be used to add texture to the surface to mimic the density and texturing of physiological environments. Behavior consistent with an osmotic engine model[34], motor clutch model[45], and bleb-based motility[38] has been observed on these surfaces. 3D gels, most commonly collagen gels, are an additional *in vitro* method used to study cell migration. The addition of the third dimension provides a better mimic of cell migration in the body, and a variety of cell phenotypes have been observed in 3D collagen gels[42]. 3D hydrogels utilizing hyaluronic acid (HA), the primary ECM of the brain, of varying stiffnesses have also been used. While phenotypes in a HA hydrogel are different from those in a collagen gel, cell behavior was still consistent with a motor-clutch mode of migration[46]. However, the gels contain a single or a limited number of ECM proteins, do not account for other cell types and signaling in the body, and do not account for tissue heterogeneity.

1.7.2. *In vivo* and *in vivo*-like systems for investigating cell migration

Ideally, cell migration could be observed in humans in the disease state that is being studied, but this is not feasible. Many assays have been developed to bridge the gap between *in vitro* and *in vivo* assays. Microfluidic devices can be used to simulate

various processes such as extravasation/intravasation and wound healing as these devices can add an additional components to better simulate the process occurring in the body[47], [48], however they still lack the complexity of the *in vivo* microenvironment and signaling.

Another method used to study cell migration is *ex-vivo* tissue slices; cell migration has been observed in mouse brain slices[49], [50], tumor explants[38], lymph nodes[51], and other tissues. These methods better mimic *in vivo* migration, as the cells experience the same environment as *in vivo* including ECM proteins and other cell types, though a few key differences exist. There may be mechanical differences in a tissue explant relative to an intact tissue, slicing and removing the tissue may initiate a wound healing response, and signaling from outside the tissue is no longer included.

Studies have begun to develop methods of imaging cells *in vivo* using cranial window technology in mice. A portion of the skull is removed and replaced with glass such that the head of the mouse can be anchored to a two-photon microscope and fluorescent cells can be imaged inside the brain while the mouse is awake and even running on a treadmill[52]. As this technology is still new, there are significant limitations, including very small fields of view and limited imaging depth. In addition, imaging can only occur over small time frames. Though this is currently a low throughput method for imaging cells, it can provide important information on the relevance of other systems of studying cell migration.

1.8. Molecular motors

Many of these experimental techniques have been used to identify the molecules involved in cell migration. Non-muscle myosin II (NM II) motors are the primary motor involved in generating force in the motor-clutch mode of cell migration, but they also play critical roles in cell adhesion, cell division, and cell shape regulation. NM II molecules are comprised of a globular head domain containing binding sites for ATP and actin, an α-helix coiled rod domain, and lever arms that connect the head and rod domains, shown in Figure 1.4. The lever arms are bound to two heavy chains of regulatory light chains (RLCs) and two essential light chains (ELCs)[53]. Phosphorylation of the RLC unfolds the NM II and results in increasing the ATPase activity of myosin in the presence of actin. Once the myosin has bound to actin, ATPase activity results in conformational changes in the myosin that pull the actin filaments[54]. The drug blebbistatin is a small molecule inhibitor that blocks ATPase activity of for NM II and therefore inhibits the ability of the myosin to move F-actin filaments[55].

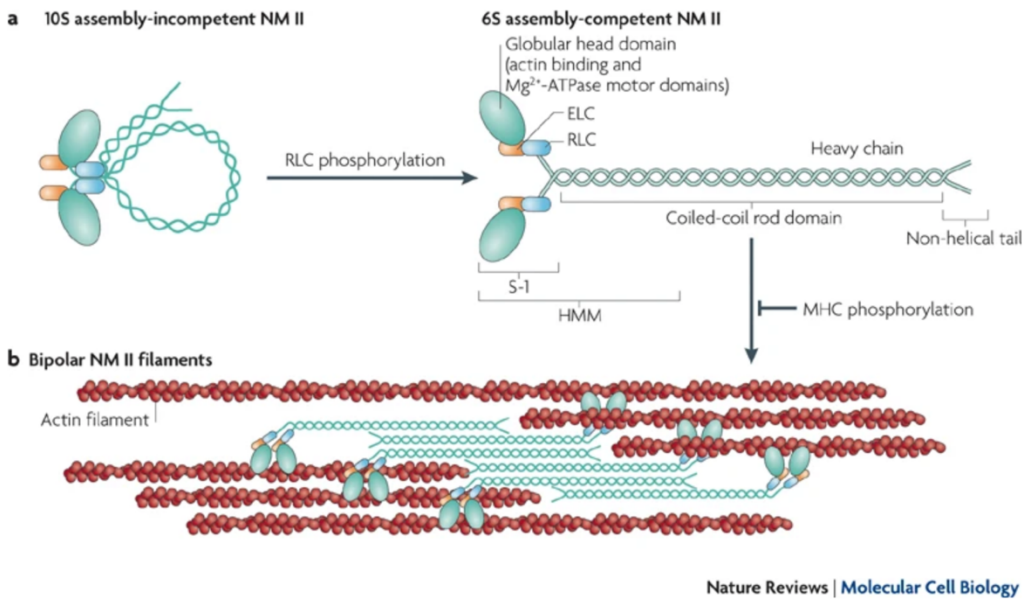

Figure 1.4. Non-muscle myosin II
Schematics demonstrating NM II domains and unfolding in response to RLC phosphorylation, taken from Vicente-Manzanares et al., Nat Rev, 2009.

NM II is involved in a variety of pathways that control cell adhesion, cell shape, and cell migration, including the Rho/ROCK pathway. Kinases including focal adhesion kinase (FAK) and Src are recruited to focal adhesions and can upregulate myosin phosphorylation [53]. Cells utilize these pathways to regulate myosin activity which allows for optimization of cell shape, adhesion, and migration. These pathways can also influence the regulation of adhesion molecules, or molecular clutches.

1.9. Molecular clutches

Adhesion molecules, or molecular clutches, sit in the cell membrane and connect the ECM outside of the cell to the actin cytoskeleton through adaptor proteins[56], as described in Figure 1.5. While the role of myosin II in motor-clutch cell migration is

relatively well understood, it is not known which molecule or molecules acts as the molecular clutch *in vivo*, though many have been studied.

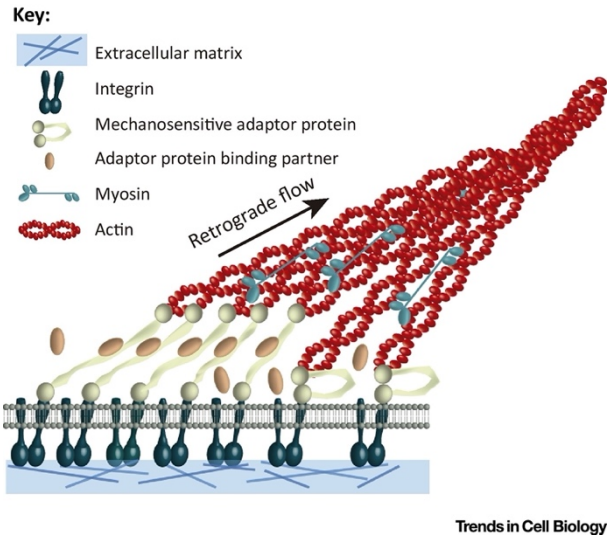

Figure 1.5. Components of the motor clutch model

Schematic depicting myosin motors pulling on actin filaments, which pulls on the molecular clutch (integrins) via adaptor proteins, from Elosegui-Artola et al., Trends in Cell Biology, 2018[57].

1.9.1. Integrins

Integrins are heterodimeric adhesion molecules that span the plasma membrane to connect the actin cytoskeleton to the ECM, and they have been a major focus of research into cell adhesion[58]. Integrins are made up of two heterodimers, an alpha and beta subunit, and the specific combination of subunits determines which ECM protein they bind to. Integrins can bind to collagen, laminin, and RGD sequences, which are found in fibronectin, fibrinogen, vitronectin, osteopontin, and a variety of cell surface proteins[59] [57], [60], [61]. Integrins bind to the actin cytoskeleton via the adaptor protein talin, which has two isoforms, talin1 and talin2. As talin experiences force, it can

unfold, revealing binding sites for the molecule vinculin, which increases the strength of the actin-ECM bond. Without talin, force cannot be transmitted from the actin network to the integrins[62], [63]. Many studies have found integrins to be significant for cell migration[64]. Additionally, integrins have been implicated in cancer progression and metastasis [65]–[68].

A 2014 clinical trial investigated the effect of Cilengitide, a drug targeting two types of integrins, $\alpha_v\beta_3$ and $\alpha_v\beta_5$, but the drug did not show a benefit to survival[69]. In a post-hoc analysis by David Odde, these types of integrins were not found to correlate with survival in a control group, so it may be that these adhesion molecules are not used in GBM cell migration. Alternatively, motor clutch modeling suggests a biphasic relationship between survival and adhesion molecule expression, so targeting of adhesion molecules must take into account individual expression levels, as a partial reduction of adhesion in cells with an intermediate expression would slow migration, in cells with low expression would not impact migration, and in cells with high expression could worsen outcomes. On a population level, the drug would appear to have no impact on migration and survival.

Integrins have generally been regarded as the primary adhesion molecule used in cell migration[58]. However, Lämmermann et al. developed a pan-integrin knockout mouse and found dendritic cells were still be able to localize to the lymph nodes, implying that migration can occur independent of integrins [70]. At the time, these results raised the possibility that cells could migrate in 3D without adhesion, but it was not considered that an adhesion molecule other than integrins, such as CD44 (see

below), could be used to migrate via the classic motor-clutch mechanism and no specific mechanism for adhesion-free migration was proposed as an alternative.

1.9.2. CD44

CD44 is an adhesion protein that binds to hyaluronic acid and hyaluronan and connects to the actin cytoskeleton via adaptor proteins ezrin, radixin, and moesin, the so-called ERM proteins, and ankyrin[71]. It is expressed on many cell types including connective tissues, bone marrow, and leukocytes[72]. CD44 has been implicated and found to be upregulated in a variety of cancers including GBM[73]–[77]. While there is a primary isoform of CD44 (CD44s), alternative isoforms (CD44v) are present and may be associated with more metastatic cells. While primary gliomas express CD44s, intracranial metastatic tumors often express CD44v[76]. Many groups have found CD44 to be important for glioma progression[78], [79]. Klank et al. found a biphasic relationship between survival in both humans and mice and CD44 expression, where an intermediate expression of CD44 correlated with fastest migration in mice and lowest survival in both mice and humans[80].

1.10. Thesis statement

In this dissertation, I sought to identify the mechanism of glioblastoma migration and better understand how targeting cell migration could impact disease progression. I hypothesize that glioblastoma cells migrate via a motor clutch mode of migration mediated through both integrins and CD44 in brain tissue (Chapter 2). In addition, I hypothesize that cytotoxic T cells also migrate via a motor clutch mode of migration, and I seek to identify a method to slow down migration of cancer cells while not impacting,

or possibly increasing, migration of T cells (Chapter 3). A treatment for glioblastoma that targets cell migration must not impair the ability of T cells to migrate into the tumor, migrate within the tumor, and seek out and kill cancer cells, as this could worsen disease outcomes.

2. Chapter 2: Glioblastoma cells use an integrin- and CD44-mediated motor-clutch mode of migration in brain tissue

Authors: Sarah M Anderson[1], Marcus Kelly[1], David J. Odde[1*]

[1] Department of Biomedical Engineering, University of Minnesota, Minneapolis, Minnesota, USA

* Corresponding author: oddex002@umn.edu

2.1. Authors' Contributions

MK performed the traction force experiments on U251 CD44 KO cells. The rest of the work in the paper was done by SMA.

2.2. Summary

Glioblastoma (GBM) is an aggressive malignant brain tumor with 2-year survival rates of 6.7% [14], [81]. One key characteristic of the disease is the ability of glioblastoma cells to migrate rapidly and spread throughout healthy brain tissue[9], [82]. To develop treatments that effectively target cell migration, it is important to understand the fundamental mechanism driving cell migration in brain tissue. Several models of cell migration have been proposed, including the motor-clutch, bleb-based motility, and osmotic engine models. Here we utilized confocal imaging to measure traction dynamics and migration speeds of glioblastoma cells in mouse organotypic brain slices to identify the mode of cell migration. We found that nearly all cell-vasculature interactions reflected pulling, rather than pushing, on vasculature at the cell leading edge, a finding consistent with a motor-clutch mode of migration, and inconsistent with an osmotic engine model or confined bleb-based migration. Reducing myosin motor activity, a key component in the motor-clutch model, was found to decrease migration speed at high doses for all cell types including U251 and 6 low-passage patient-derived xenograft lines (3 proneural and 3 mesenchymal subtypes). Variable responses were found at low doses, consistent with a motor-clutch mode of migration which predicts a biphasic relationship between migration speed and motor-to-clutch ratio. CRISPR/Cas9

knockouts of Talin1, a molecule that mechanically links integrins to the actin cytoskeleton, and of CD44 both slowed migration of U251 cells. Consistent with these findings, targeting integrins with Cyclo-RGD was found to decrease migration in some PDX lines and in U251 cells while incubation with IM7, an antibody for CD44, slowed migration in U251 cells. Overall we find that glioblastoma cell migration is most consistent with a motor-clutch mechanism to migrate through brain tissue *ex vivo*, and that both integrins and CD44, as well as myosin motors, play an important role in constituting the adhesive clutch.

2.3. Introduction

Glioblastoma multiforme (GBM) is an aggressive malignant brain tumor with extremely low 5-year survival rates[81]. The current standard of care includes surgery, radiation, and temozolomide chemotherapy, though these treatments have failed to prevent recurrence and fail to result in long-term survival. One key characteristic that drives the aggressiveness of the disease is the ability of the tumor cells to migrate rapidly and spread throughout the brain[9], [82], [83]. Developing an in depth understanding of the mechanisms that cancer cells use to migrate could provide opportunities for developing novel strategies for limiting cancer spread.

Several models of cell migration have been proposed. The motor-clutch mechanism of force transmission describes the process of transmitting intracellular forces to the extracellular matrix (ECM). In this model, forces in the cell are generated through non-muscle myosin II motors and F-actin polymerization, leading to retrograde movement of the F-actin filaments away from the leading edge toward the cell center

[84]. Adhesion molecules, or molecular “clutches”, connect the F-actin network to the ECM to transmit force to the environment[85]–[87]. The motor-clutch model simulates this behavior by describing the stochastic breakage and rebinding of clutches in response to a moving actin filament network/bundle[30], [31]. Though other versions of the model have been developed[88], the simplest version regards the F-actin network/bundle as a rigid rod, which can bind to an array of linear springs, or clutches. The clutches exhibit force-dependent unbinding and transmit force to a linear substrate spring that describes the elastic properties of the extracellular environment. Eventually, the clutches at one protrusion fail stochastically, while the clutches at other protrusions persist, thus breaking the symmetry, so that the failed protrusion becomes the trailing edge, and the persisting protrusions constitute the leading edge. This results in net movement of the cell towards the leading edge. The movement of the cell thus moves opposite of the direction of substrate deformation, which is one of the key predictions of the motor-clutch model. The trailing edge experiences pulling forces until the protrusions fail and the substrate mechanically relaxes. The behavior of the entire cell was simulated by Bangasser et al. (2017) [32], who developed a cell migration simulator (CMS), which links multiple motor clutch modules via a spring at the cell body, to stochastically simulate whole-cell migration. One key finding of this model is the biphasic relationship between cell migration speed and motor-to-clutch ratio in which balanced motors and clutches leads to optimal cell migration[32], [89].

The physical paths that glioma cells use to invade healthy tissue has been studied extensively. Post-mortem histological analysis was used to determine that

glioma cells migrate along the brain parenchyma, blood vessels, white matter tracts, and the subarachnoid space below the meningeal covering of the brain[90], [91]. Several studies have used dynamic analysis in brain tissue to identify the vasculature as the primary tract of cell migration[92]–[96]. Liu et al. imaged the deformation of vasculature during migration of U251 glioma cells and found that cells primarily exert a pulling force at their leading edge, consistent with a motor-clutch model and inconsistent with other proposed modes of migration, though they analyzed only a small number of cells and one high-passage cell line[49].

Within the motor clutch framework, integrins are generally thought of as the primary cell adhesion molecule that acts as the clutch, linking the actin cytoskeleton to the extracellular matrix via the adaptor proteins talin, vinculin, and alpha-actinin [57], [60], [61]. Integrins are a family of adhesion proteins that bind directly to ECM proteins and play a critical role in cell migration and signaling in many cell types and in cancer[65], [66], [67]. They have a heterodimeric structure composed of alpha and beta subunits. These subunits bind directly to specific peptide sequence, such as RGD, on ECM substrates, including collagen, laminin, and fibronectin[68]. Talin, which has two human isoforms, talin1 and talin2, acts as a force-bearing connection, or adaptor, between integrin cytoplasmic tails and actin filaments. Recent studies have identified other molecules that could have the potential to act as a molecular clutch, such as the adhesion molecule CD44. CD44 binds to hyaluronic acid via its extracellular domain and connects to the actin cytoskeleton intracellularly via adaptor proteins ezrin, radixin, and moesin, the so-called ERM proteins, and ankyrin[71], [73], [74], [97]. CD44 has also

been implicated in mediating glioma cell migration[75]–[77]. Klank et al. found a biphasic relationship between survival in both humans and mice and CD44 expression, where an intermediate expression of CD44 correlated with fastest migration in mice and lowest survival in both mice and humans, as predicted by the CMS[80]. This study also demonstrated that natural variations in expression of CD44 across subtypes biphasically correlates with patient survival. Specifically, the proneural subtype was shown to have lower CD44 expression and the mesenchymal subtype was shown to have higher CD44 expression, with the former subtype exhibiting modestly longer survival. These findings have been supported by other studies demonstrating that glioblastoma cells can migrate through hyaluronic acid-rich matrices via CD44 adhesion [77] and that cells from mesenchymal glioma tumors have higher CD44 expression and migrate faster than their proneural counterparts[28].

However, the universality of the motor-clutch model has been questioned. In particular, Lämmerman et al. showed that dendritic cells in 3D could migrate without integrins[70], a key component of the molecular clutch. However, there are potential limitations of this finding, in particular not all integrins were knocked out, and other adhesion molecules that could mediate motor-clutch migration, such as CD44, were presumably still active. It is worth noting that a high copy number of relatively weak, i.e. non-specific, adhesive bonds could still serve the function of a clutch in the motor-clutch framework. However, as a result of this finding, alternate models of cell migration were proposed. Stroka et al. proposed the osmotic engine model, in which cell migration is driven by a spatial gradient of ion/osmolyte pumps in the plasma membrane that lead to

directed water fluxes throughout the cell [34]. In this model, migration does not require on adhesion to the environment. Instead, the cell establishes a spatial gradient of ion pumps that creates a net influx of ions at the leading edge and net outflux of ions at the trailing edge. This creates an electro-osmotic gradient across the cell cytoplasm, driving water to permeate into the cell at the leading edge and out of the cell at the trailing edge, leading to net movement of the cell forward. Following this hypothesis, Stroka et al. found cell migration is sensitive to changes in Na+/H+ exchangers, changes in aquaporin water channels, specifically AQP5, and osmotic shock. However, their experiments were conducted in confined microchannels in vitro, and whether this mode of migration occurs in physiological relevant environments, such as for glioblastoma cells in brain tissue, is an open question [34]. A cell migrating under this mechanism could still maintain adhesion to the environment, so as the osmotic forces propel the cell forward adhesions would presumably exert a frictional force resisting the motion, and so blocking adhesions would result in an increased cell migration speed. In addition, the cell would push the environment away from the leading edge, which is inconsistent with the small set of observations from Liu et al. for U251 cells in normal mouse brain slices. However, again, these results were based on a limited number of observations for a highly passaged cell line, and it is unknown whether lower passage glioblastoma cells use the osmotic engine model for migration in brain tissue.

Another mechanism of cell migration that has been proposed is bleb-based motility[35]. A variety of cell types have been shown to produce blebs *in vitro*, including A375 melanoma cells, breast cancer cells, and T cells[36]–[38], [98]. The most *in vivo*-

like environment blebbing has been observed in is 3D collagen gels[38], [39]. A bleb is a local transient loss of plasma membrane to F-actin cortex cohesion that causes a plasma membrane-bounded blister-like protrusion to rapidly extend from the cell[39], [40]. Blebbing enables the plasma membrane to rapidly advance, faster than F-actin can polymerize. Subsequently, the actin-myosin cortex reforms under the plasma membrane, adhesions can form, and the intracellular forces can be transmitted to the environment. In order for the cell to migrate following the rapid extension of the plasma membrane, adhesions must presumably form at the leading edge and engage the cell's motor-clutch modules, pulling the cell forward before the bleb can be retracted. In this description, bleb-based motility can be regarded as a form of motor-clutch-mediated migration, where the plasma membrane advances by blebbing rather than F-actin self-assembly, as in the original motor-clutch model. Even so, during bleb extension, this model predicts that the extracellular environment will be pushed away from the leading edge, whereas the F-actin assembly-based motor-clutch model predicts only pulling forces at the leading edge.

In the present study, the migration of a high passage gliomblastoma cell line, U251, and 6 low passage patient-derived xenograft (PDX) glioblastoma lines were investigated in mouse brain-slice organotypic culture to discern the cell migration mechanism in brain tissue *ex vivo*. Brain slices have been found to preserve the cytoarchitecture of the brain and additionally be an effective way to study the effects of small molecule inhibitors on cell migration [99], [100]. Traction dynamics and cell migration speeds in mouse brain slices were assessed using two-color swept-field

confocal imaging with glioma cells either expressing GFP-actin or a green membrane dye and the brain vasculature labeled with a red fluorescent marker (isolectin-b4-rhodamine). Genetic modification and drug perturbations were used to target specific motor and clutch molecules potentially involved in migration. We find that the observed traction dynamics are consistent with glioma cells using a motor clutch mode of migration and argue against other models, including the osmotic engine model and bleb-based motility model. We also find myosin, integrins and CD44 to be important for cell migration, with implications for therapeutic targeting of glioblastoma cell migration.

2.4. Materials and Methods

2.4.1. U251 cell culture

The U251 human glioblastoma cell line was obtained from Dr. G. Yancey Gillespie (University of Alabama at Birmingham) and was authenticated using the short tandem repeat assay (University of Arizona Genetics Core). Stably transfected U251-GFP-actin cells were used[32]. Cells were cultured in T25 plastic tissue culture flasks (353108; Becton Dickinson, Franklin Lakes, NJ) in a humidified 37^{o}C, 5% CO_2 incubator. Dulbecco's modified Eagle's medium/F-12 (31765-035; Gibco, Gaithersburg, MD) supplemented with 8% fetal bovine serum (FBS; 10438-026; Gibco) and 1x penicillin/streptomycin (100 IU/mL Penicillin, 100 μg/mL Streptomycin; 30-001-CI; Corning, Corning, NY) (P/S) was used to culture the cells. Before plating cells onto brain slices for migration studies, cells were removed from the flask using a 5 minute incubation with 0.25% trypsin with EDTA in Hanks' balanced salt solution (25-052-CI; Gibco).

2.4.2. Mayo PDX cell culture

PDX lines were obtained from the Mayo Clinic Brain Tumor Patient-Derived Xenograft National Resource[101]. Cell lines that were frozen in FBS-containing media (GBM44, GBM85, GBM80) were cultured in T25 plastic tissue culture flasks (353108; Becton Dickinson, Franklin Lakes, NJ) in a humidified 37^{o}C, 5% CO_2 incubator with Dulbecco's modified Eagle's medium/F-12 (31765-035; Gibco, Gaithersburg, MD) with 8% fetal bovine serum (10438-026; Gibco) and 1x penicillin/streptomycin (30-001-CI; Corning,

Corning, NY). Cells that were frozen without FBS (GBM12, GBM117, GBM39, GBM85) were cultured on T25 plastic culture dishes coated in 10% Matrigel with DMEM/F12 with 1x B-27 supplement (12587010; Gibco) and 1x P/S.

2.4.3. Creation and maintenance of cell lines

CD44 knockout (KO) was achieved as described previously [102]. TLN1 KO was achieved using the CRISPR/Cas9 system. A guide RNA (sequence AACUGUGAAGACGAUCAUGG) was created to target TLN1. U251 cells were transfected with Cas9 nuclease and gRNA using the Neon Electroporation system (Voltage = 1150V, Pulse width = 30ms, number of pulses = 2, interval between pulses = 1 ms). Serial dilution was then used to generate several hundred single cell clones. Amplification and sequencing of the TLN1 gene for some of the single clones was used to identify 4 clones with a homozygous TLN1 KO. Western blot was used to confirm knockout of TLN1 and verify that TLN2 expression was not upregulated in response to TLN1 KO (Supplementary Figure 2.2).

2.4.4. Preparation of mouse brain slices

All animal treatments and experiments were conducted in accordance with Institutional Animal Care and Use Committee at the University of Minnesota approved protocols. Adult B57BL/6 mice aged 8-12 weeks from the Jackson Labs were terminally anesthetized in a CO_2 chamber and then perfused transcardially with ~20mL isotonic saline until the liver appeared tan colored. The brains were extracted and transferred into chilled oxygenated artificial cerebrospinal fluid (124 mM NaCl, 2.5 mM KCl, 2.0 mM

$MgSO_4$, 1.25 mM KH_2PO_4, 26 mM $NaHCO_3$, 10 mM glucose). The cerebrum was sectioned into 300 μm coronal slices using a vibratome at 80 Hz vibration speed, 2.5mm amplitude, and 0.5mm/sec advance speed (Lafayette Instruments; 7000SMZ-2).

2.4.5. Organotypic brain-slice coculture with glioma cells

Brain slices were transferred into DMEM/F12 media containing 8% FBS and 1x P/S and stored in an incubator at 37°C and 5% CO_2. Two hundred thousand cells were plated onto a slice and incubated overnight to allow cells to infiltrate into the slice. Cells typically invade up to 100 μm into the tissue. Isolectin GA-IB4 (Alexa Fluor 568; Molecular Probes, Eugene, OR) was added to the slice to stain the vasculature at least 30 minutes before imaging. The slice was transferred into a 6-well glass-bottom 35 mm culture dish (P35G-0-20-C; MatTek, Ashland, MA) with fresh media. A tissue culture anchor (SHD 42-15; Warner Instruments, Hamden, CT) was placed on top of the brain slice to prevent it from drifting during imaging.

2.4.6. Brain slice incubation with drugs and antibodies

For experiments that included drug targeting, the drug was added to the dish containing the brain slice and cell co-culture 3 hours before imaging to allow the drug to diffuse into the slice. When the slice was moved into fresh media for imaging, drug was added to keep the concentration consistent. For experiments with IM7, the slice and cells were incubated with IM7 for 30 minutes before cell plating.

2.4.7. Confocal imaging of brain slices

For experiments with brain slices, the slice was imaged using a Zeiss LSM 7 Live dual-color swept-field laser confocal microscope (Carl Zeiss, Oberkochen, Germany) with a 20x 0.45 NA objective lens capable of simultaneous imaging in both the green (GFP) and red (IB4) channels as previously described[49]. Maximal intensity projections from multiple z-stacks were used to generate 2D images for quantitative shape and motion analysis. A 3x3 tile scan was imaged, and the number of z-stacks was adjusted to ensure that the data acquisition of the whole slice was completed in under 10 min (eight to nine planes with 10 μm separation were typically used). The z-stacks were then imaged every 10 min for up to 10 h at 37^{o}C in a humidified 5% CO_2 environment.

2.4.8. Brain slice registration and cell tracking

To track single cell migration, relevant z planes were first selected to exclude cells migrating outside of the brain slice, particularly on the glass. Maximum intensity projections from these z-stacks were used to assess single cell migration speeds. Stage drift and tissue relaxation were registered using an affine transformation in MATLAB's imregister_tform function. Single cells were then tracked using ImageJ's TrackMate with radius of 10-15 μm and threshold of 2-10 μm. The random motility coefficient (D) was calculated by linear fitting to the mean-squared displacement (MSD) versus time (t).

2.4.9. Motor clutch modeling

The motor clutch model as described by Chan & Odde [30] and Bangasser et al.[31] was used to simulate substrate load-and-fail dynamics and output plots of substrate

displacement versus time. A custom Matlab code was developed to isolate peaks in displacement and fit a line to the loading of the substrate, which estimates the stretching rate of the substrate.

2.4.10. Stochastic cell migration simulator

The cell migration simulator as described by Bangasser et al.[32] and Klank et al.[80] was used to simulate 10 migrating cells under various numbers of motors and clutches for 6 hours each. The simulation parameters are shown in Table 1.

2.4.11. 2D polyacrylamide gel synthesis

Polyacrylamide hydrogels (PAGs) were cast onto No. 0 glass bottom 35 mm culture dishes (MatTek P35G-0-20-C) using a previously described method and formulation [32], [103]. Cast gels were then coated using sulfo-SANPAH (Thermo Fischer Scientific, Waltham, MA) as previously described (Bangasser et al., 2017; Wang and Pelham, 1998). In this study, Type I Collagen (354236, Corning, Corning, NY) or anti-CD44 antibody IM7 (BDB553131, BD Biosciences, San Jose, CA) were used to coat PAGs. In general, 200 µg/mL Col I solution was used and 1-300 µg/mL IM7 solution was used depending on the experiment. In addition, 0.7, 4.6, 9.3, 19.8, 98.5, 195 kPa stiffnesses were used in this study, which were obtained by varying the cross-linker and polymer concentrations as previously described[32].

2.4.12. Statistical analysis

Statistics were completed in PRISM using a Kruskal-Wallis/Mann-Whitney test with multiple comparisons to account for the number of datasets that were being compared.

2.5. Results

2.5.1. Human glioblastoma cells exert pulling forces on brain vasculature

Glioma cells, including high passage U251 cells and patient derived xenograft (PDX) lines from the Mayo Clinic, were plated on 300 μm thick normal mouse brain slices. The cells, which were stained to be green fluorescent, adhered to and migrated into the brain slice and were imaged inside the slice using confocal microscopy. This method allowed us to both assess single-cell migration speed and investigate interactions between cells and the vasculature. As described by Liu et al., the direction and speed that cells are deforming vasculature can be determined by generating a kymograph of the leading edge of the cell. Figure 2.1A shows example kymographs for two scenarios: motor-clutch-predicted pulling and osmotic engine-predicted pushing. Figure 2.1B-E shows examples of single cells from PDX lines and U251 cells migrating along vasculature. Cells can be seen pulling the blood vessel towards itself while at the same time moving in that direction. This behavior can be captured by generating a kymograph of the leading edge. Figure 2.1F-I shows kymographs for 4 cells pulling on the vasculature. Green lines show the movement of the cell and magenta lines show the movement of the vasculature. These examples show the movement of the blood vessel towards the cell, opposite the direction the cell is moving, as is consistent with a motor-clutch mode of migration but inconsistent with an osmotic engine mode of migration. The angle of the vascular movement in the kymograph, marked by a red dotted line, can be used to quantify the speed at which the vasculature is being deformed. This process was repeated for many cells, including both U251 and a variety of PDX lines. While the

majority of cells are either not adhered to vasculature or show no deformation, of the cells visibly interacting with vasculature, 14 cells from 4 different PDX lines (GBM39, GBM44, GBM85, GBM80) and 8 U251 cells were analyzed and all deformations but one were consistent with a motor-clutch mode of migration (Fig 1J). The mean maximum speed of deformation was 2.2 with s.e.m. 0.52 nm/sec, well within the capabilities of myosin motor sliding velocities, which have been found to be around 3 μm/sec [104]. Observed rates of deformation would be expected to be significantly smaller than maximum myosin motor sliding velocities because the actin filaments experience resistance from the bound adhesion molecules, which we next modeled using a motor-clutch model. Overall, these results are consistent with a motor-clutch model for cell migration, and inconsistent with an osmotic engine model for cell migration.

2.5.2. Motor clutch model predicts cell traction dynamics on vasculature

Under a motor clutch mode of migration, F-actin retrograde flow applies inward forces to the environment, i.e. towards the advancing cell. When the cell moves forward and the trailing edge releases, there would be a pulling at the leading edge and relaxation at the trailing edge. By contrast, in an osmotic engine model, the cell would be moving forward independent of its adhesions, applying frictional forces to the surrounding environment. This would result in a *pushing* at the leading edge and a pulling at the trailing edge. Thus, the directions of the forces at the leading edge in the two models are in opposite directions, providing an excellent opportunity for model discrimination, as summarized above and in Fig. 1.

The motor clutch model with the substrate modeled as a Kelvin-Voigt (KV) material [105] (Fig 2A) was used to simulate deformation of the substrate in response to cellular forces. A KV model was used because the simplification of the substrate to a simple Hookean spring could not achieve substrate displacements as large as what was observed experimentally due to load and foal of the substrate spring, while a KV model allows the substrate to deform further. Additionally, with the substrate modeled as a simple Hookean spring, the displacement must snap back to its original state, which was not always observed experimentally. A KV model can describe plateauing of the displacement. Adebowale et al., previously used a Standard Linear Solid (SLS) model for viscoelasticity, but the KV model is a special case of the SLS model where one spring is considered infinitely stiff, and is therefore simpler[41]. Model parameters are shown in

Table 2.1. The substrate deformation can be plotted over time in response to changing various motor-clutch parameters. The stiffness of the substrate spring determines the maximum displacement to which the substrate can be stretched (Figure 2.2B). A magenta dashed line indicates the average stretching speed of 2.2 nm/sec that was found experimentally. The damping constant impacts the rate at which it approaches the maximum displacement (Figure 2.2C). Altering a parameter that impacts the strength of the clutches, including number of clutches, characteristic clutch bond force, and unloaded off-rate of the clutches, will also change the rate at which the substrate approaches maximum deformation. In Figure 2.2D, the clutch unloaded off-rate constant is varied (k_{off}). In order to simulate deformations of 20-40 μm at a speed on the order of 1 nm/sec, small spring constants (0.01-0.001 pN/nm) and relatively large damping constants (10-60 pN/nm) were used. Pogoda et al. analyzed the time-dependent viscoelastic properties of brain[106]. Though they did not analyze storage and loss moduli at frequencies as low as 10^{-3}-10^{-4} Hz, the trends in their data would imply that at these frequencies, the viscous loss modulus would be significantly higher than the elastic storage modulus, as was found to be the case here. Thus, inward deformations of the vasculature at the leading edge observed experimentally can be computationally reproduced in a motor-clutch model assuming a Kelvin-Voigt model for local brain-vasculature mechanics. These experimental and computational results together support the hypothesis that cells migrate using a motor clutch mode of migration and contradict the hypothesis that cells migrate using an osmotic engine mode of migration.

2.5.3. Cell Migration Simulator predicts response to motor and clutch targeting drugs

To further test whether cells migrate via a motor clutch mode of migration in brain slices, we first sought to understand theoretically how migration would be affected by drugs targeting motors and clutches is important. The cell migration simulator, described by Bangasser et al., was used to model migration speed in response to changes in number of motors and clutches. Table 2 shows the parameters used in simulations. A unique prediction of the cell migration simulator is the optimality of the motor-to-clutch ratio (Figure 2.2E-F). If a cell is operating at the optimal motor-to-clutch ratio or has too few motors, decreasing motor activity will result in slower migration, as this directly decreases the cell's ability to pull itself forward via detachment at the rear. However, if a cell has too many motors relative to the number of the clutches, a slight decrease in motor activity will allow the force to better distribute among the clutches, resulting in less clutch breakage, more efficient force transmission, and faster migration (Figure 2.2E). A similar effect can be seen in Figure 2.2F upon targeting of clutches. Of note, these simulations predict that cell migration would be more sensitive to decreasing motors, as a decrease in motors from the optimum has a very steep decrease from fast migration to no migration while a decrease in clutches from the optimum has a more gradual decrease in migration speed. This suggests that cell migration speed would be more sensitive to motor targeting drugs than to clutch targeting drugs.

2.5.4. Glioma cell motility is biphasic with respect to myosin motor activity

After incubating green fluorescent glioblastoma cells (U251 and 6 PDX lines) with brain slices overnight, cells were imaged inside the slice for 10 hours. Figure 2.3A-B shows example tracks (wind rose plots) of single cell trajectories and Fig 3C-D shows the corresponding mean squared displacement (MSD) plots for this same subset of cells. The MSD plots, while variable, are generally linear and the cells therefore migrate via a random walk. Activity of myosin II motors can be decreased with blebbistatin treatment. Introducing various doses of blebbistatin into the brain slice assay leads to a progressive decrease in migration speed in U251 cells, with an over 4-fold decrease in random motility coefficient (RMC) at 250 μM blebbistatin (Figure 2.3E), implying that control U251 cells are sitting near or below the optimal motor-clutch level. At high doses of blebbistatin, all PDX lines exhibit a significant decrease in migration speed. At an intermediate dose, GBM85 + FBS, GBM 39, and GBM 117 exhibit an increase in migration speed (Figure 2.3F-G). This is a finding unique to a motor-clutch mode of migration, implying that these lines have too many motors relative to the number of clutches for optimal migration. By contrast, the osmotic engine does not utilize myosin, and so presumably operates in a manner independent of blebbistatin concentration. Each cell line has a unique estimated motor-to-clutch ratio predicted by response to motor targeting drugs and the ratio for each line relative to the optimum can be estimated based on these findings, as shown in Figure 2.3H. For example, GBM44 + FBS exhibits a progressive decrease in migration, implying that this line has either balanced motors and clutches or too few motors relative to the number of clutches,

similar to U251 cells. By contrast, GBM80 + FBS, GBM85, and GBM12 exhibit no change in migration at intermediate doses, implying that they are slightly above the optimal motor to clutch ratio, so decreasing motors slightly pushes them over the optimum and we observe only modest change in migration speed, except at very high dose of blebbistatin. Lastly, GBM117, GBM39, and GBM85+FBS all exhibited a peak in migration at intermediate blebbistatin, consistent with their having a higher motor-to-clutch ratio under control conditions than the other cell lines. Supplementary Figure 2.1 includes the statistics for each curve. Altogether, we observed cell migration dynamics and sensitivity to motor perturbation consistent with a motor-clutch mode of migration for glioblastoma cells in brain tissue.

2.5.5. Integrins contribute to cell motility in brain tissue

Next we sought to determine the role of the clutch in cell migration. Initial studies examined migration on 2D polyacrylamide gels of various stiffnesses coated in various substrates to confirm the expected phenotype of a reduction in clutches. In this setup, the cell is forced to migrate using the specific clutch that binds to the ECM coating the gel. For example, on collagen I-coated PAG, cells migrate via integrins. In U251 cells, a knockout of talin1, an adaptor protein between integrins and F-actin, was developed using CRISPR/Cas9. These cells were unable to migrate on collagen gels (Figure 2.4A), indicating that integrin-mediated migration is nearly halted by knockout of talin1. In addition, the cells are smaller in projected area, as measured by a 65% decrease in projected area (Figure 2.4B), and more rounded, as measured by a 63% decrease in aspect ratio (Figure 2.4c), consistent with the hypothesis that the knockout of integrins

prevents proper adhesion and cell spreading. U251 cells with talin1 knocked out migrated slower in brain tissue than controls by 3.5-fold (Figure 2.4D), though they were still migratory, indicating that integrin-mediated adhesion contributes to cell migration in brain tissue but is not the only mechanism the cells use to migrate.

For both U251 and PDX lines, cyclo-RGD (cRGD) was used to target RGD-binding integrins (Figure 2.4E). This decreased migration speed in U251 by 1.5-fold, indicating that U251 cells are using RGD-binding integrins to migrate. In PDX lines (Figure 2.4F-G), some lines (GBM44+FBS, GBM85+FBS, GBM80+FBS, GBM39) exhibited a decrease in migration speed while GBM12, GBM85, and GBM117 did exhibit a significant effect. The statistics for this finding is summarize in Supplementary Figure 1. This indicates that while some lines do partially use integrins to migrate, others do not or can compensate for loss of RGD-binding integrins.

2.5.6. CD44 contributes to cell motility

CRISPR/Cas9 was used to develop a knockout of CD44 in U251 cells. CD44 KO cells were extremely inefficient at adhering to IM7 PAGs and the few cells that did adhere exerted lower traction force than control cells (Figure 2.5A). These cells also migrated slower in brain tissue with a 4-fold and 1.5-fold decrease in RMC observed in two knockout lines relative to control cells, indicating that both integrins and CD44 are important for cell migration in brain tissue (Figure 2.5B). When IM7 was introduced into the brain slice assay with U251 cells, migration speed decreased by 1.5-fold, further indicating that CD44 is important for U251 migration (Figure 2.5C). PDX lines did not experience a decrease in migration speed in response to IM7 incubation (Figure 2.5D).

This is consistent with modeling results in Fig. 2 suggesting that cell migration is not particularly sensitive to clutch targeting. As these cells migrate slower than U251, a small decrease in migration speed would be difficult to detect.

2.5.7. Additive effects of simultaneous targeting of CD44 and integrins

In order to determine the interplay between CD44 and integrins, we targeted both integrins and CD44 simultaneously. When cRGD was used on the talin1 KO cells it had no impact on migration speed in brain tissue (Figure 2.6A), indicating that targeting integrins via talin knockout and RGD targeting drugs is not additive. On the other hand, cRGD was used on the CD44 KO cells and this further decreased migration in brain tissue (Figure 2.6B). When combined, there was a 10-fold decrease in RMC in cRGD targeting of CD44 KO cells relative to control, suggesting that targeting of CD44 and integrins is additive. In wild-type U251 cells, simultaneous targeting of IM7 and cRGD further decreased migration speed compared to either condition alone with a 2.3-fold decrease relative to control (Figure 2.6C). These results are consistent with the finding that glioma cells utilize both integrins and CD44 as clutches independently to migrate. While targeting one may be able to partially decrease migration, both integrins and CD44 must to be targeted to observe a large decrease in migration speed.

2.6. Discussion

In this study, we utilized imaging of GBM cell migration to identify the mechanism of single-cell migration in brain tissue for both high passage U251 cells and low passage patient-derived xenograft lines. Confocal imaging of green-fluorescent cancer cells on red-fluorescent vasculature revealed the cells pulling on the vasculature at the leading edge, a prediction unique to a motor clutch mode of migration and contradictory to an osmotic engine mode of migration. In addition, blebbistatin was used to target myosin II motors and demonstrated the significance of motors to cell migration. Further, some PDX lines were found to have a biphasic response to blebbistatin as described by an increase in migration speed at intermediate doses, another finding that is a specific prediction of a motor clutch model. Through knockouts and drug targeting, both integrins and CD44 were found to act as clutches and the slowest migration was achieved by targeting both clutches simultaneous. This is significant because it both describes a mechanism for how these cells are migrating and suggests that the optimal way to treat GBM via targeting cell migration would be to target both integrins and CD44 simultaneously.

There are a few notable limitations to the methods used. In analyzing the environmental mechanical deformations, many cells showed no visible interaction with the environment, especially in the PDX lines, which could be due to a number of reasons. For example, the cells could be adhered to ECMs that are not visualized by the microscope such as ECMs associated with white matter tracts. They could also simply be non-migratory or the deformation is too small for the microscope to resolve,

which is likely the case in the PDX lines as those are slower migrating. In addition, televascular cell-ECM interactions were not imaged and could behave differently than cell-vasculature interactions.

Despite these limitations, the present findings are significant because the prediction of cells pulling on vasculature is unique to a motor clutch mode of migration, and of the cells whose interaction with vasculature could be visualized all but one demonstrated pulling at the leading edge. This is very strong evidence that these cells use a motor clutch mode of migration while also arguing strongly against the competing osmotic engine model. Had the cells been migrating using an osmotic engine, pushing at the leading edge would have been observed. The hypothesis that cells migrate using a motor-clutch mode of migration was further supported by targeting of motor-clutch components. Most significantly, some lines were found to have a biphasic response to blebbistatin treatment. This optimality of motors and clutches is a also unique prediction of the motor-clutch model. While it's possible that blebbistatin treatment could indirectly impact migration under an osmotic engine model, there is no obvious mechanism for a biphasic response to blebbistatin in this model. Further, as adhesions purely act as frictional resistance to migration in an osmotic engine model, the decrease in migration in response to targeting multiple clutches through a variety of mechanisms argues against the osmotic engine model and supports the motor-clutch model.

While a previous study examined a limited number of U251-mediated vasculature deformations in brain tissue *ex vivo* [49], traction analysis in brain slices of low passage glioblastoma lines had not been done previously. The low-passage PDX cells behaved

similarly to U251 cells, though they generally migrated slower overall. The present study analyzed PDX lines with and without media containing fetal bovine serum per Mayo PDX culture protocol, and noted significant differences between the two conditions. It was consistently found that lines cultured in serum exhibited significantly faster migration, including GBM85 which was studied in both serum and serum-free conditions. FBS therefore has some activating effect on cell migration in the PDX lines. Serum exposure is not an unrealistic experimental effect, as tumors experience breakdown of the blood-brain barrier that presumably exposes tumor cells to serum. Thus, we speculate that the breakdown of the blood-brain barrier in the central regions of the tumor [107] could provide an impetus for accelerating glioblastoma cell migration, which presumably would enhance cell invasion into adjacent relatively normal brain parenchyma where the vasculature barrier function is still intact.

Our study also found that for U251 cells, the slowest migration was achieved by dual targeting of integrins and CD44, suggesting that both molecules are important clutches. This implies that in developing clutch-targeting treatments, targeting both mechanisms of migration simultaneously will have the greatest effect. In the PDX lines, IM7 incubation did not decrease migration speed as hypothesized. This could be because the cells migrate so slowly that detecting a partial decrease in migration speed is not feasible, as results from the CMS simulations indicate that migration is less sensitive to targeting of clutches than motors. This further suggests that targeting one clutch at a time may not be sufficient to adequately slow down migrating cells. It is also possible that the PDX lines do not use CD44 as a clutch, however previous findings strongly

suggest a role of CD44 in glioblastoma migration [80]. An alternative strategy would be to target myosin II motors[108], which the CMS predicts is very sensitive (Figure 2.2E).

In summary, our study investigated a variety of glioblastoma cell lines ranging from low to high passage in an environment that closely mimics cells in the invasive front of a brain tumor. We find that treatment of glioblastoma via targeting migration should either simultaneously target both integrins and CD44, or else target myosin II. This study also highlights the importance of determining whether cells are at an optimal motor-clutch ratio, as insufficient targeting of motors or clutches can potentially increase migration. The motor-clutch-based CMS predicts that the former is more sensitive, and may be a better strategy, although it will be important to assess the effects of drugs on immune cells in the glioblastoma tumor microenvironment, especially antitumoral CD8+ T cells. If the drugs impair T cells to a similar or greater extent than they impair glioblastoma cells, then there will be no benefit or potentially harm to the patient. Overall, our study provides a framework for further development of antimigratory strategies in glioblastoma, and potentially other invasive cancers as well.

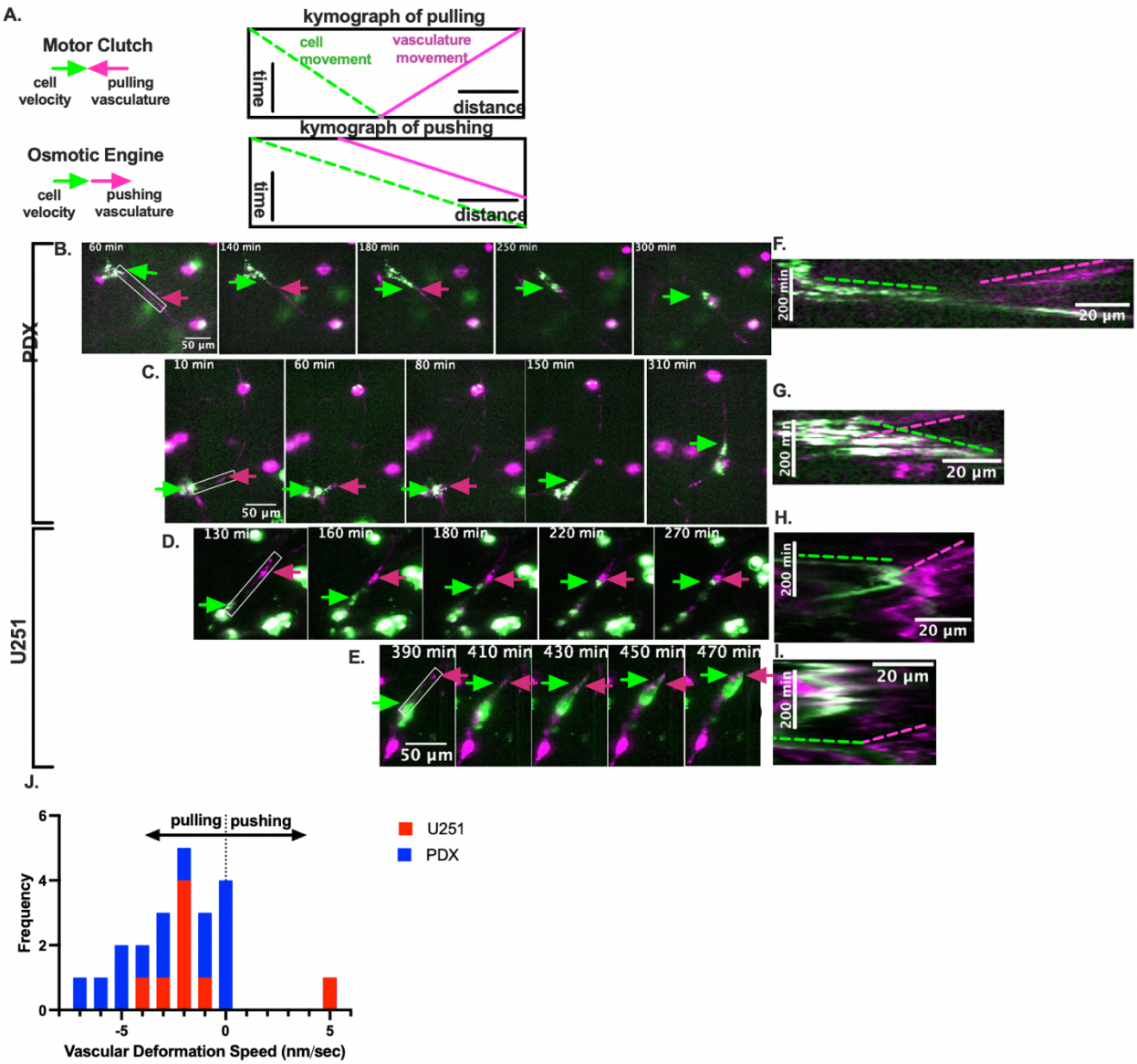

Figure 2.1. Glioblastoma cells exert pulling forces during migration that are consistent with a motor-clutch model for migration.

A) Schematic depicting example kymographs of a cell pulling on vasculature vs. pushing on vasculature. Examples of B-C) Mayo PDX cells (GBM44) and D-E) U251 cells (green) imaged by confocal microscopy migrating along blood vasculature (magenta). Green arrows indicate the leading edge of the cell and magenta arrows indicate the vasculature being deformed. The cell can be seen pulling the vasculature towards itself as it moves forward. F-I) Kymographs of the leading edge of the cell as denoted by the white box on a-d showing motion of the vasculature towards the cell. j) Calculated rates of vasculature movement show that for PDX and U251 cells the vascular is pulled towards the cell at 0-7 nm/sec with one U251 cell observed to push

the vasculature away. The mean speed of vasculature deformation is 2.2 nm/sec with s.e.m. 0.52 nm/sec (n=22 observations).

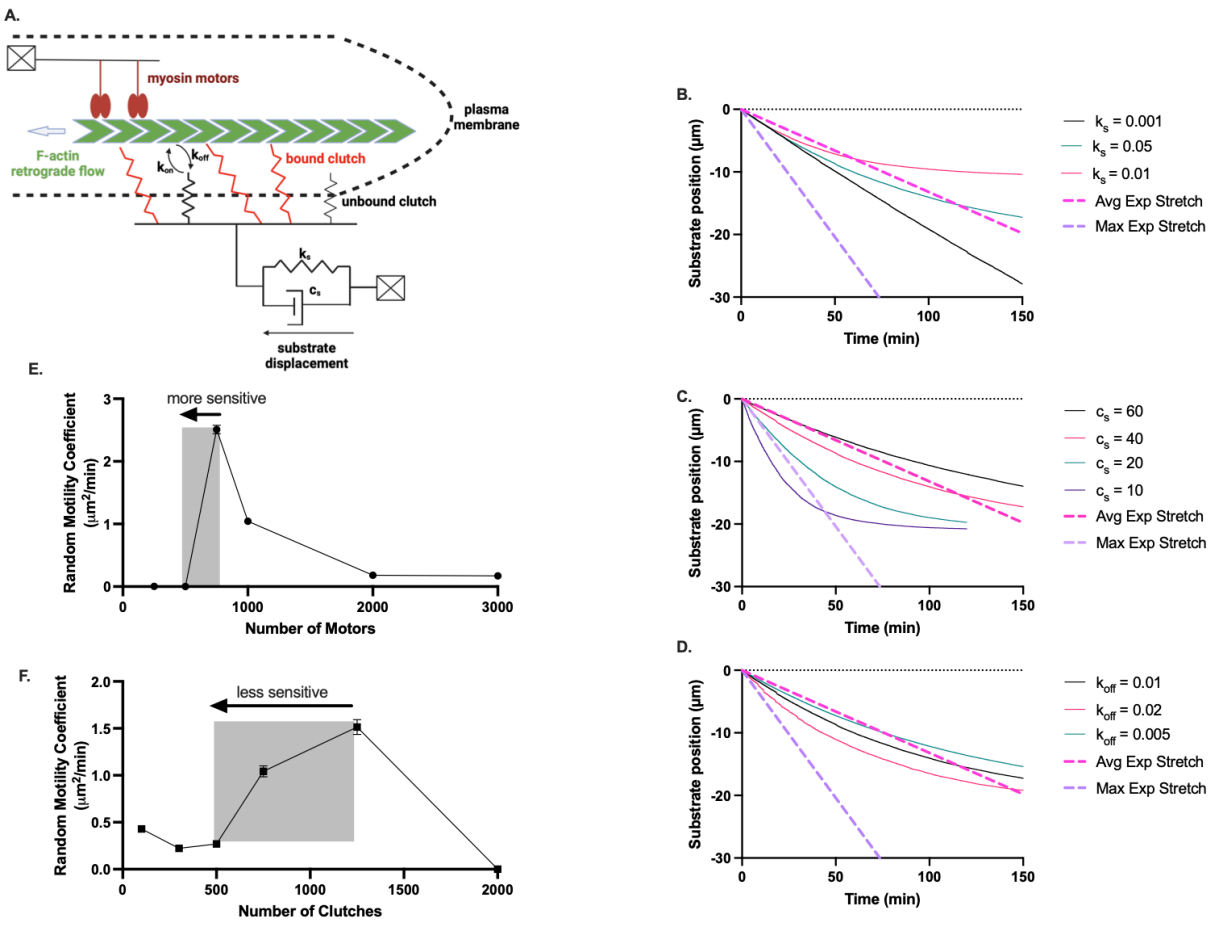

Figure 2.2. Motor clutch model and cell migration simulator predict cell traction and migration behavior in brain slices.

A) Schematic of the motor clutch model with the substrate modeled as a Kelvin-Voigt viscoelastic material. Displacement of the substrate simulated over time in response to changes in B) k_s, the substrate spring constant, C) c_s, the substrate damping constant, and D) k_{off}, the unloaded clutch unbinding rate. A dashed magenta line indicates the mean speed of vascular deformation found experimentally and a dashed purple line indicates the maximum speed of vascular deformation observed experimentally. The cell migration simulator was used to model the relationship between E) number of motors and F) number of clutches and RMC. Cells are more sensitive to decreases in motor number below the optimum than clutch number below the optimum.

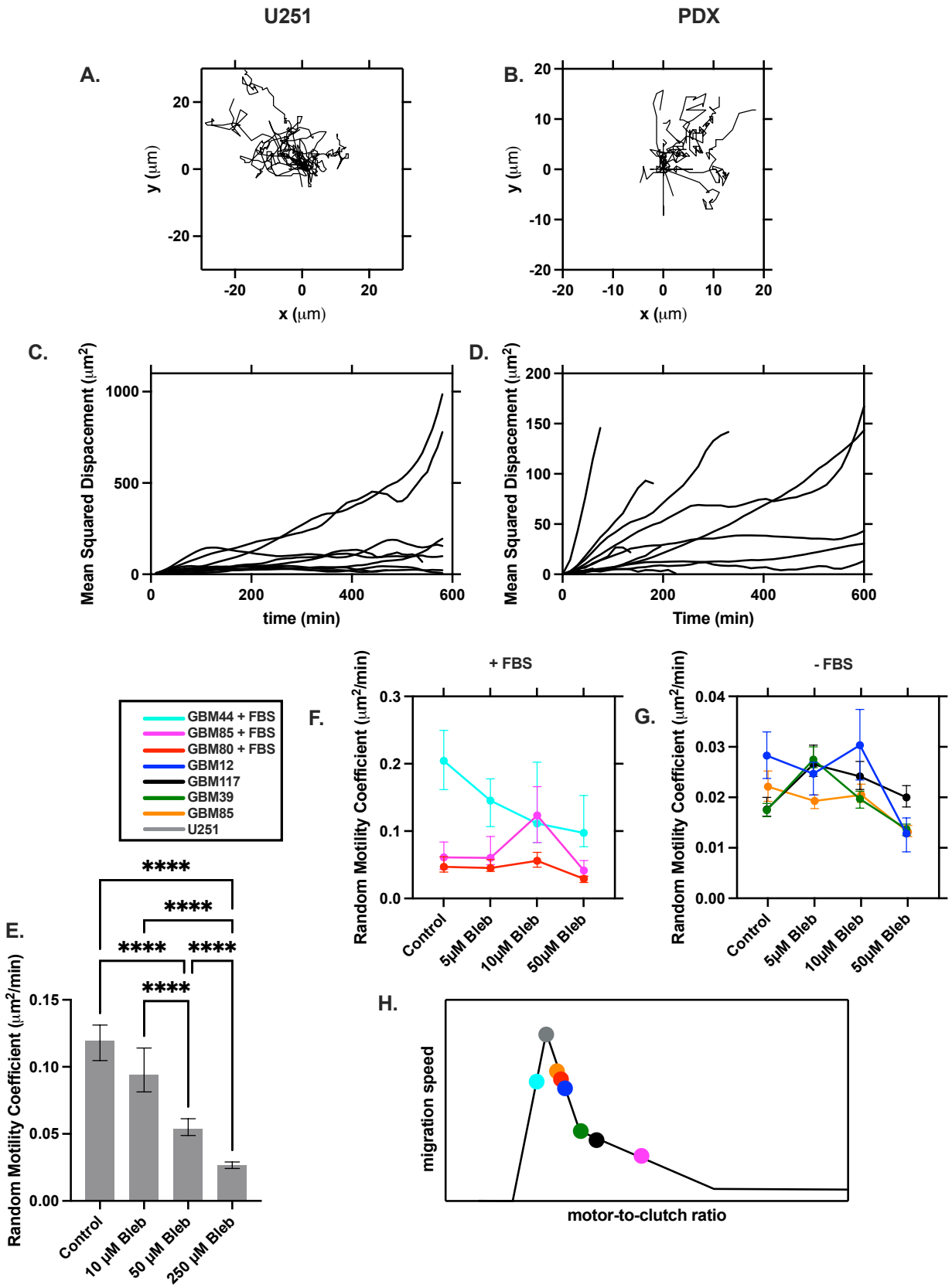
U251
PDX
A.
B.
y (μm)
x (μm)
C.
D.
Mean Squared Dispacement (μm²)
time (min)
Time (min)
GBM44 + FBS
GBM85 + FBS
GBM80 + FBS
GBM12
GBM117
GBM39
GBM85
U251
E.
F.
G.
+ FBS
- FBS
Random Motility Coefficient (μm²/min)
Control
5μM Bleb
10μM Bleb
50μM Bleb
10 μM Bleb
50 μM Bleb
250 μM Bleb
****
H.
migration speed
motor-to-clutch ratio

Figure 2.3. Migratory behavior of glioma cells in brain slices and response to myosin motor-targeting.

Tracks of a) U251 cells and b) GBM80 (-FBS) PDX cells on brain slices. c-d) Corresponding mean squared displacement as a function of time interval for the same cells. e) RMC of U251 cells in mouse brain slices in response to increasing doses of blebbistatin. f-g) Response of PDX lines to varying doses of blebbistatin for cells that were cultured in the presence or absence of FBS. h) Simulated normalized migration speed vs. motor-to-clutch ratio with estimates motor-to-clutch ratio for each analyzed cell line.

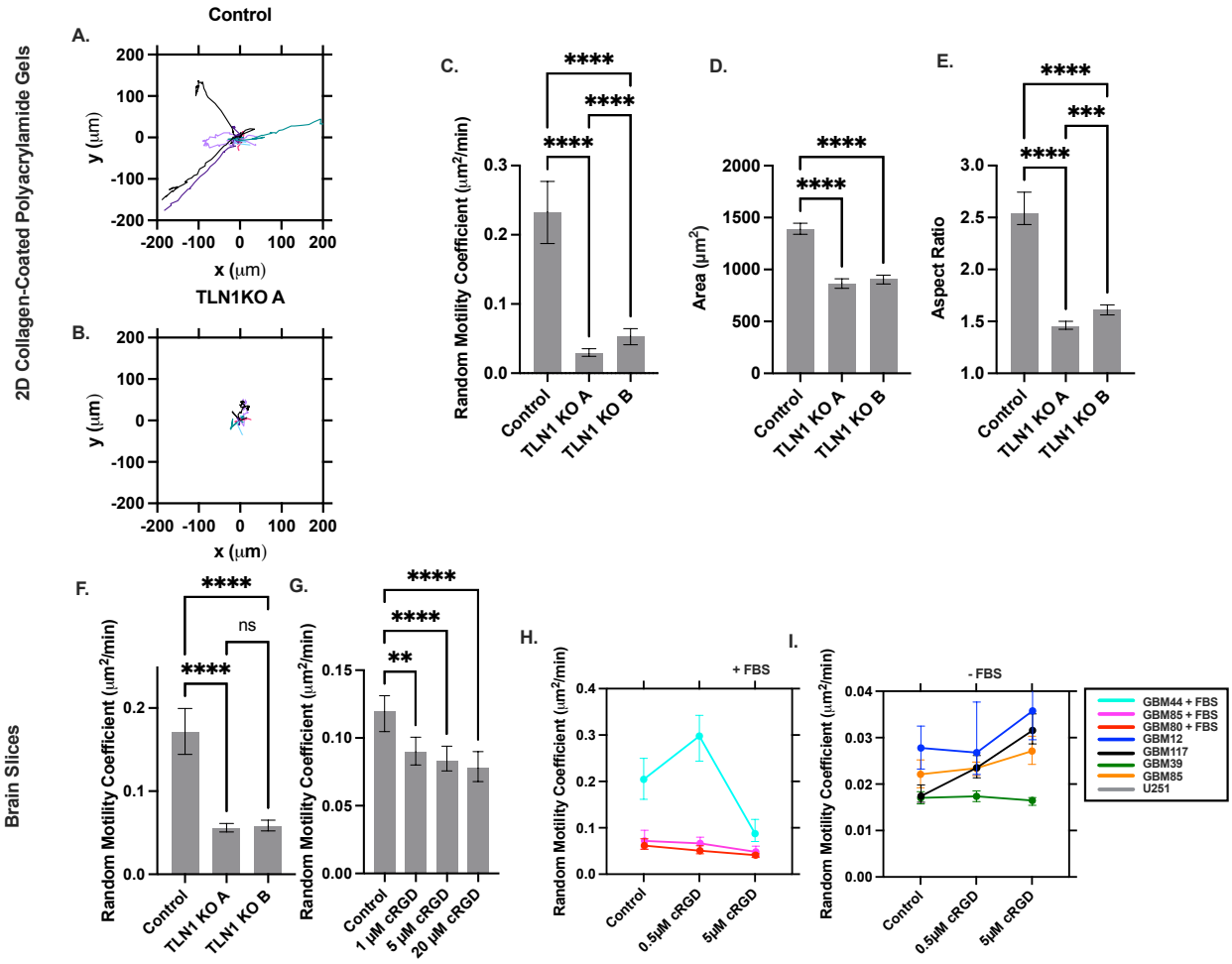

Figure 2.4. The role of integrins in GBM cell migration on PAGs and brain slices.

Wind-rose plots for A) control cells and B) TLN1 KO cells. C) TLN1 KO cells migrate significantly slower than control lines on collagen-coated polyacrylamide gels. D) TLN1 KO cells are smaller in projected area and E) more round than control cells. F) TLN1 KO cells migrate slower on mouse brain slices. Inhibiting RGD-binding integrins with cyclo-RGD in G) U251 and H-I) PDX lines slows cell migration in some lines, while others are unaffected.

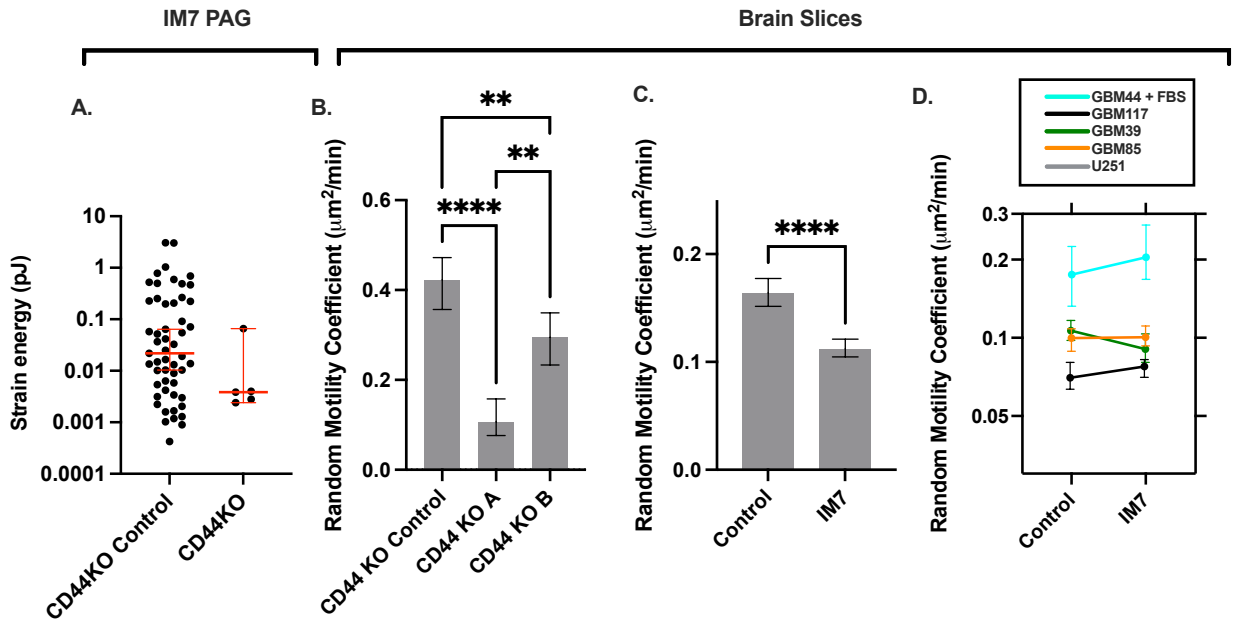

Figure 2.5. The role of CD44 in GBM cell migration on brain slices.

A) CD44 knockout cells migrate slower on brain slices relative to the control line. B) U251 cells on brain slices migrate slower with IM7 incubation. C) Migration of PDX lines is unaffected by IM7 incubation.

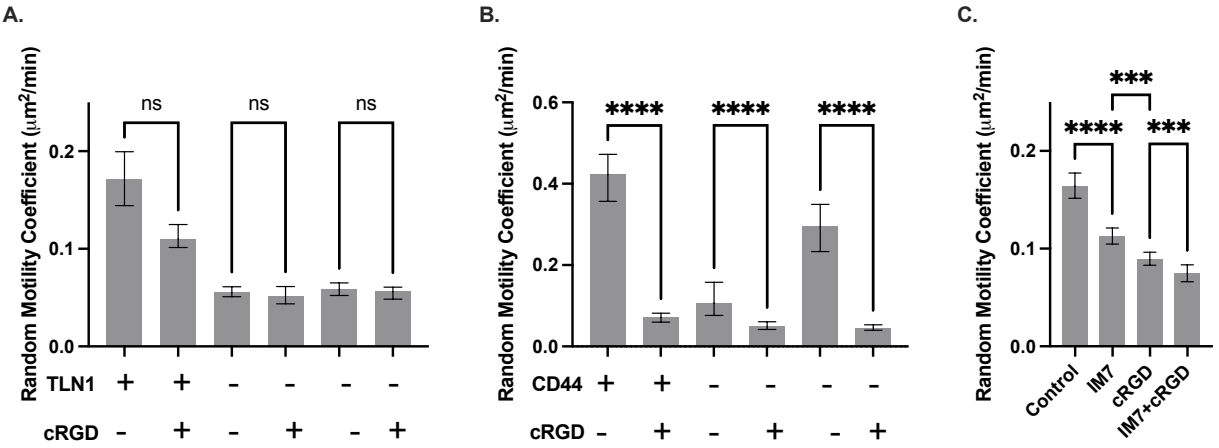

Figure 2.6. Combined targeting of integrins and CD44 maximally inhibits migration on brain slices

A) cRGD targeting of TLN1 KO cells does not further decrease migration. B) cRGD targeting of CD44KO cells decreases migration further on brain slices. C) Combination targeting of U251 cells on brain slices with IM7 and cRGD decreases migration more than either by itself.

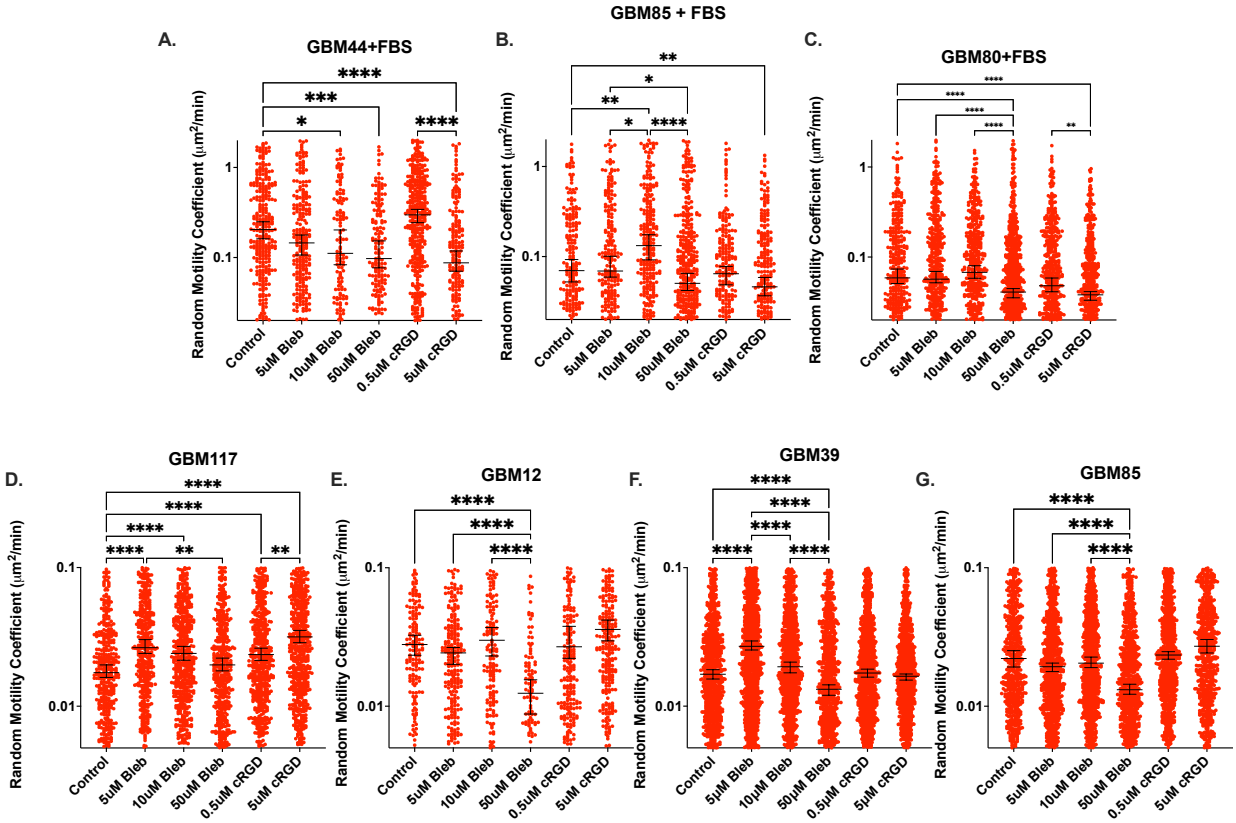

Supplementary Figure 2.1. Migratory behavior of individual glioma cells in brain slices in response to blebbistatin and cyclo-RGD

RMC of cells in response to varying doses of blebbistatin and cRGD for A) GBM44 + FBS, B) GBM 85 + FBS, C) GBM 80 + FBS, D) GBM 117, E) GBM 12, F) GBM 39, and G) GBM 85. Each dot represents a single cell. The black line denotes the median value and 95% confidence interval. Statistics were done using a Kruskal Wallis test.

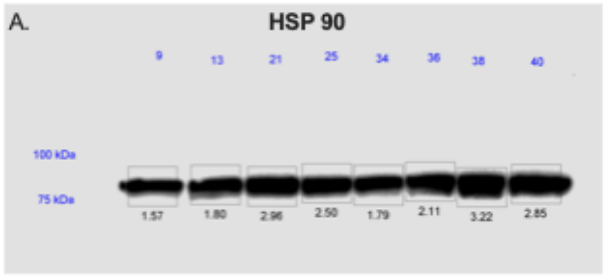

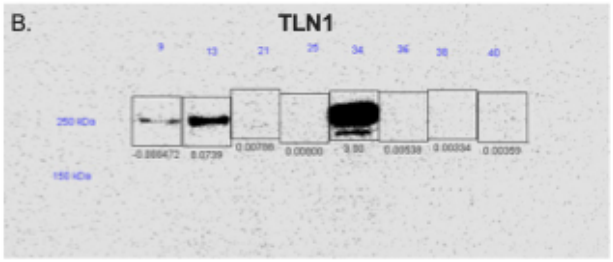

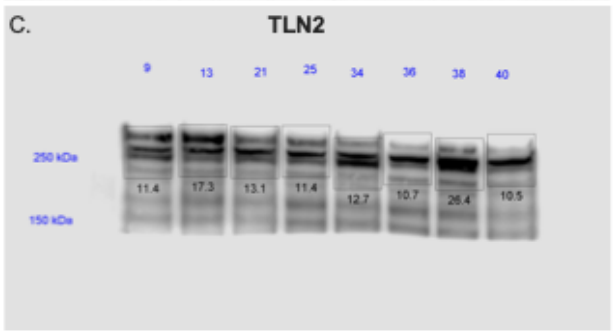

D.

	9	13	21	25	34	36	38	40
HSP90	1.57	1.8	2.96	2.5	1.79	2.11	3.22	2.85
Talin 1	0.000472	0.07392	0.00788	0.008	3	0.00538	0.00334	0.00359
TLN1 norm	0.000301	0.041067	0.002662	0.0032	1.675978	0.00255	0.001037	0.00126
Talin 2	11.4	17.3	13.1	11.4	12.7	10.7	26.4	10.5
TLN2 norm	7.261146	9.611111	4.425676	4.56	7.094972	5.07109	8.198758	3.684211

Supplementary Figure 2.2. Western Blot demonstrating knockout of talin1

Western Blot results for the A) control HSP90, B) Talin1, and C) Talin2 in development of Talin1 knockout. D) Calculations demonstrating knockout of talin1 in given samples and no significant upregulation of talin 2.

Table 2.1. Motor clutch model (MCM) with Kelvin-Voigt substrate parameters

n_m	Total number of motors	50	
n_c	Total number of clutches	50	
k_s	Substrate spring constant	variable	pN/nm
c_s	Substrate damping coefficient	variable	pN/nm
F_m	Myosin motor stall force	2	pN
v_u	Unloaded actin flow rate	120	nm/sec
k_{on}	Clutch on-rate constant	1	sec^{-1}
k_{off}^*	Unloaded clutch off-rate	variable	sec^{-1}
k_c	Clutch spring constant	1	pN/nm
F_b	Characteristic clutch rupture force	2	pN

Table 2.2. Cell Migration Simulator (CMS) parameters. All references values from Bangasser et al. [32].

n_m	Total number of module motors	variable	
n_c	Total number of module clutches	variable	
A_{tot}	Maximum total actin length	10^5	nm
v_{poly}	Maximum actin polymerization rate	200	nm/sec
k_{mod}	Maximum module nucleation rate	1	sec^{-1}
k_{cap}	Module capping rate	0.001	sec^{-1}
l_{in}	Initial module length	5000	nm
l_{min}	Minimum module length	100	nm
k_{cell}	Cell spring constant	1000	pN/nm
$n_{c,cell}$	Total number of cell body clutches	10	
k_s	Substrate spring constant	0.1	pN/nm
F_m	Myosin motor stall force	2	pN
v_u	Unloaded actin flow rate	120	nm/sec

k_{on}	Clutch on-rate	1	sec^{-1}
k_{off}^{*}	Unloaded clutch off-rate	0.1	sec^{-1}
k_c	Clutch spring constant	0.8	pN/nm
F_b	Characteristic clutch rupture force	2	pN

3. Chapter 3: Targeting of CD44 and LFA-1 increases T cell migration in brain tissue

Authors: Sarah M Anderson[1], Nikolaos Memmos[1], Menal Abdella[1], Aamir Ansari[1], Hongrong Zhang[1], Paolo Provenzano[1], David J. Odde[1*]

[1] University of Minnesota, Department of Biomedical Engineering, Minneapolis, Minnesota, USA.

* Corresponding author: oddex002@umn.edu

3.1. Authors' Contributions

NM developed the gaussian mixture model code that was used and advised SMA to utilize the HMM. MA performed the experiments with T cells on PAGs and AA developed codes to analyze this data, both under advisement from SMA. HZ did the T cell extraction and isolation and gave frozen T cells to SMA. The remainder of experiments were completed by SMA.

3.2. Summary

Infiltration of cytotoxic CD8+ T cells into the brain is an important indicator of disease progression and survival for a variety of diseases including multiple sclerosis and glioblastoma. While T cell infiltration in multiple sclerosis has negative implications on disease progression[109], one key hallmark of glioblastoma is the suppression of the immune response, allowing tumor growth[110]–[112]. In this study we use mouse organotypic brain slices co-cultured with CD8+ T cells to develop long time scale (> 30 minutes) movies of migrating CD8+ T cells in normal brain tissue. We found the T cells migrated with two distinct modes, a fast (~2 μm^2/min) mode representing about 20% of steps and a slow (~0 μm^2/min) mode representing the remaining 80% of the steps. We targeted myosin motors and several adhesion molecules to assess how they contribute to T cell migration, and found that targeting of myosin with blebbistatin and targeting of RGD-binding integrins with cyclo-RGD both result in a decrease in migration speed. We also find that targeting LFA-1 with α-CD11a monoclonal antibodies (mAb) and targeting CD44 with α-CD44 mAb increase migration. As U251 cancer cells in brain tissue have decreased migration speed in response to α-CD44 mAb, the present results suggest

that CD44 could be a potential target for improving glioblastoma outcomes by simultaneously slowing cancer cell migration and speeding up CD8+ T cells.

3.3. Introduction

T cell migration in the brain has critical implications for a variety of diseases including gliomas and other brain tumors[113], multiple sclerosis (MS)[109], neurodegeneration[114], and viral infection[115]. One key hallmark of glioblastoma, for example, is the suppression of the immune response, allowing the tumor to grow and spread faster. Infiltration of cytotoxic CD8+ T cells into the tumor has been shown to be an important indicator of disease progression and survival[110]–[112]. In particular, a clinical study by Yang et al. investigated the level of CD8+ T cell infiltration in patient tumors and tracked subsequent survival and determined that patients with higher CD8+T cell infiltration were more likely to survive longer (>403 days)[25]. Additionally, Shamsan et al. demonstrated that in mice the mesenchymal subtype of glioblastoma experiences faster migration of cancer cells but longer survival due to increased infiltration of CD8+ T cells [28]. Several studies have begun to investigate if targeting of cancer cell migration can slow down disease progression[80], however, the effects of cell migration-targeting drugs and antibodies on T cell migration in brain tissue has not been studied. Thus, the mechanism of T cell migration in brain tissue is unknown and it is unclear how targeting cancer cell migration would impact T cell migration. Understanding the mechanism of T cell migration in tissue and specifically brain tissue could inform the development of immune therapies that improve T cell intra-tumoral migration and killing of glioma cancer cells. In addition, increasing T cell migration could be used to improve T cell response to infection, whereas decreasing it could be beneficial in MS and neurodegeneration.

Two primary modes of cell migration have been observed *in vitro*: amoeboid and mesenchymal. Mesenchymal migration is characterized by intracellular force generation via actin-myosin complexes pulling on adhesive molecular “clutches” bound to the extracellular matrix (ECM) and asymmetric breakage of these adhesions to define the trailing edge[30], [116]. By contrast, amoeboid migration occurs in the absence of adhesions[117]. One potential mechanism for amoeboid migration is an osmotic engine model, in which cell migration is driven by a spatial gradient of electro-osmotic pumps and channels in the plasma membrane that lead to directed water fluxes throughout the cell [34]. *In vitro*, some studies have found T cells to migrate via an amoeboid mode of migration[70], [117]–[119] while other studies have found that they use a motor-clutch mesenchymal migration [118], [120], [121]. These results are consistent with a more general framework where T cells are able to plastically switch between the different modes of migration depending on their environment, which is regulated by microtubule instability[38], [70], [122], [123].

Several studies have investigated cytotoxic CD8+ T cells in physiologically relevant environments. Cytotoxic CD8+ T cells, which are primarily responsible for finding and killing cancer cells [16], have been found to migrate rapidly in 3D aligned collagen gels [124] and in 2.5D nanotextured ICAM-1 gels [38]. They have also been imaged in melanoma tumors [125], lung squamous cell carcinoma tumors[126], the trachea[127], lymph nodes[128], and live larval zebrafish fins[129]. Several studied have imaged CD8+ T cells in brain tissue. These studies all inoculated mice with an infection and imaged CD8+ T cell migration in the CNS, and the migrating T cells were consistently

found to have 2 subpopulations: a slow-migrating (“arrested”) subset and a fast-migrating subset [130]–[132]. The most in-depth investigation of CD8+ T cell migration in brain tissue was done by Harris et al., who found that CD8+ T cells in chronically infected mouse brain explants migrated via a Lévy walk and that the migration speed is decreased by the chemokine CXCL10[50]. However, like the other studies in brain tissue, they only imaged cells on relatively short time scales (10-30 minutes) and several studies have questioned the Lévy walk approach as a useful framework for any biological motion, described below. In a subsequent study by Banigan et al., a two-state model was used to describe CD8+ T cell migration in lymph nodes[133]. When Jerison and Quake observed T cells in the live larval zebrafish over millimeter fields of view and for periods of a few hours, they found that the cells do not follow a Lévy walk over long periods but instead the cells had a large heterogeneity in both speed and turning behavior [129]. Additionally, all of these studies that investigate T cell migration in brain tissue utilized the brains of infected mice; to our knowledge, migration speeds of CD8+ T cells in normal brain tissue has yet to be reported. This is relevant for glioblastomas, as the most invasive cells are migrating into relatively normal brain tissue beyond the tumor margin[134]. The mechanical processes mediating T cell migration *in vivo* are not clear.

Many adhesion molecules have been hypothesized to act as a molecular “clutch” for T cell migration. The primary class of molecules that has been identified as a molecular clutch in T cell adhesion and migration are integrins, particularly LFA-1, which has been found to be important for both T cell migration and activation [135]–[138]. LFA-1, a

surface-expressed heterodimer composed of an alpha subunit (CD11a/αL) and beta subunit (CD18/β2), is a leukocyte-specific integrin that binds to the ICAM proteins[139]. LFA-1 has been specifically targeted on T cells using a drug, efalizumab, to treat autoimmune diseases, particularly psoriasis[140], though it was withdrawn from the market due to severe side effects including fatal brain infections[141]. While T cells have been shown to use a mesenchymal mode of migration on both ICAM-1 and collagen *in vitro* [120], [38], a few studies question this by demonstrating that dendritic cell migration can occur independent of most integrin subtypes[70], [117]. While one explanation of this is that cells use an amoeboid mode of migration, it is also possible that they use another molecule as a molecular clutch.

One potential molecule is CD44, which is widely expressed on activated T cells, is one of the most common surface markers used for T cells, and has been shown to regulate tethering and rolling interactions with cells that express hyaluronic acid such as vascular endothelial cells[142], [143]. In addition to being a potential clutch for migration, CD44 has been suggested to potentially play a role in activation of CD8+ T cells. Klement et al. found that upregulation of osteopontin, a ligand of CD44, decreases activation of CD8+ T cells [144]. Further, Mrass et al. found that T cells with a CD44 knockout were less efficient in scanning of tissue and therefore made fewer contacts with tumor cells. These cells did not maintain a stable polarized shape and did not migrate with the same persistence as wild type cells [145]. While these studies suggest an important role for CD44 in T cell migration, it is not clear how targeting CD44 via

mAbs would influence migration. In addition, the role of CD44 in T cell migration in brain tissue is unclear.

In this study, we used normal organotypic mouse brain slices *ex vivo* co-cultured with CD8+ T cells to assess the mode of migration in an *in vivo*-like environment. We also utilized drugs and antibodies to investigate the molecular basis of migration via perturbation of motor-clutch components. This allowed us to investigate the impact of adhesion and migration molecules of the integrin class, most notably LFA-1, and CD44 over long time scales (10 hours) on CD8+ T cell migration.

3.4. Methods

3.4.1. T cell isolation

All animal treatments and experiments were in accordance with Institutional Animal Care and Use Committee at the University of Minnesota approved protocols. Adult B57BL/6 mice aged 8-12 weeks from the Jackson Laboratory were euthanized in a CO_2 chamber and sterile surgical tools were used to separate the mouse spleen, which was stored in ice-cold PBS with 25% penicillin streptomycin (100 IU/mL Penicillin, 100 µg/mL Streptomycin; 30-001-CI; Corning, Corning, NY) (P/S). A syringe plunger was used to disrupt the spleen inside a 70 µm nylon strainer (Fisherbrand, cat#: 22363548) over a 50 mL tube and rinsed with 10 mL of 1x PBS with 2% FBS. Splenocytes were then resuspended in 1XPBS + 2% FBS + 1mM EDTA at 10^8 cells/mL. CD8+ T cells were negatively selected using the EasySep Mouse CD8+ T Cell Isolation Kit (StemCell Technologies cat #: 19853) following the manufacturer's recommendation. After isolation, the enriched cells were resuspended in pre-warmed media (Immunocult-XF T Cell Expansion Medium, StemCell Technologies Cat #10981) supplemented with 30U Mouse Recombinant IL-2 (StemCell Technologies Cat #78081) and 1% P/S and plated in a 96 well round bottom plate (Corning, Cat #38018) at 10^5 cells in 100µL per well.

3.4.2. T cell activation with Dynabeads

To activate the T cells, CD3/CD28 DynaBeads (DynaBeads Mouse T-Activator CD3/CD28 for T-Cell Expansion and Activation, Gibco Cat #11456D) were washed and resuspended in T cell culture media. Two and a half µL of the resuspended DynaBeads

were added to each well of the T cells, and incubated in a CO_2 incubator at 37C overnight. If the media turned yellow, fresh media was added. After 20-24 hours, the cell-contained medium was transferred to a round bottom tube and placed in the magnet for 2.5 minutes to remove the DynaBeads. After beads removal, the cells were counted and resuspended in FBS with 15% DMSO at 1-2 million cells per mL before transferring to cryovials for long term storage in liquid nitrogen.

3.4.3. T cell thawing and expansion

To thaw T cells, a cryovial was placed in a 37^{o}C water bath. As soon as it was thawed, the solution was moved into 10mL of pre-warmed Immunocult medium. The cell solution was then counted and centrifuged at 220G for 5 minutes. The supernatant was removed, and the cells were resuspended in fresh Immunocult + 30U IL-2 medium and plated in a round bottom 96 well plate at 10^5 cells per 100µL in each well. After 24 hours, an additional 100µL of Immunocult + IL-2 medium was added and the cells were ready to be used. The cells were used within 72 hours of thawing to preserve activation.

3.4.4. 2D polyacrylamide gel synthesis

Polyacrylamide hydrogels (PAGs) were cast onto No. 0 glass bottom 35 mm culture dishes (MatTek P35G-0-20-C) using a previously described method and formulation[32], [103]. Briefly, the dishes are treated with 0.1 M NaOH, 97% (3-aminoproyl)trimethoxysilane and 0.5% glutaraldehyde to activate the glass surface. Then, 4 µL of a prepolymer mixture of 40% acrylamide solution, 2% bis-acrylamide solution, 1M HEPES solution, and deionized water was added to the dish and covered

with a 12 mm No. 1.5 circular cover slip. Once the gel has polymerized, the cover slip was removed. Cast gels were then coated using sulfo-SANPAH (Thermo Fischer Scientific, Waltham, MA) conjugated to a substrate as previously described [32], [103]. In this study, 165 µg/mL Type I Collagen (354236, Corning, Corning, NY), 165 µg/mL laminin (Corning 35423), 200 µg/mL fibronectin (Sigma-Aldrich F1141), 100 µg/mL a-CD44 mAb (clone IM7) (BD Biosciences 553131), 100 µg/mL ICAM1 (BioLegend 553006), and 100 µg/mL a-CD11a mAb (clone TS1/22) (Thermo Fisher Scientific MA11A10) were used to coat PAGs. In addition, 0.7, 9.3, 19.5, 100 kPa stiffnesses were used in this study.

3.4.5. Live Imaging of T cells

Two phase-contrast microscopes (Nikon TiE, Nikon Ti-2) were used for imaging. A Zyla 5.5 sCMOS camera (Andor Technology, Belfast, United Kingdom) and a 20x/0.95NA Ph1 lens with 3.07 pixels/µm was used. Cells were maintained at 37^{o}C and 5% CO_2 for the duration of imaging using an Oko lab Bold Line top stage humidified incubator (Okolab, Ottaviano, Italy). Ten positions on each gel were identified for imaging and a phase contrast image of the cells was acquired every 5 minutes for 8 hours.

3.4.6. Tracking of cells on 2D PAGs

A custom MATLAB® code was developed for cell segmentation. Specifically, .tiff movies were imported as frames. To ensure high accuracy, movies that were too crowded and contained more than 40 spots per frame on average were not considered for further analyses. A Gaussian filter with a 3×3 kernel was applied to each frame to

remove noise followed by a Sobel filter for edge detection. The identified objects were morphologically closed using a disc-shaped structural element of size 108-870 μm^2. The objects that either touched the frame's boundaries or were too small or big to be a cell were removed.

After segmentation, LapTracker from TrackMate v7 was used for tracking. The centroid of the cell in the next frame closest to the centroid of the current cell is linked together to create an edge. The search for the next cell is limited within a disc of radius 'max-linking distance' (50 μm for slow setting, 167 μm for fast setting) centered at the centroid of the current cell. Joining many such edges creates a track for a single cell which can then be used to calculate cell speed and random motility coefficient (RMC).

3.4.7. Determination of the Number of the Percent Adherent Cells

The experimental settings had modest natural convection in the nutrient medium that drove the unadhered cells at a speed of around ~12 μm/min, which was much faster than the adhered cells, which were clearly not moving. A threshold of 6 μm/min was therefore used to distinguish adhered cells from unadhered cells as adhered cells were never observed to be moving faster than this threshold.

3.4.8. Preparation of mouse brain slices

All animal treatments and experiments were in accordance with Institutional Animal Care and Use Committee at the University of Minnesota approved protocols. Adult B57BL/6 mice aged 8-12 weeks from the Jackson Labs were terminally anesthetized in a CO_2 chamber and then perfused transcardially with ~20mL isotonic

saline until the liver appeared tan colored. The brains were extracted and transferred into chilled oxygenated artificial cerebrospinal fluid (124 mM NaCl, 2.5 mM KCl, 2.0 mM $MgSO_4$, 1.25 mM KH_2PO_4, 26 mM $NaHCO_3$, 10 mM glucose). The cerebrum was sectioned into 300 μm coronal slices using a vibratome at 80 Hz vibration speed, 2.5 mm amplitude, and 0.5 mm/sec advance speed (Lafayette Instruments; 7000SMZ-2). The slices were transferred into DMEM/F12 media (Thermo Fisher Scientific 11-320-033) containing 8% FBS and 1x P/S and stored in an incubator at 37°C and 5% CO_2.

3.4.9. Organotypic brain-slice coculture with T cells

The media in the dish with the brain slice was removed and replaced with 2 mL of Immunocult + IL2 media. Three hundred thousand T cells per brain slice were transferred into a 10 mL conical and incubated with 5 μL/mL of Vybrant DiO Cell-Labeling Solution (Thermo Fisher Scientific, Cat #V22886) and incubated for 15 minutes in a 37°C, 5% CO_2 incubator to stain the cells. The cells were centrifuged and washed with PBS 3x then resuspended into immunocult + IL2 medium and added to dish with a brain slice and incubated overnight to allow cells to infiltrate into the slice. Cells typically invade up to 150 μm into the tissue. Isolectin GS-IB_4, Alexa Fluor 568 Conjugate (Invitrogen I21412) was added to the slice at least 30 minutes before imaging. This binds to and stains lectins, which are highly expressed on endothelial cells (vasculature) and microglia[146], [147]. The slice was transferred into a 6-well glass-bottom 35 mm culture dish (MatTek P35G-0-20-C) with fresh media. A tissue culture anchor (Warner Instruments SHD 42-15) was placed on top of the brain slice to prevent it from drifting during imaging.

3.4.10. Brain slice incubation with drugs and antibodies

For experiments that included drug targeting, the drug was added to the dish containing the brain slice and cell co-culture 3 hours before imaging to allow the drug to diffuse into the slice. When the slice was moved into fresh media for imaging, drug was added to keep the concentration consistent. For experiments with α-CD44 mAb and α-CD11a mAb, the slice and cells were incubated for 30 minutes with 20 μg/mL mAb before cell plating and the brain slice/cell co-culture was left to incubate in 20 μg/mL mAb.

3.4.11. Confocal imaging of brain slices

For experiments on brain slices, the slice was imaged on a Zeiss LSM 7 Live swept-field laser confocal microscope (Carl Zeiss, Oberkochen, Germany) with a 20x 0.45 NA objective lens (1.53 pixels/μm) capable of simultaneous imaging in both the green (GFP) and red (IB4) channels as previously described[49]. Maximal intensity projections from multiple z-stacks were used to generate 2D images for quantitative shape and motion analysis. The number of z-stacks was adjusted to ensure that the data acquisition of the whole slice was completed in under 5 min (9 planes with 10 μm separation were typically used). The z-stacks were then imaged every 5 min for up to 10 hours at 37^{o}C in a humidified 5% CO_2 environment.

3.4.12. Brain slice registration and cell tracking

To track single cell migration, relevant z planes were first selected to exclude cells migrating outside of the brain slice, particularly on the glass. Maximum intensity

projections from these z-stacks into 2D images were used to assess single cell migration speeds. Stage drift and tissue relaxation were registered using an affine transformation in MATLAB's imregister_tform function. Single cells were then tracked using ImageJ's TrackMate with radius of 5 μm and threshold of 10-15 μm. The random motility coefficient (RMC) was calculated by linear fitting to the mean-squared displacement (MSD) versus time (t).

3.4.13. Double Gaussian Fitting

A custom Python code was developed to fit multiple Gaussians to the cell displacements. In the algorithm, it was assumed that the mean of the Gaussian distributions is equal to zero and the covariance matrix is diagonal. To calculate the covariance matrix and the mixing coefficients, the Expectation Maximization algorithm is used[148]. First, the covariance matrix and the mixing coefficients are initialized. In the Expectation step the probability, γ_{nk} for each data point to belong to each Gaussian distribution based on equation 4:

$$\gamma_{nk} = \frac{\varphi_k N(\boldsymbol{x_n}|0, \boldsymbol{\Sigma_k})}{\sum_{n=1}^{K} \varphi_k N(\boldsymbol{x_n}|0, \boldsymbol{\Sigma_k})} \quad (4)$$

where *K* the number of clusters. In the Maximization step the covariance matrix and the mixing coefficients are updated based on equations 5 and 6 respectively. The process is continued until the absolute difference for the log likelihood is less than 10^{-3}.

$$\boldsymbol{\Sigma_k^{new}} = \frac{1}{N_k} \sum_{n=1}^{N} \gamma_{nk} N(\boldsymbol{x_n}|0, \boldsymbol{\Sigma_k})\, \boldsymbol{x_n x_n^T} \quad (5)$$

$$\varphi_k = \frac{N_k}{N} \quad (6)$$

where N_k is equal to $N_k = \sum_{n=1}^{N} \gamma_{nk}$. The Akaike Information Criterion (AIC) plots were generated by fitting a variable number of Gaussians to the data and tracking the corresponding error via AIC.

3.4.14. Hidden Markov Model

In order to model the step lengths as a two-state Hidden Markov Model (HMM) the moveHMM R package was used. Data was prepared as a .csv file with one column representing cell ID and columns for the x and y coordinates in μm for all experiments under the same conditions. The data was prepped using the prepData() function. As the HMM analysis is sensitive to initial parameter values, a random number generator was used to choose initial values between specified ranges. The initial estimate of the mean step length for state 1 ranged from 0.5 to 1.5 and the initial estimate of the mean step length for state 2 ranged from 2 to 8. The standard deviations ranged from 0.5 to 1.5 and 2 to 8 for states 1 and 2, respectively. The initial zero-mass parameters were calculated to be the proportion of step lengths equal to 0. For each set of initial parameters, the fitHMM() function was used to generate a fit and a corresponding maximum log likelihood value. The fit with the highest maximum log likelihood was used. The model outputs the corresponding parameters for the gamma fits for each state, the mean, standard deviation and transition probability matrix.

3.5. Results

3.5.1. Functional assessment of T cell adhesion molecules *in vitro*

In order to test functional surface expression of various adhesion molecules, T cells were plated on 2D polyacrylamide gels (PAGs) coated with various substrates including collagen, fibronectin, laminin, ICAM1, a-CD11a mAb (clone TS1/22), and α-CD44 mAb (clone IM7) at four stiffnesses: ~1 kPa, 10kPa, 20kPa, and 100 kPa. As shown in Figure 3.1A, T cells exhibited extremely poor adhesion to several substrates, particularly the integrin-engaging extracellular matrix proteins (ECMs) collagen, fibronectin, and laminin. This indicates that the cells have a very low surface expression of the ECM-cognate integrins. Adhesion to ICAM-1 and a-CD11a mAb, an antibody mimicking the ligand of ICAM1, were slightly better at 17% and 35%, respectively, indicating that LFA-1, the ligand of ICAM-1 and a-CD11a mAb, may be the dominant integrin expressed on the surface of these T cells, consistent with previous literature[149]. Remarkably, the adhesion to a-CD44 mAb was nearly 100%. This suggests that T cells have a high surface expression of CD44, a known T cell marker, and that they can use CD44 to adhere strongly to surfaces.

3.5.2. T cells exhibit poor migration on 2D substrates

Of the cells that adhered to the PAGs, it was noted that cells exhibit “tethered migration”, in which cells attach to the surface at a single point/small region and the body of the cell moves around this point, but the point of contact with the gel does not move significantly (Figure 3.1B). Despite the tethering point of the cell not moving, the

cells were extremely active, with blebs, filopodia, and lamellipodia consistently seen in high spatial-temporal resolution movies. This behavior is reflected in plots of the mean squared displacement (MSD) of cells (Figure 3.1C). There is a linear increase in MSD at very short time periods followed by a plateau, which indicates confined migration. As the MSD v. time plot is non-linear, a random walk model was not applicable and therefore instantaneous speed over the 5 min acquisition time intervals was used to quantify motility on the PAGs, which was similar across all substrates (Figure 3.1D). The migration speed was consistently very low, 0.083 μm/min (+/- 0.012 μm/min, s.e.m.). Additionally, when speed is measured on varying stiffness substrates, ranging from 0.7 kPa to 100 kPa, there is no major effect of stiffness on migration speed, cell area, or cell aspect ratio (Figure 3.1E-G). These results imply that CD8+ T cells are not able to migrate under a classic mesenchymal mode of migration in these conditions due to firm adhesion in a single subregion of the cell surface [31].

3.5.3. Migratory behavior of T cells in brain slices

To understand T cell migration in a 3D physiologically relevant environment, T cells (green) were co-cultured with 300 μm thick mouse organotypic brain slices. Isolectin B4 (magenta) was used to stain the vasculature and microglia [150]. T cells invaded up to 150 μm into the slice following a 4 hour incubation and confocal microscopy was used to visualize T cells migration, as shown in a maximum intensity z-projection of the T cells (green) with vasculature/microglia (magenta) in Figure 3.2A. There appears to be strong associations between the T cells and both vasculature and

microglia. As shown in Figure 2B, T cells (green) are seen migrating along vasculature (magenta). Example 2D projected tracks of individual T cells relative to a common origin, a so-called wind-rose plot, are shown in Figure 3.2C. The tracks do not trend toward a specific direction and appear random. Notably, there appears to be a significant fraction of cells that migrate very little and stay close to the origin and a smaller fraction that is more migratory. This finding is similarly reflected in the mean squared displacement plot in Figure 3.2D where a few cells have higher MSD than others.

3.5.4. Identification of two distinct migration speeds

In order to determine if T cell migration can be modeled as a population of fast- and slow- moving cells, Akaike information criterion (AIC) plots were generated for each position, shown in Supplementary Figure 3.1. Akaiki Information Criterion (AIC) plots for the Gaussian mixture model demonstrate that the data is best described as a two-state modelSupplementary Figure 3.1. The AIC plots estimate the error associated with the number of Gaussian distributions being fitted to the displacement data. In all plots, a large decrease is seen between 1 and 2 states, indicating that a 2 state model is a better fit than a 1 state model. In some datasets, further decreases are seen at higher number of states (>4 states), which are likely due to fitting noise. Some datasets, even those that are repeats of the same experiment, have decreases at intermediate number of states, while others do not. While this could imply that some datasets could be better fit with a 3 or 4 state model, a 2 state model is a good fit for all data sets, so we used

this model for further analysis. The displacements were then fit to a double Gaussian, which can then be used to calculate the diffusion coefficient (random motility coefficient) and the relative proportion of cells in each Gaussian. Two states were observed, a slow migrating state (mean RMC 0.01-0.05 μm^2/min) including 65-95% of the displacements, and a fast migrating state (mean RMC 1.5-8 μm^2/min) making up 5-35% of the displacements, as shown in Supplementary Figure 3.2. Since the slow migrating cells are imaged at least 10 μm into the brain slice, and in some cases up to 150 μm in, they must have been migratory in their past history before switching to a non-migratory state. Each point on the plot represents a single movie containing ~50-300 cells imaged over 1 mm^2. Given these findings, a Hidden Markov Model (HMM) was used to characterize the two states, fast and slow, as two gamma distributions of step lengths, or, equivalently, instantaneous speeds. In Figure 3.2E, a cell can be seen starting in the fast migrating state at the origin before transitioning to a slow migrating state after 65 min. The cell then spends the remaining 520 minutes in the slow state. For the entire cell population, Figure 3.2F shows the histogram of step lengths overlayed with the fits for both states. Notably, there are two states, a slow state with a mean of 0.79 μm and standard deviation 0.20 μm, and a fast state with a mean of 4.31 μm and standard deviation 3.79 μm.

3.5.5. Motor-clutch targeting drugs affects cell migration speed

Since T cell migration in brain tissue could potentially be mediated via a motor-clutch mechanism, we next sought to determine how perturbation of myosin motors and

various cell adhesion molecules impacted migration speed. Figure 3.3A summarizes the number of cells that were tracked for each perturbation. First, blebbistatin, a drug targeting myosin II, was incubated for 1 hour with the brain slices at 10 and 50 μM. The cells were tracked and the random motility coefficient (RMC) was estimated. Though no statistically significant effect was seen at 10 μM, a significant decrease ($p<0.0001$) in migration speed can be seen at the higher dose of blebbistatin (Figure 3.3B). While there was no statistically significant difference in cell area in response to the blebbistatin (Figure 3.3C), a slight trend of increasing area was noted. This increase was expected, as decreasing the contractility of the cells via decreasing motors will cause them to spread and result in a larger area[32]. Cyclo-RGD, which targets RGD-binding integrins, was used to target a potential molecular clutch. At the lower dose of 1 μM, a small decrease in RMC was seen with a larger decrease in RMC observed at the higher dose of 5 μM (Figure 3.3D). Further, a decrease in cell area was seen with increasing dose of cRGD (Figure 3.3E). This is consistent with the blebbistatin data, as decreasing adhesions should inhibit cell spreading. These results are consistent with the motor-clutch model for cell migration, and suggest that T cells use canonical adhesion-based migration in brain tissue, rather than an adhesion-independent mechanism as has been suggested in the literature[70].

3.5.6. Antibody targeting of either CD44 or ICAM1 increases migration speed

In order to investigate the effect of other potential clutches, CD44 and LFA-1, antibodies, α-CD44 mAb and α-CD11a mAb, were separately used to target their respective adhesion molecules, CD44 and LFA-1 Contrary to our hypothesis that

targeting adhesion molecules should decrease migration, we saw an increase in RMC in response to both α-CD44a mAb (Figure 3.3F) and α-CD11a mAb (Figure 3.3H). There was also an increase in cell area in both cases (Figure 3.3G,I).

3.5.7. Impact of motor-clutch targeting drugs on distinct subpopulations

We wanted to further test how each drug and antibody impacted the fast and slow states predicted by the HMM. The HMM described above was used to determine the gamma distribution of step lengths, described as a mean and standard deviation of the step lengths of each subpopulation (state 1 and state 2) in response to the drugs and antibodies. Figure 3.4A-J describes the gamma parameters of each state, overlayed with a histogram of the step lengths while figure 4K lists the parameters of the distributions. Notably, increasing doses of blebbistatin (Figure 3.4A-C) result in more steps in state 1, the slow migrating group, and fewer steps in state 2, the fast migrating group, described by a higher peak in state 1 and lower peak in state 2. The mean step size of state 2 also decreases from 3.6 to 2.3 μm (Figure 3.4K). This implies that blebbistatin both decreases the speed of the migrating cells and shifts cells towards the slow migrating group. Cyclo-RGD had a similar effect with more steps in the slow group and fewer in the fast group and a decrease in mean step size of the fast group from 4.3 to 3.4 μm, shown in Figure 3.4D-F. By contrast, cells treated with α-CD44 mAb exhibit a decrease in the number of cells in state 1 and an increase in cells in state 2 with no major change in the step size of either group (Figure 3.4G-H). This suggests that the increase in RMC in response to α-CD44 mAb is due to more cells being activated to the

fast migrating state. Treatment with α-CD11a mAb had minimal effects on the cells in state 1, but it did increase the mean step length of the fast group (Figure 3.4I-J). The HMM also calculates a transition probability matrix, describing the probability that a cell in a given state will switch to another state. This can be used to calculate the average time in each state, as summarized in Figure 3.4L. Blebbistatin treatment reduces the time spent in either state, likely because the blebbistatin also decreases the standard deviation of state 1. At 5 μM cRGD, cells will remain in the slow state significantly longer than in the fast state. α-CD44 mAb and α-CD11a mAb treatments have minimal effect on the time in each state. In summary, we find that drugs that perturb motor-clutch components alter not only the overall cell motility, but also the transitions between the fast and slow states, and in some case also alter the speed of the fast state.

3.6. Discussion

In this study, T cell migration was imaged in 2D PAGs and mouse brain slices and a variety of drugs and antibodies were used to elucidate the mechanism of migration. Migration was decreased in response to targeting of myosin motors with blebbistatin and targeting of RGD-binding integrins with cRGD, consistent with a motor clutch mode of migration. By contrast, migration increased in response to targeting adhesion molecules CD44 and ICAM-1 with a-CD44a mAb and a-CD11a mAb, the same antibodies that T cells experienced high adherence to on PAGs.

The studies of T cells on PAGs demonstrated an intriguing discrepancy in which cells were only able to adhere to α-CD44a mAb and to a lesser extent to α-CD11a mAb, which turned out to be the two molecules that resulted in an increase in migration in

brain slices. We hypothesize that this is because these cells have a high surface expression of CD44 and LFA-1 and can best utilize these molecules to adhere to a 2D surface. Ultimately, the behavior observed in these cells was a single anchor point tethering the cell to the surface and therefore these studies did not result in migratory cells, apparently contradicting results seen in the literature. Other studies have found CD8+ T cells to be migratory on ECM-coated glass [151], [152] and nanotextured PAGs [38]. Another study imaged Jurkat T cells on PAGs coated in CD3 and CD28 mAbs but migration was not studied[153]. Based on this, it is possible that CD8+ T cells do not migrate in a 2D hydrogel environment coated with ECM proteins. The movement of the cell body in the z direction appears as if the cell is actively searching for additional anchor points in the third dimension.

To understand migration of these cells in 3D, we used confocal microscopy to generate long time scale movies of CD8+ T cells migrating in normal brain tissue, which to our knowledge has not been previously reported in the literature. Normal mouse organotypic brain slices were co-cultured with the T cells and incubated with various drugs and antibodies. This setup describes a method to study cell migration in response to various stimuli in a physiologically relevant environment, as the use of a 6 well plate, with each well containing a 300 μm thick brain slice, allows the testing of 6 conditions at once. There are several limitations to this method. In order to compress the very large image files for analysis, we used a maximum intensity projection of 9-10 z-stacks, as this allowed us to compress each image file to reduce computation time. Migration in the third dimension was therefore lost, however the calculation of random motility

coefficient accounts for the dimensionality of the tracking data. In addition, cells that migrated further than the maximum linking distance of 40 μm in one 5 minute time frame could be lost by the tracking software, though these events were observed to be rare. On the other hand, the nature of co-culturing cells and brain slices and imaging the cells that infiltrate the slice means that the assay is selecting for cells that can migrate in a brain slice, therefore biasing the data towards migratory cells.

Despite its limitations, the brain slice assay provides critical information on identifying the mode of T cell migration. The decrease in migration observed with both blebbistatin and cRGD treatment is consistent with a motor-clutch mode of migration. Had the cells been migrating via an amoeboid mode of migration, specifically through an osmotic engine model[34], it is feasible that blebbistatin targeting of myosin motors could indirectly impact migration speed by impacting cell shape and length scale. However, adhesions, if present, would act as frictional resistance to migration and targeting adhesions would either have no effect on migration speed or would increase migration speed. The decrease in migration in response to cRGD targeting of integrins is inconsistent with the osmotic engine hypothesis. On the other hand, both cRGD and blebbistatin disrupt the motor-to-clutch ratio in opposite directions and lead to a decrease in migration speed, suggesting that the cells are migrating via a motor clutch mechanism and are relatively close to the optimal motor-to-clutch ratio. This near-optimality is similar to results seen for cancer cells[32].

On the other hand, treatment with α-CD44a mAb and α-CD11a mAb increased migration speed. While this appears to be inconsistent with findings from Klement et al.

and Mrass et al., there may be an optimality to CD44 expression causing opposing results, as these studies used complete knockouts. One explanation of this finding consistent with a motor-clutch hypothesis is that the T cells are somewhat hyperadhesive, meaning their adhesions are too strong to allow them to migrate efficiently. Therefore, decreasing the number of adhesions shifts the cells to a more optimal motor-to-clutch ratio and improves migration. In this case, while we would have expected to see a similar increase or no effect from cRGD, it is possible that the effect of even the lower dose of cRGD (1 μM) was strong enough to push the cells past the optimum and decrease migration whereas the antibodies had a smaller effect to just shift the cells to the optimum, as described in Figure 3.5A. An alternate explanation is that while blebbistatin and cRGD targeted the motor-clutch components, α-CD44a mAb and α-CD11a mAb impacted the activation/signaling of the T cells. This is consistent with the increased area of the T cells and explains the opposing response to cRGD and α-CD44a mAb/α-CD11a mAb. The mechanism of activation could be explained through a motor-clutch model, which would predict that the only ways to increase migration are through optimizing the motor-to-clutch ratio and increasing the F-actin polymerization rate. As crosstalk between integrins and CD44 has been found in cancer cells [Kelly et al., in preparation], CD44 could be negatively regulating RGD-binding integrins, so blocking CD44 in turn upregulates integrins and shift the T cells closer to the optimum, as summarized in Figure 3.5B. This is consistent with the cRGD results suggesting the T cells are at or below the optimal number of integrins. Similarly, blocking LFA-1 could

be upregulating other integrins and optimizing the motor-to-clutch ratio. Alternatively, blocking CD44 and LFA-1 could be increasing F-actin polymerization rate.

Though elucidating the exact mechanism for increasing T cell migration via α-CD44a mAb/α-CD11a mAb treatment requires further investigation, this finding is significant because it demonstrates that targeting known adhesion molecules could potentially increase migration. In diseases such as MS, this could potentially exacerbate the disease, so it is critical to further our understanding of the role of adhesion molecules in T cell migration before developing treatments. For GBM, this finding is a critical example of a deviation between cancer cell and T cell behavior. Previous work by Anderson et al. found that in a similar brain slice assay with U251 glioma cells, decreasing CD44 and RGD-binding integrins both significantly decreased migration speed. While these results suggest that targeting molecular clutches could be used to hinder progression of glioblastoma, it was not known how this could affect T cell migration. Because T cell infiltration into the tumor has critical implications for survival, slowing down T cell migration with cancer cell migration could potentially make outcomes worse. Here we identify CD44 as a potential clutch that could be targeted to slow down migration of cancer cells while simultaneously improving T cell migration.

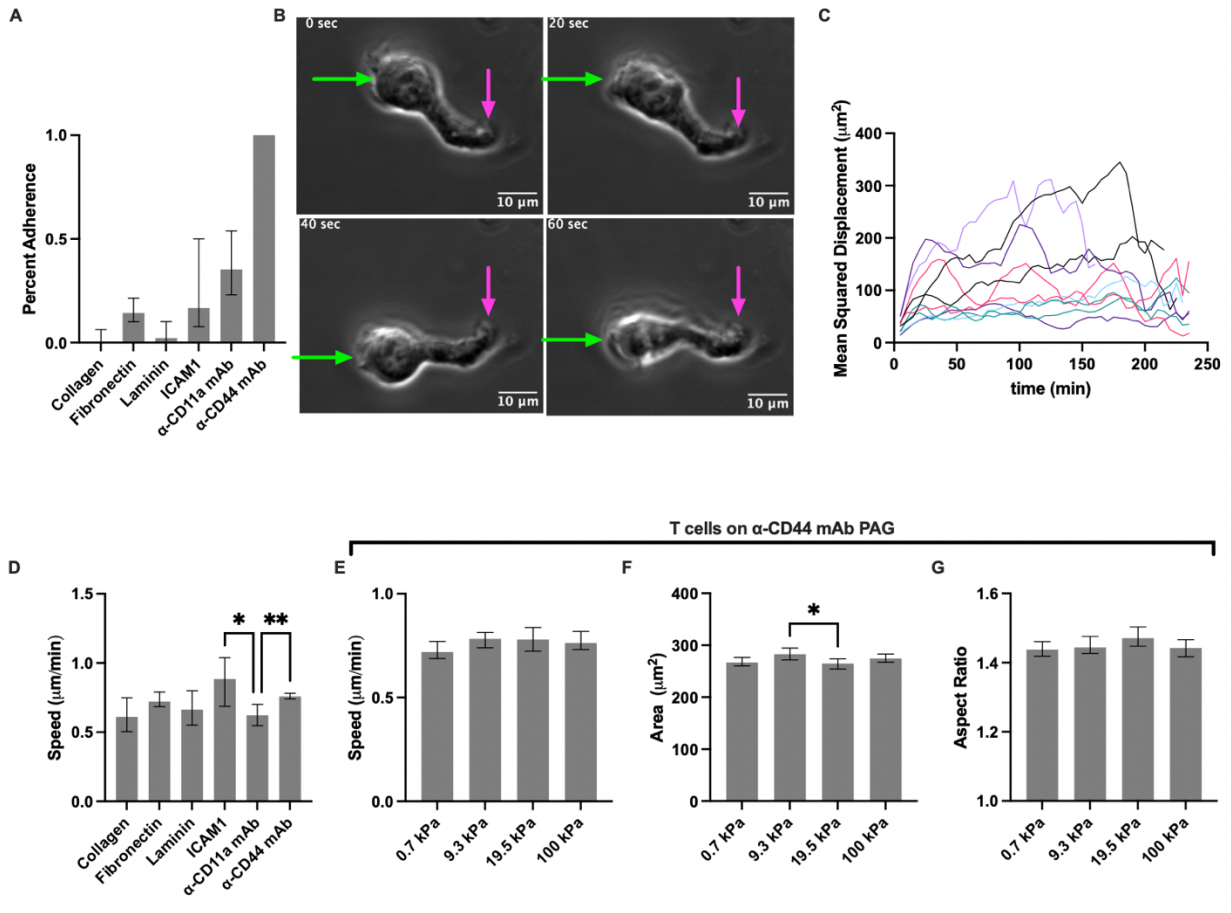

Figure 3.1. T cells primarily adhere to α–CD44 mAb-coated PAGs and exhibit tethered movement when adhered.

A) Percent of cells that adhered to each ECM with data from 4 stiffnesses (Young's modulus) of 0.7, 9.3, 19.5, and 100kPa lumped together. B) Images of a T cell on α-CD44a mAb-coated PAG demonstrating tethered movement. Magenta arrows indicates the point of tethering that does not move while the cell body, indicated by a green arrow, moves around this point. C) Mean squared displacement plotted against time for 10 example cells. D) Instantaneous speed of T cells during tethered migration, measured by tracking the cell centroid. E) T cell speed, F) area, and G) aspect ratio of adhered cells on α-CD44a mAb-coated gels as a function of substrate stiffness.

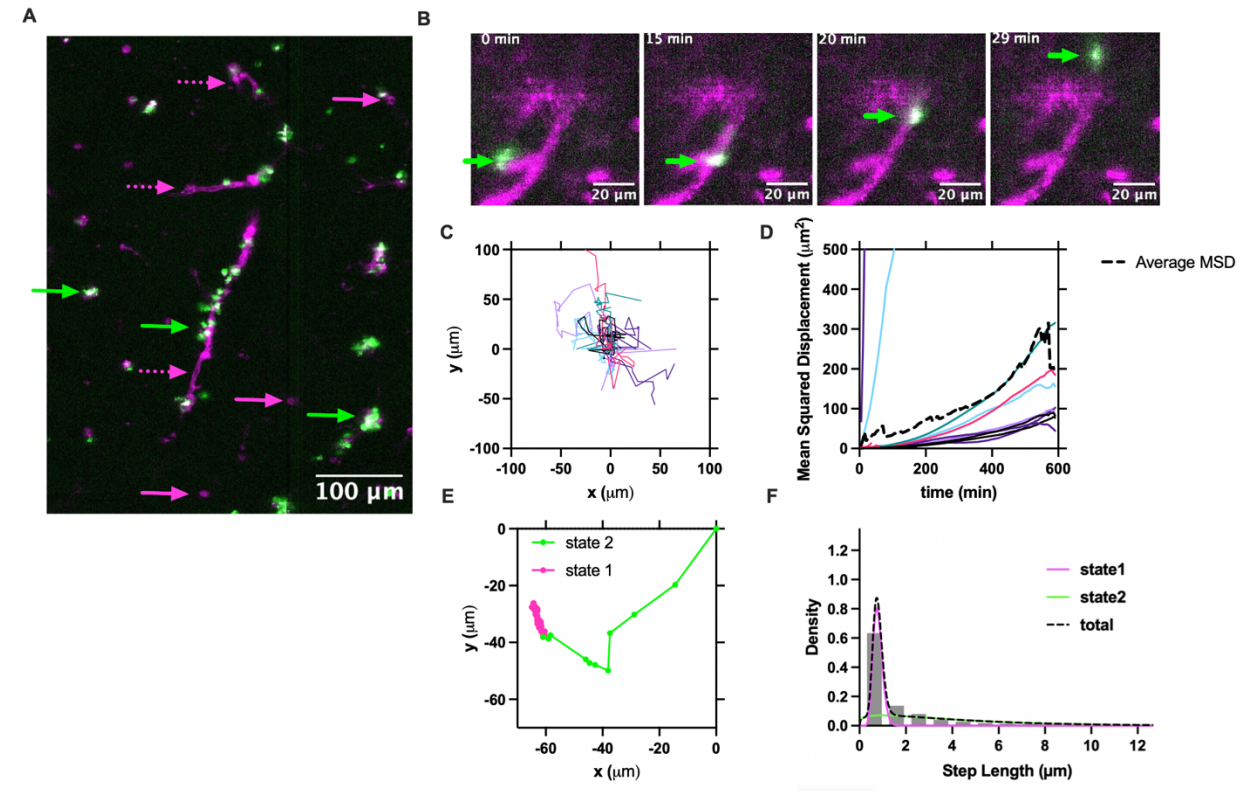

Figure 3.2. T cell migration in brain slices

A) T cells (green) often associate with vasculature and microglia (both magenta) in brain tissue. Examples of T cells are noted in green arrows, microglia in solid magenta arrows, and vasculature in dashed magenta arrows. B) An example T cell (green) migrating along vasculature (magenta). Green arrows indicate the location of the T cell. C) Wind-rose plot showing 2D projected trajectories of a subset of T cells for clarity. D) Mean squared displacement vs. time for the same cells with the mean MSD for all cells in the position in a dashed black line. Displacements for control T cells were fitted to a HMM, and E) shows a the wind-rose plot of a single cell starting at the origin with magenta corresponding to when it is in state 1 (slow) and green corresponding to when it is in state 2 (fast). F) A histogram of step lengths with the HMM-determined Gaussian distributions of step lengths overlayed in magenta (state 1) and green (state 2). A dashed black line indicates the total distribution.

A

Number of Cells Analyzed

Control Bleb	562
10μM Bleb	300
50μM Bleb	229
Control cRGD	983
1μM cRGD	754
5μM cRGD	1049
Control α-CD44 mAb	1626
α-CD44 mAb	3156
Control α-CD11a mAb	1120
α-CD11a mAb	1485

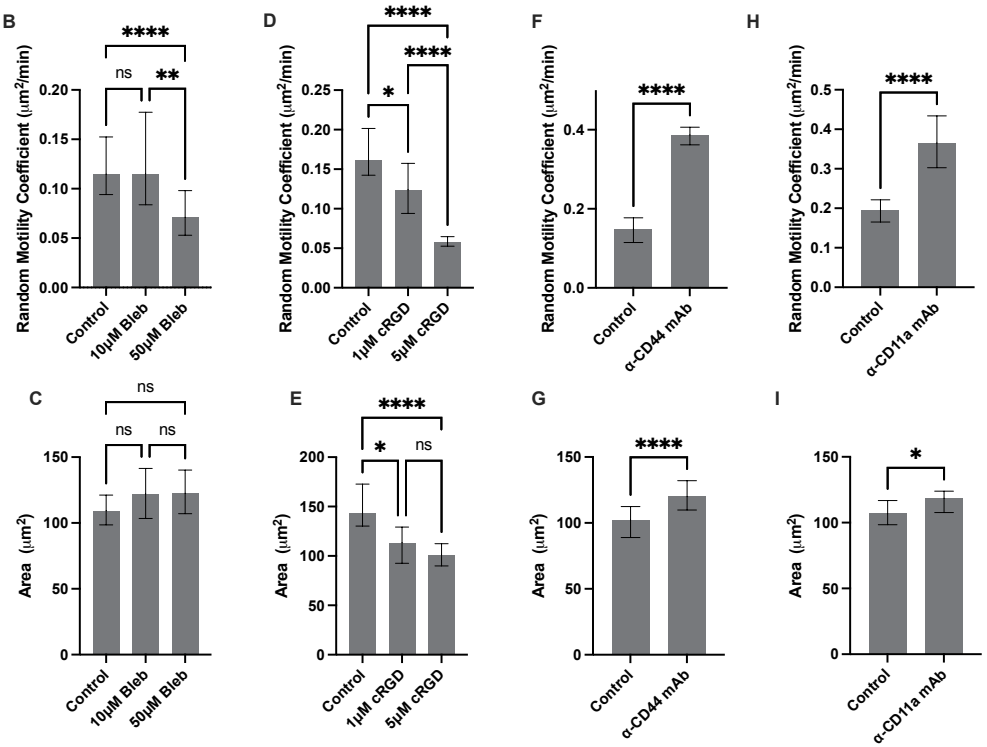

Figure 3.3. Perturbations of motor-clutch components impact T cell migration and area.

A) Table summarizing the number of cells tracked for each condition. Random motility coefficient and area in response to B,C) 0, 10, and 50 μM Blebbistatin, D,E) 0, 1, and 5 μM cyclo-RGD, F,G) 20 μg/mL (130 nM) α-CD44 mAb, H,I) 20 μg/mL (130 nM) α-CD11a mAb.

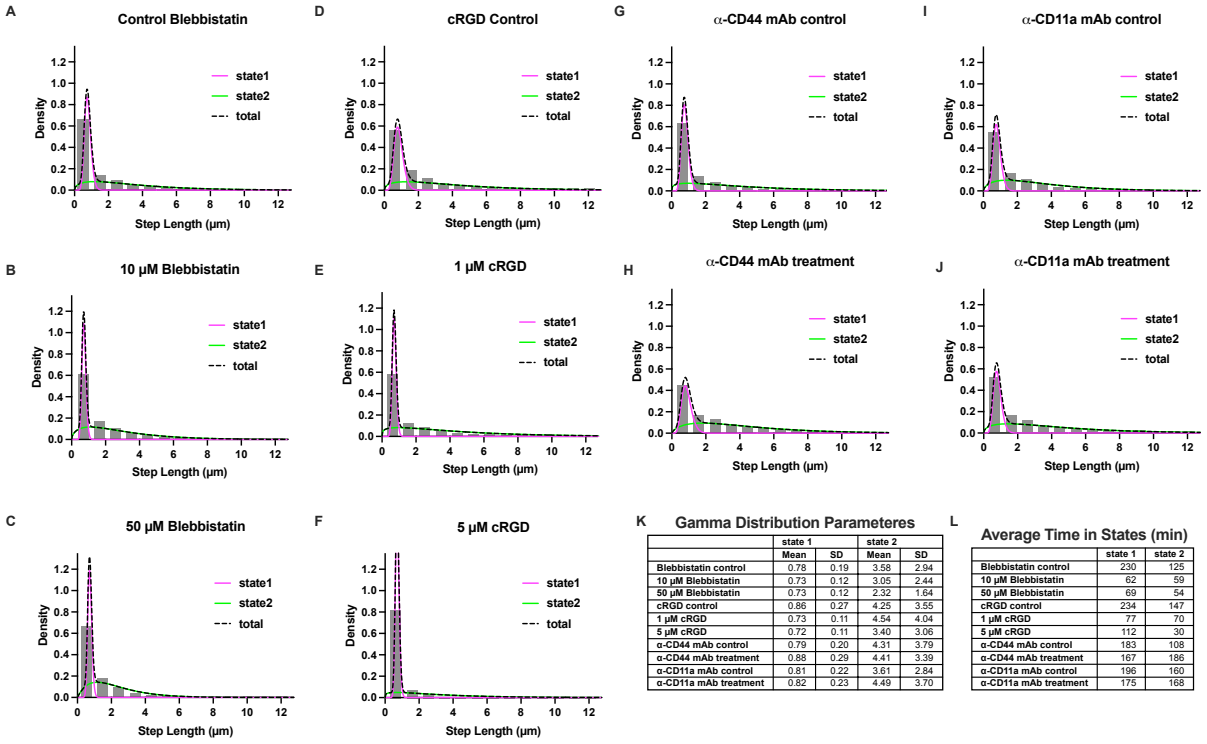

K Gamma Distribution Parameteres

	state 1		state 2	
	Mean	SD	Mean	SD
Blebbistatin control	0.78	0.19	3.58	2.94
10 μM Blebbistatin	0.73	0.12	3.05	2.44
50 μM Blebbistatin	0.73	0.12	2.32	1.64
cRGD control	0.86	0.27	4.25	3.55
1 μM cRGD	0.73	0.11	4.54	4.04
5 μM cRGD	0.72	0.11	3.40	3.06
α-CD44 mAb control	0.79	0.20	4.31	3.79
α-CD44 mAb treatment	0.88	0.29	4.41	3.39
α-CD11a mAb control	0.81	0.22	3.61	2.84
α-CD11a mAb treatment	0.82	0.23	4.49	3.70

L Average Time in States (min)

	state 1	state 2
Blebbistatin control	230	125
10 μM Blebbistatin	62	59
50 μM Blebbistatin	69	54
cRGD control	234	147
1 μM cRGD	77	70
5 μM cRGD	112	30
α-CD44 mAb control	183	108
α-CD44 mAb treatment	167	186
α-CD11a mAb control	196	160
α-CD11a mAb treatment	175	168

Figure 3.4. Hidden Markov Model (HMM) describes T cell migration as a two-state model with fast and slow states described by gamma distributions of displacements and random switching between states

Histograms of step lengths and corresponding HMM-generated gamma distribution fits for state 1 (magenta, slow), state 2 (green, slow), and total (black, dashed) for A-C) 0, 10, and 50 μM Blebbistatin, D-F) 0, 1, and 5 μM cyclo-RGD, G-H) 20 μg/mL (130 nM) α-CD44 mAb, I-J) 20 μg/mL (130 nM) α-CD11a mAb. K) Mean and standard deviation of the gamma distributions for each fit. L) Average time in each state for each condition, calculated using the transition probability matrix.

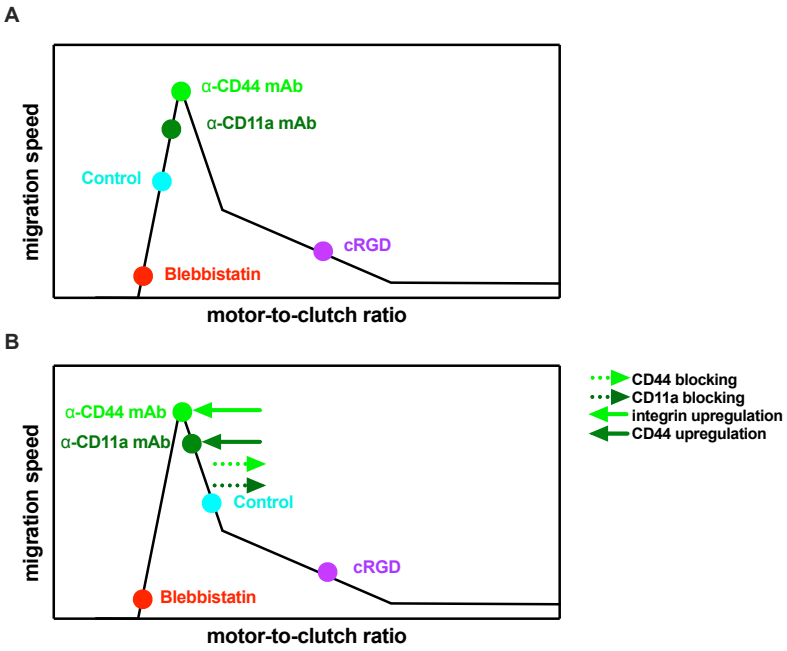

Figure 3.5. Schematics depicting potential mechanisms for increase in migration in response to targeting CD44 and LFA-1

A) T cells are initially hyperadhesive, so targeting with α-CD44 mAb or α-CD11a mAb decreases clutches and optimizes migration. Targeting RGD-binding integrins with cyclo-RGD decreases migration beyond the optimal to lower migration. B) T cells are initially hypoadhesive. Though blocking clutches with α-CD44 mAb or α-CD11a mAb decreases adhesion, integrins or CD44, respectively, are upregulated in response, optimizing the motor-to-clutch ratio.

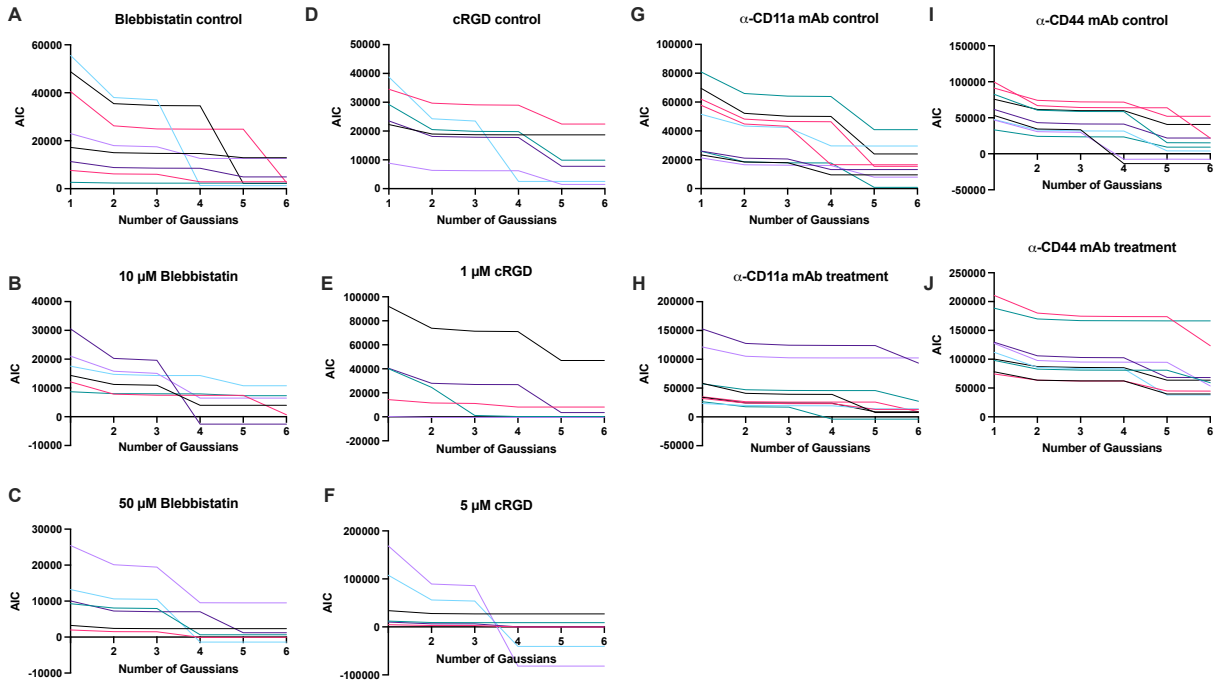

Supplementary Figure 3.1. Akaiki Information Criterion (AIC) plots for the Gaussian mixture model demonstrate that the data is best described as a two-state model

AIC Plots for A-C) 0, 10, and 50 μM Blebbistatin, D-F) 0, 1, and 5 μM cyclo-RGD, G-H) 20 μg/mL (130 nM) α-CD44 mAb, I-J) 20 μg/mL (130 nM) α-CD11a mAb. Each line is for a single field containing 50-300 cells.

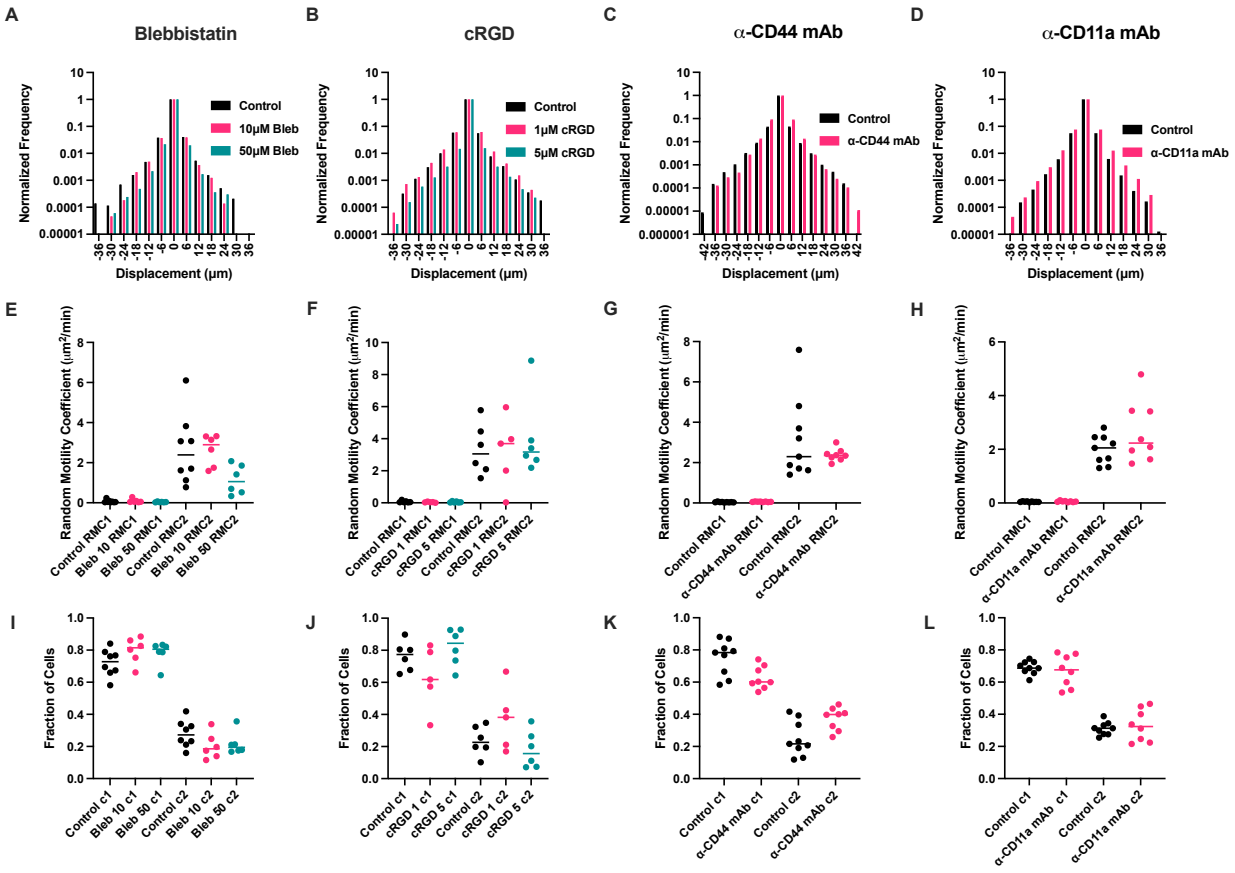

Supplementary Figure 3.2. T cell displacements are best fit by fast- and slow-migrating subgroups via a Gaussian mixture model analysis

A normalized histogram of x and y displacements combined for A) blebbistatin, B) cyclo-RGD, C) α-CD44 mAb, and D) α-CD11a mAb incubation. Estimated RMC values for each subgroup for E) blebbistatin, F) cyclo-RGD, G) α-CD44 mAb, and H) α-CD11a mAb incubation. The fraction of cells in each subgroup for I) blebbistatin, J) cyclo-RGD, K) α-CD44 mAb, and L) α-CD11a mAb incubation.

4. Chapter 4: Conclusions and Future Directions

The goal of this dissertation was to identify the mechanisms by which glioblastoma cells and T cells migrate in brain tissue to further our understanding of how targeting cell migration could impact disease progression. Although cell migration is an area of interest for potential treatments, developing an effective treatment is in need of better mechanistic understanding in order to have a rational approach.

In Chapter 2, healthy mouse brain slices were used to investigate the mechanism that glioblastoma cells use to migrate in brain tissue. Cell-vascular interactions for high-passage and low-passage patient derived xenograft lines were imaged and were found to be consistent with a motor-clutch mode of migration and inconsistent with the osmotic engine model. Furthermore, blebbistatin was used to target myosin II motors and the variable response at low doses and decrease in migration speed at high doses were consistent with the unique prediction of optimality of motors in a motor-clutch mode of migration. Two primary clutches were investigated, integrins and CD44, and both molecules were found to contribute to cell migration, with the slowest migration occurring when both integrins and CD44 were targeted simultaneously. These findings are significant because it furthers our understanding of how glioblastoma cells migrate in brain tissue and identifies potential targets for slowing cell migration.

Although the results in Chapter 2 suggest that the optimal way to target cell migration in glioblastoma is by simultaneous targeting of integrins and CD44, it is critical to understand how this would impact migration of anti-glioblastoma T cells. In Chapter 3, we identify that T cell migration in healthy brain tissue can be described by a double

Gaussian distribution and a two-state Hidden Markov Model that represents the displacements of a mixture of fast migrating and slow migrating cells. In addition, cell migration is decreased in response to motor-targeting blebbistatin and integrin-targeting cyclo-RGD, as predicted by a motor clutch mode of migration. Interestingly, cell migration is increased by α-CD44 mAbs and α-CD11a mAbs. We conclude that this increase is likely due to improved activation of the T cells, potentially via an upregulation of alternative clutch molecules. Of significance, the increase in migration in response to α-CD44 mAb is a critical divergence in phenotype between T cells and cancer cells. This finding identifies CD44 as a potential target for glioblastoma treatments that could slow down migration of cancer cells while improving the ability of cytotoxic T cells to kill cancer cells.

Additional studies can be done to further our understanding of cell migration *in vivo*. While these findings identified integrins and CD44 as the primary clutches in cancer cells, using CRISPR/Cas9 to develop a cell line with talin1, talin2, and CD44 all knocked out could tell us if cells are still able to migrate without either integrins or CD44. Though these results suggest that the cells will migrate significantly slower than a control cell, if the cells can still migrate at all, it would be important to determine if other molecules can act as a clutch and drive the cells to migrate. Additionally, though ezrin, radixin, and moesin, the ERM proteins, are thought to be the adaptor molecules for CD44, developing a knockout of the ERM proteins could better elucidate their role in cell migration and improve our understanding of CD44-mediated migration. Many additional molecules that were not studied are thought to contribute to cell migration and may

make up part of the clutch framework, including vinculin, alpha-actinin, and ankyrin. Knockout cells of each of these proteins could elucidate their specific contribution to cell migration.

There are several elements of T cell migration that are still not understood. In these studies, we were unable to observe deformations in vasculature in response to T cell migration, but higher resolution images of migrating T cells could inform on traction dynamics of T cells in tissue and determine if they are consistent with a motor clutch mode of migration. In addition, these studies utilized drugs and antibodies to disrupt motor-clutch components, but complete knockouts of each molecule would give more complete information about their role in cell migration. This is especially true in the case of CD44 and ICAM-1, in which the antibodies resulted in increased migration speed. Future studies could investigate the mechanism of this increase, which could be due to an upregulation of a different clutch or an increase in the actin polymerization rate.

In order to determine how translatable these findings are to a clinical environment, similar studies could be done in ways that better mimic human disease. For example, brain slices could be taken from a mouse with red-fluorescent T cells with an induced brain tumor expressing GFP. Migratory behavior of the cancer cells and T cells would better reflect how they behave and interact with each other in a disease state. Drug and antibody targeting of clutches could be used to determine how blocking CD44 impacts migration of both cancer and T cells simultaneously and the ability of T cells to kill cancer cells. Alternatively, cranial window imaging of an induced tumor could be used to

image migrating cancer cells in a mouse brain and dissect how it varies from *ex vivo* brain slices.

Overall, this dissertation advanced our understanding of the mechanics of cell migration and how it is relevant to glioblastoma progression using both high- and low-passage cell lines in brain tissue. We identified CD44 as an adhesion molecule that blocking could slow down migration of cancer cells while speeding up migration of T cells. These findings open doors to effectively targeting cancer cell migration as a means to slow down glioblastoma progression while also having implications for a variety of types of solid tumors.

5. Appendix: Motor-Clutch Modeling of Single-Integrin Force Dynamics

One of the first projects I worked on in graduate school was a collaborative project with Alexander Dunn's lab at Stanford University. Their lab developed FRET-based tension sensors that sit outside a cell between an integrin and the substrate, in this case a glass surface with functionalized PEG brush. These sensors measure the force on a single integrin, a measurement directly predicted by the motor clutch model that, until this point, the technology had not existed to test. Interestingly, the majority of the observed forces on the integrins were primarily low force (<7 pN) and static. They also observed high, static forces (>7 pN) and dynamic events, as shown in Figure A. 1. The dynamic events observed could be a step event, meaning an instantaneous change, or a ramp event, meaning a more gradual change. The motor clutch model in its base form did not produce forces on the clutches that were static, as the clutches experience continuous load and fail dynamics. Additionally, the dynamic events could only be ramp increases and step decreases, but the sensors observed the opposite events as well.

We sought to challenge the assumptions made in the motor clutch model to see if we could determine an explanation for the static forces as well as ramp decreases in force and step increases in force. We developed several variations of the motor clutch model, summarized in Figure A. 2C. The first model was a "multiple connections model," which aimed to represent the adaptor molecule talin and reinforcing vinculin as an additional set of springs in series with the clutch spring. Unbinding occurred at the adaptor clutch springs. While this did achieve some level of static forces, the clutch

force was far more variable than what was observed experimentally. Next, we modeled the clutches as a viscoelastic element, which allowed for slower relaxation of the clutch spring and rapid rebinding. While the forces were more static than the base model, they still experienced gradual increases. The final model we explored included reversible actin crosslinkers, which meant breakage could occur within the actin network and create discrete clusters of motors. As these clusters form and change, clusters can experience temporary mechanical equilibrium. These dynamics lead to static forces, as well as step and ramp increases and decreases in force. Interestingly, this model also reduced force dissipation, as complete clutch failure occurred less often. It also was able to recreate the same force distribution observed by the sensors experimentally. These results are published under Tan et al., Science Advances, 2020[88].

This project is what allowed me to develop such a deep understanding of the motor clutch model that I used throughout the duration of my dissertation. It also shaped what the dissertation would eventually be about, as learning about the dynamics of clutches motivated me to study the clutch in *in vivo*-like environments.

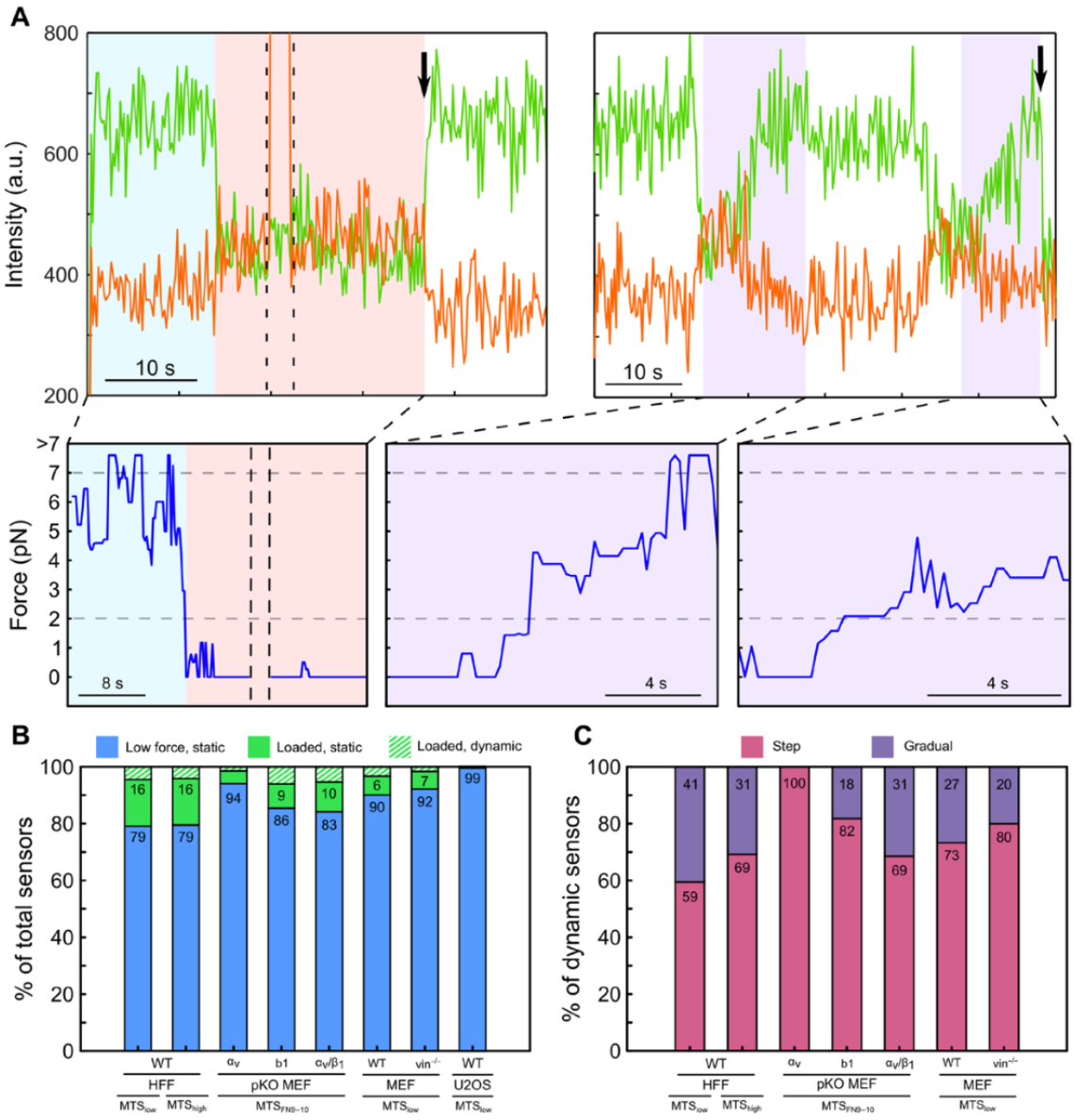

Figure A. 1. Dynamic transitions in load constitute a minority of sensor measurements[88]

(**A**) Representative traces showing step (left) and gradual ramp (right) load transitions (FRET donor: green; FRET acceptor: orange; load: blue) for HFFs adhering MTS_{low}. Black arrows mark acceptor or donor bleaching; dashed black lines indicate direct excitation of the FRET acceptor. Horizontal gray dashed lines indicate upper and lower force measurement limits for MTS_{low}. (**B**) Percentage low force (defined as <2 for MTS_{low} or < 7 pN for MTS_{high}) (blue), higher force but static (green), and dynamic (hashed; subset of loaded integrins) sensors for a variety of cell types adhering to different MTSs.

(**C**) Percent of dynamic sensors with step (magenta) and ramp (purple) transitions. U2OS cells had no observable dynamic events.

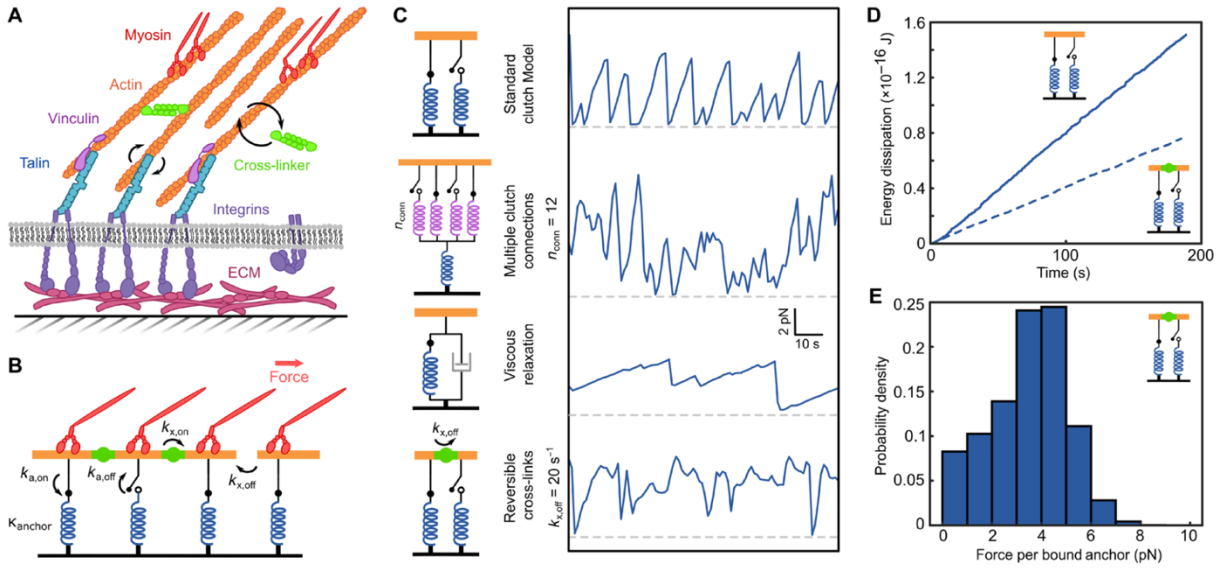

Figure A. 2. A modified model of cytoskeletal force transduction yields mechanical equilibrium at individual integrins[88].

(**A**) Simplified cartoon of a FA: Nonmuscle myosin II pulls on reversibly cross-linked actin filaments, which are linked to integrins by vinculin and talin. (**B**) Cytoskeletal dynamics model: F-actin filaments bind to anchors (blue) and are linked by cross-linking proteins (green). (**C**) An example force trace of the standard clutch model and possible clutch model extensions that account for multivalent clutch connections, viscous relaxation, or reversible cross-links. Reversible cross-links allow for stable force plateaus as well as sporadic ramp and step events. The dashed gray lines indicate zero force. (**D**) Calculated energy dissipation from simulations with irreversible (top) and reversible (bottom) cross-links. (**E**) Force distribution for simulated anchors with reversible cross-linking ($k_{x,off}$ = 20 s^{-1}).

Bibliography

[1] D. Hanahan and R. A. Weinberg, “Hallmarks of Cancer: The Next Generation,” *Cell*, vol. 144, no. 5, pp. 646–674, Mar. 2011, doi: 10.1016/j.cell.2011.02.013.

[2] J. Shortt and R. W. Johnstone, “Oncogenes in Cell Survival and Cell Death,” *Cold Spring Harb. Perspect. Biol.*, vol. 4, no. 12, p. a009829, Dec. 2012, doi: 10.1101/cshperspect.a009829.

[3] R. A. Weinberg, *The Biology of Cancer*, 2nd ed. Garland Science, Taylor & Francis Group, LLC, 2014.

[4] L. R. Yates and P. J. Campbell, “Evolution of the cancer genome,” *Nat. Rev. Genet.*, vol. 13, no. 11, Art. no. 11, Nov. 2012, doi: 10.1038/nrg3317.

[5] J. Roche, “The Epithelial-to-Mesenchymal Transition in Cancer,” *Cancers*, vol. 10, no. 2, p. 52, Feb. 2018, doi: 10.3390/cancers10020052.

[6] A. Ray and P. P. Provenzano, “Aligned forces: Origins and mechanisms of cancer dissemination guided by extracellular matrix architecture,” *Curr. Opin. Cell Biol.*, vol. 72, pp. 63–71, Oct. 2021, doi: 10.1016/j.ceb.2021.05.004.

[7] A. W. Lambert, D. R. Pattabiraman, and R. A. Weinberg, “Emerging Biological Principles of Metastasis,” *Cell*, vol. 168, no. 4, pp. 670–691, Feb. 2017, doi: 10.1016/j.cell.2016.11.037.

[8] F. Hanif, K. Muzaffar, K. Perveen, S. M. Malhi, and S. U. Simjee, “Glioblastoma Multiforme: A Review of its Epidemiology and Pathogenesis through Clinical Presentation and Treatment,” *Asian Pac. J. Cancer Prev. APJCP*, vol. 18, no. 1, pp. 3–9, 2017, doi: 10.22034/APJCP.2017.18.1.3.

[9] F. Lefranc, J. Brotchi, and R. Kiss, “Possible future issues in the treatment of glioblastomas: special emphasis on cell migration and the resistance of migrating glioblastoma cells to apoptosis,” *J. Clin. Oncol. Off. J. Am. Soc. Clin. Oncol.*, vol. 23, no. 10, pp. 2411–2422, Apr. 2005, doi: 10.1200/JCO.2005.03.089.

[10] H. Xu *et al.*, “Epidermal growth factor receptor in glioblastoma,” *Oncol. Lett.*, vol. 14, no. 1, pp. 512–516, Jul. 2017, doi: 10.3892/ol.2017.6221.

[11] A. Liu, C. Hou, H. Chen, X. Zong, and P. Zong, “Genetics and Epigenetics of Glioblastoma: Applications and Overall Incidence of IDH1 Mutation,” *Front. Oncol.*, vol. 6, p. 16, Jan. 2016, doi: 10.3389/fonc.2016.00016.

[12] N. Singh, A. Miner, L. Hennis, and S. Mittal, “Mechanisms of temozolomide resistance in glioblastoma - a comprehensive review,” *Cancer Drug Resist.*, vol. 4, no. 1, pp. 17–43, Mar. 2021, doi: 10.20517/cdr.2020.79.

[13] J. R. Wesolowski, P. Rajdev, and S. K. Mukherji, “Temozolomide (Temodar),” *AJNR Am. J. Neuroradiol.*, vol. 31, no. 8, pp. 1383–1384, Sep. 2010, doi: 10.3174/ajnr.A2170.

[14] S. Mohammed, M. Dinesan, and T. Ajayakumar, “Survival and quality of life analysis in glioblastoma multiforme with adjuvant chemoradiotherapy: a retrospective study,” *Rep. Pract. Oncol. Radiother.*, vol. 27, no. 6, pp. 1026–1036, Dec. 2022, doi: 10.5603/RPOR.a2022.0113.

[15] A. Orimo and R. A. Weinberg, “Stromal Fibroblasts in Cancer: A Novel Tumor-Promoting Cell Type,” *Cell Cycle*, vol. 5, no. 15, pp. 1597–1601, Aug. 2006, doi: 10.4161/cc.5.15.3112.
[16] H. Raskov, A. Orhan, J. P. Christensen, and I. Gögenur, “Cytotoxic CD8+ T cells in cancer and cancer immunotherapy,” *Br. J. Cancer*, vol. 124, no. 2, Art. no. 2, Jan. 2021, doi: 10.1038/s41416-020-01048-4.
[17] C. Yunna, H. Mengru, W. Lei, and C. Weidong, “Macrophage M1/M2 polarization,” *Eur. J. Pharmacol.*, vol. 877, p. 173090, Jun. 2020, doi: 10.1016/j.ejphar.2020.173090.
[18] H. Gonzalez, C. Hagerling, and Z. Werb, “Roles of the immune system in cancer: from tumor initiation to metastatic progression,” *Genes Dev.*, vol. 32, no. 19–20, pp. 1267–1284, Oct. 2018, doi: 10.1101/gad.314617.118.
[19] B. Alberts, A. Johnson, J. Lewis, M. Raff, K. Roberts, and P. Walter, “T Cells and MHC Proteins,” in *Molecular Biology of the Cell. 4th edition*, Garland Science, 2002. Accessed: Jun. 30, 2023. [Online]. Available: https://www.ncbi.nlm.nih.gov/books/NBK26926/
[20] K. Kondělková, D. Vokurková, J. Krejsek, L. Borská, Z. Fiala, and A. Ctirad, “Regulatory T cells (TREG) and their roles in immune system with respect to immunopathological disorders,” *Acta Medica (Hradec Kralove)*, vol. 53, no. 2, pp. 73–77, 2010, doi: 10.14712/18059694.2016.63.
[21] Y. Ohue and H. Nishikawa, “Regulatory T (Treg) cells in cancer: Can Treg cells be a new therapeutic target?,” *Cancer Sci.*, vol. 110, no. 7, pp. 2080–2089, Jul. 2019, doi: 10.1111/cas.14069.
[22] I. Hwang *et al.*, “Tumor-associated macrophage, angiogenesis and lymphangiogenesis markers predict prognosis of non-small cell lung cancer patients,” *J. Transl. Med.*, vol. 18, no. 1, p. 443, Nov. 2020, doi: 10.1186/s12967-020-02618-z.
[23] Y. Hua and G. Bergers, “Tumors vs. Chronic Wounds: An Immune Cell’s Perspective,” *Front. Immunol.*, vol. 10, p. 2178, Sep. 2019, doi: 10.3389/fimmu.2019.02178.
[24] S. C. Frederico, J. C. Hancock, E. E. S. Brettschneider, N. M. Ratnam, M. R. Gilbert, and M. Terabe, “Making a Cold Tumor Hot: The Role of Vaccines in the Treatment of Glioblastoma,” *Front. Oncol.*, vol. 11, p. 672508, 2021, doi: 10.3389/fonc.2021.672508.
[25] I. Yang *et al.*, “CD8+ T-cell infiltrate in newly diagnosed glioblastoma is associated with long-term survival,” *J. Clin. Neurosci.*, vol. 17, no. 11, pp. 1381–1385, Nov. 2010, doi: 10.1016/j.jocn.2010.03.031.
[26] I. S. Mauldin *et al.*, “Proliferating CD8+ T Cell Infiltrates Are Associated with Improved Survival in Glioblastoma,” *Cells*, vol. 10, no. 12, p. 3378, Dec. 2021, doi: 10.3390/cells10123378.
[27] J. Dejaegher *et al.*, “DNA methylation based glioblastoma subclassification is related to tumoral T-cell infiltration and patient survival,” *Neuro-Oncol.*, vol. 23, no. 2, pp. 240–250, Feb. 2021, doi: 10.1093/neuonc/noaa247.

[28] G. A. Shamsan *et al.*, “Differential migration mechanics and immune responses of glioblastoma subtypes.” bioRxiv, p. 2022.06.26.497270, Jun. 29, 2022. doi: 10.1101/2022.06.26.497270.
[29] A. Narita, “Minimum requirements for the actin-like treadmilling motor system,” *Bioarchitecture*, vol. 1, no. 5, pp. 205–208, Sep. 2011, doi: 10.4161/bioa.18115.
[30] C. E. Chan and D. J. Odde, “Traction dynamics of filopodia on compliant substrates,” *Science*, vol. 322, no. 5908, pp. 1687–1691, Dec. 2008, doi: 10.1126/science.1163595.
[31] B. L. Bangasser, S. S. Rosenfeld, and D. J. Odde, “Determinants of maximal force transmission in a motor-clutch model of cell traction in a compliant microenvironment,” *Biophys. J.*, vol. 105, no. 3, pp. 581–592, Aug. 2013, doi: 10.1016/j.bpj.2013.06.027.
[32] B. L. Bangasser *et al.*, “Shifting the optimal stiffness for cell migration,” *Nat. Commun.*, vol. 8, no. 1, Art. no. 1, May 2017, doi: 10.1038/ncomms15313.
[33] F. Lang *et al.*, “Functional significance of cell volume regulatory mechanisms,” *Physiol. Rev.*, vol. 78, no. 1, pp. 247–306, Jan. 1998, doi: 10.1152/physrev.1998.78.1.247.
[34] K. M. Stroka *et al.*, “Water Permeation Drives Tumor Cell Migration in Confined Microenvironments,” *Cell*, vol. 157, no. 3, pp. 611–623, Apr. 2014, doi: 10.1016/j.cell.2014.02.052.
[35] E. K. Paluch and E. Raz, “The role and regulation of blebs in cell migration,” *Curr. Opin. Cell Biol.*, vol. 25, no. 5, pp. 582–590, Oct. 2013, doi: 10.1016/j.ceb.2013.05.005.
[36] J. S. Logue, A. X. Cartagena-Rivera, M. A. Baird, M. W. Davidson, R. S. Chadwick, and C. M. Waterman, “Erk regulation of actin capping and bundling by Eps8 promotes cortex tension and leader bleb-based migration,” *eLife*, vol. 4, p. e08314, doi: 10.7554/eLife.08314.
[37] A. Laser-Azogui, T. Diamant-Levi, S. Israeli, Y. Roytman, and I. Tsarfaty, “Met-induced membrane blebbing leads to amoeboid cell motility and invasion,” *Oncogene*, vol. 33, no. 14, pp. 1788–1798, Apr. 2014, doi: 10.1038/onc.2013.138.
[38] E. D. Tabdanov *et al.*, “Engineering T cells to enhance 3D migration through structurally and mechanically complex tumor microenvironments,” *Nat. Commun.*, vol. 12, no. 1, Art. no. 1, May 2021, doi: 10.1038/s41467-021-22985-5.
[39] A. Lorentzen, J. Bamber, A. Sadok, I. Elson-Schwab, and C. J. Marshall, “An ezrin-rich, rigid uropod-like structure directs movement of amoeboid blebbing cells,” *J. Cell Sci.*, vol. 124, no. 8, pp. 1256–1267, Apr. 2011, doi: 10.1242/jcs.074849.
[40] A. Estecha *et al.*, “Moesin orchestrates cortical polarity of melanoma tumour cells to initiate 3D invasion,” *J. Cell Sci.*, vol. 122, no. Pt 19, pp. 3492–3501, Oct. 2009, doi: 10.1242/jcs.053157.
[41] K. Adebowale *et al.*, “Enhanced substrate stress relaxation promotes filopodia-mediated cell migration,” *Nat. Mater.*, vol. 20, no. 9, Art. no. 9, Sep. 2021, doi: 10.1038/s41563-021-00981-w.
[42] K. M. Yamada and M. Sixt, “Mechanisms of 3D cell migration,” *Nat. Rev. Mol. Cell Biol.*, vol. 20, no. 12, Art. no. 12, Dec. 2019, doi: 10.1038/s41580-019-0172-9.

[43] A. Elosegui-Artola *et al.*, “Mechanical regulation of a molecular clutch defines force transmission and transduction in response to matrix rigidity,” *Nat. Cell Biol.*, vol. 18, no. 5, Art. no. 5, May 2016, doi: 10.1038/ncb3336.
[44] A. Isomursu *et al.*, “Directed cell migration towards softer environments,” *Nat. Mater.*, vol. 21, no. 9, pp. 1081–1090, Sep. 2022, doi: 10.1038/s41563-022-01294-2.
[45] L. S. Prahl, M. R. Stanslaski, P. Vargas, M. Piel, and D. J. Odde, “Predicting Confined 1D Cell Migration from Parameters Calibrated to a 2D Motor-Clutch Model,” *Biophys. J.*, vol. 118, no. 7, pp. 1709–1720, Apr. 2020, doi: 10.1016/j.bpj.2020.01.048.
[46] B. Ananthanarayanan, Y. Kim, and S. Kumar, “Elucidating the mechanobiology of malignant brain tumors using a brain matrix-mimetic hyaluronic acid hydrogel platform,” *Biomaterials*, vol. 32, no. 31, pp. 7913–7923, Nov. 2011, doi: 10.1016/j.biomaterials.2011.07.005.
[47] Y.-H. V. Ma, K. Middleton, L. You, and Y. Sun, “A review of microfluidic approaches for investigating cancer extravasation during metastasis,” *Microsyst. Nanoeng.*, vol. 4, no. 1, Art. no. 1, Apr. 2018, doi: 10.1038/micronano.2017.104.
[48] P. Y. Poon, P. Y. K. Yue, and R. N. S. Wong, “A Device for Performing Cell Migration/Wound Healing in a 96-Well Plate,” *J. Vis. Exp. JoVE*, no. 121, p. 55411, Mar. 2017, doi: 10.3791/55411.
[49] C. J. Liu, G. A. Shamsan, T. Akkin, and D. J. Odde, “Glioma Cell Migration Dynamics in Brain Tissue Assessed by Multimodal Optical Imaging,” *Biophys. J.*, vol. 117, no. 7, pp. 1179–1188, Oct. 2019, doi: 10.1016/j.bpj.2019.08.010.
[50] T. H. Harris *et al.*, “Generalized Lévy walks and the role of chemokines in migration of effector CD8+ T cells,” *Nature*, vol. 486, no. 7404, pp. 545–548, Jun. 2012, doi: 10.1038/nature11098.
[51] M. F. Krummel, F. Bartumeus, and A. Gérard, “T cell migration, search strategies and mechanisms,” *Nat. Rev. Immunol.*, vol. 16, no. 3, Art. no. 3, Mar. 2016, doi: 10.1038/nri.2015.16.
[52] S. W. Cramer, R. E. Carter, J. D. Aronson, S. B. Kodandaramaiah, T. J. Ebner, and C. C. Chen, “Through the looking glass: A review of cranial window technology for optical access to the brain,” *J. Neurosci. Methods*, vol. 354, p. 109100, Apr. 2021, doi: 10.1016/j.jneumeth.2021.109100.
[53] M. Vicente-Manzanares, X. Ma, R. S. Adelstein, and A. R. Horwitz, “Non-muscle myosin II takes centre stage in cell adhesion and migration,” *Nat. Rev. Mol. Cell Biol.*, vol. 10, no. 11, Art. no. 11, Nov. 2009, doi: 10.1038/nrm2786.
[54] A. P. Somlyo and A. V. Somlyo, “Ca2+ sensitivity of smooth muscle and nonmuscle myosin II: modulated by G proteins, kinases, and myosin phosphatase,” *Physiol. Rev.*, vol. 83, no. 4, pp. 1325–1358, Oct. 2003, doi: 10.1152/physrev.00023.2003.
[55] T. Sakamoto, J. Limouze, C. A. Combs, A. F. Straight, and J. R. Sellers, “Blebbistatin, a myosin II inhibitor, is photoinactivated by blue light,” *Biochemistry*, vol. 44, no. 2, pp. 584–588, Jan. 2005, doi: 10.1021/bi0483357.
[56] G. Ren, A. I. Roberts, and Y. Shi, “Adhesion molecules,” *Cell Adhes. Migr.*, vol. 5, no. 1, pp. 20–22, 2011, doi: 10.4161/cam.5.1.13491.

[57] A. Elosegui-Artola, X. Trepat, and P. Roca-Cusachs, “Control of Mechanotransduction by Molecular Clutch Dynamics,” *Trends Cell Biol.*, vol. 28, no. 5, pp. 356–367, May 2018, doi: 10.1016/j.tcb.2018.01.008.
[58] B. Alberts, A. Johnson, J. Lewis, M. Raff, K. Roberts, and P. Walter, “Integrins,” in *Molecular Biology of the Cell. 4th edition*, Garland Science, 2002. Accessed: Jul. 02, 2023. [Online]. Available: https://www.ncbi.nlm.nih.gov/books/NBK26867/
[59] A. van der Flier and A. Sonnenberg, “Function and interactions of integrins,” *Cell Tissue Res.*, vol. 305, no. 3, pp. 285–298, Sep. 2001, doi: 10.1007/s004410100417.
[60] C. Brakebusch and R. Fässler, “The integrin-actin connection, an eternal love affair,” *EMBO J.*, vol. 22, no. 10, pp. 2324–2333, May 2003, doi: 10.1093/emboj/cdg245.
[61] S. Le *et al.*, “Mechanotransmission and Mechanosensing of Human alpha-Actinin 1,” *Cell Rep.*, vol. 21, no. 10, pp. 2714–2723, Dec. 2017, doi: 10.1016/j.celrep.2017.11.040.
[62] S. E. Lee, S. Chunsrivirot, R. D. Kamm, and M. R. K. Mofrad, “Molecular Dynamics Study of Talin-Vinculin Binding,” *Biophys. J.*, vol. 95, no. 4, pp. 2027–2036, Aug. 2008, doi: 10.1529/biophysj.107.124487.
[63] B. T. Goult, J. Yan, and M. A. Schwartz, “Talin as a mechanosensitive signaling hub,” *J. Cell Biol.*, vol. 217, no. 11, pp. 3776–3784, Nov. 2018, doi: 10.1083/jcb.201808061.
[64] B. Wehrle-Haller, “The Role of Integrins in Cell Migration,” in *Madame Curie Bioscience Database [Internet]*, Landes Bioscience, 2013. Accessed: Jun. 12, 2023. [Online]. Available: https://www.ncbi.nlm.nih.gov/books/NBK6613/
[65] J. S. Desgrosellier and D. A. Cheresh, “Integrins in cancer: biological implications and therapeutic opportunities,” *Nat. Rev. Cancer*, vol. 10, no. 1, pp. 9–22, Jan. 2010, doi: 10.1038/nrc2748.
[66] M. Munksgaard Thorén *et al.*, “Integrin α10, a Novel Therapeutic Target in Glioblastoma, Regulates Cell Migration, Proliferation, and Survival,” *Cancers*, vol. 11, no. 4, p. 587, Apr. 2019, doi: 10.3390/cancers11040587.
[67] H. Hamidi and J. Ivaska, “Every step of the way: integrins in cancer progression and metastasis,” *Nat. Rev. Cancer*, vol. 18, no. 9, pp. 533–548, Sep. 2018, doi: 10.1038/s41568-018-0038-z.
[68] S. K. Akiyama, “Integrins in cell adhesion and signaling,” *Hum. Cell*, vol. 9, no. 3, pp. 181–186, Sep. 1996.
[69] R. Stupp *et al.*, “Cilengitide combined with standard treatment for patients with newly diagnosed glioblastoma with methylated MGMT promoter (CENTRIC EORTC 26071-22072 study): a multicentre, randomised, open-label, phase 3 trial,” *Lancet Oncol.*, vol. 15, no. 10, pp. 1100–1108, Sep. 2014, doi: 10.1016/S1470-2045(14)70379-1.
[70] T. Lämmermann *et al.*, “Rapid leukocyte migration by integrin-independent flowing and squeezing,” *Nature*, vol. 453, no. 7191, pp. 51–55, May 2008, doi: 10.1038/nature06887.

[71] M. Culty, K. Miyake, P. W. Kincade, E. Sikorski, E. C. Butcher, and C. Underhill, “The hyaluronate receptor is a member of the CD44 (H-CAM) family of cell surface glycoproteins,” *J. Cell Biol.*, vol. 111, no. 6 Pt 1, pp. 2765–2774, Dec. 1990, doi: 10.1083/jcb.111.6.2765.
[72] C. Chen, S. Zhao, A. Karnad, and J. W. Freeman, “The biology and role of CD44 in cancer progression: therapeutic implications,” *J. Hematol. Oncol.J Hematol Oncol*, vol. 11, no. 1, p. 64, May 2018, doi: 10.1186/s13045-018-0605-5.
[73] R. Breyer *et al.*, “Disruption of intracerebral progression of C6 rat glioblastoma by in vivo treatment with anti-CD44 monoclonal antibody,” *J. Neurosurg.*, vol. 92, no. 1, pp. 140–149, Jan. 2000, doi: 10.3171/jns.2000.92.1.0140.
[74] A. Merzak, S. Koocheckpour, and G. J. Pilkington, “CD44 mediates human glioma cell adhesion and invasion in vitro,” *Cancer Res.*, vol. 54, no. 15, pp. 3988–3992, Aug. 1994.
[75] T. Yoshida, Y. Matsuda, Z. Naito, and T. Ishiwata, “CD44 in human glioma correlates with histopathological grade and cell migration,” *Pathol. Int.*, vol. 62, no. 7, pp. 463–470, 2012, doi: 10.1111/j.1440-1827.2012.02823.x.
[76] D. Si, F. Yin, J. Peng, and G. Zhang, “High Expression of CD44 Predicts a Poor Prognosis in Glioblastomas,” *Cancer Manag. Res.*, vol. 12, pp. 769–775, Feb. 2020, doi: 10.2147/CMAR.S233423.
[77] K. J. Wolf *et al.*, “A mode of cell adhesion and migration facilitated by CD44-dependent microtentacles,” *Proc. Natl. Acad. Sci.*, vol. 117, no. 21, pp. 11432–11443, May 2020, doi: 10.1073/pnas.1914294117.
[78] C. Kolliopoulos, M. M. Ali, C. Castillejo-Lopez, C.-H. Heldin, and P. Heldin, “CD44 Depletion in Glioblastoma Cells Suppresses Growth and Stemness and Induces Senescence,” *Cancers*, vol. 14, no. 15, p. 3747, Jul. 2022, doi: 10.3390/cancers14153747.
[79] Y. Kim and S. Kumar, “CD44-mediated adhesion to hyaluronic acid contributes to mechanosensing and invasive motility,” *Mol. Cancer Res. MCR*, vol. 12, no. 10, pp. 1416–1429, Oct. 2014, doi: 10.1158/1541-7786.MCR-13-0629.
[80] R. L. Klank *et al.*, “Biphasic Dependence of Glioma Survival and Cell Migration on CD44 Expression Level,” *Cell Rep.*, vol. 18, no. 1, pp. 23–31, Jan. 2017, doi: 10.1016/j.celrep.2016.12.024.
[81] R. Stupp, M. E. Hegi, M. R. Gilbert, and A. Chakravarti, “Chemoradiotherapy in malignant glioma: standard of care and future directions,” *J. Clin. Oncol. Off. J. Am. Soc. Clin. Oncol.*, vol. 25, no. 26, pp. 4127–4136, Sep. 2007, doi: 10.1200/JCO.2007.11.8554.
[82] D. B. Hoelzinger, T. Demuth, and M. E. Berens, “Autocrine factors that sustain glioma invasion and paracrine biology in the brain microenvironment,” *J. Natl. Cancer Inst.*, vol. 99, no. 21, pp. 1583–1593, Nov. 2007, doi: 10.1093/jnci/djm187.
[83] M. Alieva, V. Leidgens, M. J. Riemenschneider, C. A. Klein, P. Hau, and J. van Rheenen, “Intravital imaging of glioma border morphology reveals distinctive cellular dynamics and contribution to tumor cell invasion,” *Sci. Rep.*, vol. 9, no. 1, p. 2054, Feb. 2019, doi: 10.1038/s41598-019-38625-4.

[84] J. I. Puleo *et al.*, “Mechanosensing during directed cell migration requires dynamic actin polymerization at focal adhesions,” *J. Cell Biol.*, vol. 218, no. 12, pp. 4215–4235, Dec. 2019, doi: 10.1083/jcb.201902101.
[85] D. A. Lauffenburger and A. F. Horwitz, “Cell migration: a physically integrated molecular process,” *Cell*, vol. 84, no. 3, pp. 359–369, Feb. 1996, doi: 10.1016/s0092-8674(00)81280-5.
[86] R. O. Hynes, “Integrins: versatility, modulation, and signaling in cell adhesion,” *Cell*, vol. 69, no. 1, pp. 11–25, Apr. 1992, doi: 10.1016/0092-8674(92)90115-s.
[87] R. Oria *et al.*, “Force loading explains spatial sensing of ligands by cells,” *Nature*, vol. 552, no. 7684, pp. 219–224, Dec. 2017, doi: 10.1038/nature24662.
[88] S. J. Tan *et al.*, “Regulation and dynamics of force transmission at individual cell-matrix adhesion bonds,” *Sci. Adv.*, vol. 6, no. 20, p. eaax0317, May 2020, doi: 10.1126/sciadv.aax0317.
[89] P. A. DiMilla, K. Barbee, and D. A. Lauffenburger, “Mathematical model for the effects of adhesion and mechanics on cell migration speed,” *Biophys. J.*, vol. 60, no. 1, pp. 15–37, Jul. 1991, doi: 10.1016/S0006-3495(91)82027-6.
[90] H. J. Scherer, “Structural Development in Gliomas,” *Am. J. Cancer*, vol. 34, no. 3, pp. 333–351, Nov. 1938, doi: 10.1158/ajc.1938.333.
[91] V. A. Cuddapah, S. Robel, S. Watkins, and H. Sontheimer, “A neurocentric perspective on glioma invasion,” *Nat. Rev. Neurosci.*, vol. 15, no. 7, Art. no. 7, Jul. 2014, doi: 10.1038/nrn3765.
[92] A. Farin, S. O. Suzuki, M. Weiker, J. E. Goldman, J. N. Bruce, and P. Canoll, “Transplanted glioma cells migrate and proliferate on host brain vasculature: A dynamic analysis,” *Glia*, vol. 53, no. 8, pp. 799–808, 2006, doi: 10.1002/glia.20334.
[93] E. Hirata *et al.*, “In vivo fluorescence resonance energy transfer imaging reveals differential activation of Rho-family GTPases in glioblastoma cell invasion,” *J. Cell Sci.*, vol. 125, no. 4, pp. 858–868, Feb. 2012, doi: 10.1242/jcs.089995.
[94] F. Winkler *et al.*, “Imaging glioma cell invasion in vivo reveals mechanisms of dissemination and peritumoral angiogenesis,” *Glia*, vol. 57, no. 12, pp. 1306–1315, 2009, doi: 10.1002/glia.20850.
[95] S. Watkins, S. Robel, I. F. Kimbrough, S. M. Robert, G. Ellis-Davies, and H. Sontheimer, “Disruption of astrocyte–vascular coupling and the blood–brain barrier by invading glioma cells,” *Nat. Commun.*, vol. 5, no. 1, p. 4196, Jun. 2014, doi: 10.1038/ncomms5196.
[96] B. Krusche *et al.*, “EphrinB2 drives perivascular invasion and proliferation of glioblastoma stem-like cells,” *eLife*, vol. 5, p. e14845, Jun. 2016, doi: 10.7554/eLife.14845.
[97] J. Ipsaro, “Structures of the spectrin-ankyrin interaction binding domains,” *Jonathan Ipsaro*, May 28, 2009. https://www.jonipsaro.com/publication/ipsaro-structures-2009/ (accessed Jan. 20, 2023).
[98] M. Bergert, Stanley D. Chandradoss, Ravi A. Desai, and Ewa Paluch, “Cell mechanics control rapid transitions between blebs and lamellipodia during migration,” 2015. https://www.pnas.org/doi/10.1073/pnas.1207968109 (accessed Jan. 20, 2023).

[99] T. Eisemann, B. Costa, J. Strelau, M. Mittelbronn, P. Angel, and H. Peterziel, “An advanced glioma cell invasion assay based on organotypic brain slice cultures,” *BMC Cancer*, vol. 18, no. 1, p. 103, Dec. 2018, doi: 10.1186/s12885-018-4007-4.
[100] C. Beadle, M. C. Assanah, P. Monzo, R. Vallee, S. S. Rosenfeld, and P. Canoll, “The Role of Myosin II in Glioma Invasion of the Brain,” *Mol. Biol. Cell*, vol. 19, no. 8, pp. 3357–3368, Aug. 2008, doi: 10.1091/mbc.e08-03-0319.
[101] “Translational Neuro-Oncology: Jann N. Sarkaria - Mayo GBM PDX Line Data,” *Mayo Clinic*. https://www.mayo.edu/research/labs/translational-neuro-oncology/mayo-clinic-brain-tumor-patient-derived-xenograft-national-resource/pdx-characteristics/pdx-phenotype (accessed Mar. 28, 2023).
[102] M. R. Pawlak *et al.*, “RAD-TGTs: high-throughput measurement of cellular mechanotype via rupture and delivery of DNA tension probes,” *Nat. Commun.*, vol. 14, no. 1, Art. no. 1, Apr. 2023, doi: 10.1038/s41467-023-38157-6.
[103] R. J. Pelham and Y. l Wang, “Cell locomotion and focal adhesions are regulated by substrate flexibility,” *Proc. Natl. Acad. Sci. U. S. A.*, vol. 94, no. 25, pp. 13661–13665, Dec. 1997, doi: 10.1073/pnas.94.25.13661.
[104] T. J. Stewart, V. Murthy, S. P. Dugan, and J. E. Baker, “Velocity of myosin-based actin sliding depends on attachment and detachment kinetics and reaches a maximum when myosin-binding sites on actin saturate,” *J. Biol. Chem.*, vol. 297, no. 5, p. 101178, Sep. 2021, doi: 10.1016/j.jbc.2021.101178.
[105] Z. Gong *et al.*, “Matching material and cellular timescales maximizes cell spreading on viscoelastic substrates,” *Proc. Natl. Acad. Sci. U. S. A.*, vol. 115, no. 12, pp. E2686–E2695, Mar. 2018, doi: 10.1073/pnas.1716620115.
[106] K. Pogoda and P. A. Janmey, “Glial Tissue Mechanics and Mechanosensing by Glial Cells,” *Front. Cell. Neurosci.*, vol. 12, 2018, Accessed: Jun. 16, 2023. [Online]. Available: https://www.frontiersin.org/articles/10.3389/fncel.2018.00025
[107] J. N. Sarkaria *et al.*, “Is the blood-brain barrier really disrupted in all glioblastomas? A critical assessment of existing clinical data,” *Neuro-Oncol.*, vol. 20, no. 2, pp. 184–191, Jan. 2018, doi: 10.1093/neuonc/nox175.
[108] H. S. Picariello *et al.*, “Myosin IIA suppresses glioblastoma development in a mechanically sensitive manner,” *Proc. Natl. Acad. Sci.*, vol. 116, no. 31, pp. 15550–15559, Jul. 2019, doi: 10.1073/pnas.1902847116.
[109] J. M. Fletcher, S. J. Lalor, C. M. Sweeney, N. Tubridy, and K. H. G. Mills, “T cells in multiple sclerosis and experimental autoimmune encephalomyelitis,” *Clin. Exp. Immunol.*, vol. 162, no. 1, pp. 1–11, Oct. 2010, doi: 10.1111/j.1365-2249.2010.04143.x.
[110] S. Han *et al.*, “Rescuing defective tumor-infiltrating T-cell proliferation in glioblastoma patients,” *Oncol. Lett.*, vol. 12, no. 4, pp. 2924–2929, Oct. 2016, doi: 10.3892/ol.2016.4944.
[111] A. P. Patel *et al.*, “Single-cell RNA-seq highlights intratumoral heterogeneity in primary glioblastoma,” *Science*, vol. 344, no. 6190, pp. 1396–1401, Jun. 2014, doi: 10.1126/science.1254257.

[112] K. Woroniecka *et al.*, “T-Cell Exhaustion Signatures Vary with Tumor Type and Are Severe in Glioblastoma,” *Clin. Cancer Res.*, vol. 24, no. 17, pp. 4175–4186, Sep. 2018, doi: 10.1158/1078-0432.CCR-17-1846.
[113] V. M. Ravi *et al.*, “T-cell dysfunction in the glioblastoma microenvironment is mediated by myeloid cells releasing interleukin-10,” *Nat. Commun.*, vol. 13, no. 1, p. 925, Feb. 2022, doi: 10.1038/s41467-022-28523-1.
[114] J. Kipnis *et al.*, “Dopamine, through the Extracellular Signal-Regulated Kinase Pathway, Downregulates CD4+CD25+ Regulatory T-Cell Activity: Implications for Neurodegeneration,” *J. Neurosci.*, vol. 24, no. 27, pp. 6133–6143, Jul. 2004, doi: 10.1523/JNEUROSCI.0600-04.2004.
[115] S. Ai and R. S. Klein, “Update on T cells in the virally infected brain: friends and foes,” *Curr. Opin. Neurol.*, vol. 33, no. 3, pp. 405–412, Jun. 2020, doi: 10.1097/WCO.0000000000000825.
[116] M. F. Krummel, R. S. Friedman, and J. Jacobelli, “Modes and mechanisms of T cell motility: roles for confinement and Myosin-IIA,” *Curr. Opin. Cell Biol.*, vol. 30, pp. 9–16, Oct. 2014, doi: 10.1016/j.ceb.2014.05.003.
[117] J. Renkawitz *et al.*, “Adaptive force transmission in amoeboid cell migration,” *Nat. Cell Biol.*, vol. 11, no. 12, pp. 1438–1443, Dec. 2009, doi: 10.1038/ncb1992.
[118] P. Friedl, F. Entschladen, C. Conrad, B. Niggemann, and K. S. Zänker, “CD4+ T lymphocytes migrating in three-dimensional collagen lattices lack focal adhesions and utilize β1 integrin-independent strategies for polarization, interaction with collagen fibers and locomotion,” *Eur. J. Immunol.*, vol. 28, no. 8, pp. 2331–2343, Aug. 1998, doi: 10.1002/(SICI)1521-4141(199808)28:08<2331::AID-IMMU2331>3.0.CO;2-C.
[119] K. Wolf, R. Müller, S. Borgmann, Eva.-B. Bröcker, and P. Friedl, “Amoeboid shape change and contact guidance: T-lymphocyte crawling through fibrillar collagen is independent of matrix remodeling by MMPs and other proteases,” *Blood*, vol. 102, no. 9, pp. 3262–3269, Nov. 2003, doi: 10.1182/blood-2002-12-3791.
[120] A. Smith, Y. R. Carrasco, P. Stanley, N. Kieffer, F. D. Batista, and N. Hogg, “A talin-dependent LFA-1 focal zone is formed by rapidly migrating T lymphocytes,” *J. Cell Biol.*, vol. 170, no. 1, pp. 141–151, Jul. 2005, doi: 10.1083/jcb.200412032.
[121] M. Saitakis *et al.*, “Different TCR-induced T lymphocyte responses are potentiated by stiffness with variable sensitivity,” *eLife*, vol. 6, p. e23190, Jun. 2017, doi: 10.7554/eLife.23190.
[122] J. Jacobelli, F. C. Bennett, P. Pandurangi, A. J. Tooley, and M. F. Krummel, “Myosin-IIA and ICAM-1 Regulate the Interchange between Two Distinct Modes of T Cell Migration,” *J. Immunol.*, vol. 182, no. 4, pp. 2041–2050, Feb. 2009, doi: 10.4049/jimmunol.0803267.
[123] K. Talkenberger, E. A. Cavalcanti-Adam, A. Voss-Böhme, and A. Deutsch, “Amoeboid-mesenchymal migration plasticity promotes invasion only in complex heterogeneous microenvironments,” *Sci. Rep.*, vol. 7, no. 1, p. 9237, Aug. 2017, doi: 10.1038/s41598-017-09300-3.

[124] H. C. Pruitt *et al.*, “Collagen fiber structure guides 3D motility of cytotoxic T lymphocytes,” *Matrix Biol.*, vol. 85–86, pp. 147–159, Jan. 2020, doi: 10.1016/j.matbio.2019.02.003.
[125] C. G. Tucker *et al.*, “Adoptive T-cell therapy with IL-12 pre-conditioned low avidity T-cells prevents exhaustion and results in enhanced T-cell activation, tumor clearance, and decreased risk for autoimmunity.,” *J. Immunol. Baltim. Md 1950*, vol. 205, no. 5, pp. 1449–1460, Sep. 2020, doi: 10.4049/jimmunol.2000007.
[126] E. Peranzoni *et al.*, “Macrophages impede CD8 T cells from reaching tumor cells and limit the efficacy of anti–PD-1 treatment,” *Proc. Natl. Acad. Sci.*, vol. 115, no. 17, pp. E4041–E4050, Apr. 2018, doi: 10.1073/pnas.1720948115.
[127] K. L. Emo *et al.*, “Live Imaging of Influenza Infection of the Trachea Reveals Dynamic Regulation of CD8+ T Cell Motility by Antigen,” *PLOS Pathog.*, vol. 12, no. 9, p. e1005881, Sep. 2016, doi: 10.1371/journal.ppat.1005881.
[128] J. Jacobelli *et al.*, “Confinement-Optimized 3-Dimensional T cell Amoeboid Motility is Modulated via Myosin IIA-Regulated Adhesions,” *Nat. Immunol.*, vol. 11, no. 10, pp. 953–961, Oct. 2010, doi: 10.1038/ni.1936.
[129] E. R. Jerison and S. R. Quake, “Heterogeneous T cell motility behaviors emerge from a coupling between speed and turning in vivo,” *eLife*, vol. 9, p. e53933, May 2020, doi: 10.7554/eLife.53933.
[130] E. H. Wilson *et al.*, “Behavior of Parasite-Specific Effector CD8+ T Cells in the Brain and Visualization of a Kinesis-Associated System of Reticular Fibers,” *Immunity*, vol. 30, no. 2, pp. 300–311, Feb. 2009, doi: 10.1016/j.immuni.2008.12.013.
[131] T. N. Shaw *et al.*, “Perivascular Arrest of CD8+ T Cells Is a Signature of Experimental Cerebral Malaria,” *PLOS Pathog.*, vol. 11, no. 11, p. e1005210, Nov. 2015, doi: 10.1371/journal.ppat.1005210.
[132] S. L. Urban *et al.*, “Peripherally induced brain tissue–resident memory CD8+ T cells mediate protection against CNS infection,” *Nat. Immunol.*, vol. 21, no. 8, Art. no. 8, Aug. 2020, doi: 10.1038/s41590-020-0711-8.
[133] E. J. Banigan, T. H. Harris, D. A. Christian, C. A. Hunter, and A. J. Liu, “Heterogeneous CD8+ T Cell Migration in the Lymph Node in the Absence of Inflammation Revealed by Quantitative Migration Analysis,” *PLOS Comput. Biol.*, vol. 11, no. 2, p. e1004058, Feb. 2015, doi: 10.1371/journal.pcbi.1004058.
[134] A. Armento, J. Ehlers, S. Schötterl, and U. Naumann, “Molecular Mechanisms of Glioma Cell Motility,” in *Glioblastoma*, S. De Vleeschouwer, Ed., Brisbane (AU): Codon Publications, 2017. Accessed: Jul. 04, 2023. [Online]. Available: http://www.ncbi.nlm.nih.gov/books/NBK470001/
[135] Z. Shulman *et al.*, “Lymphocyte Crawling and Transendothelial Migration Require Chemokine Triggering of High-Affinity LFA-1 Integrin,” *Immunity*, vol. 30, no. 3, pp. 384–396, Mar. 2009, doi: 10.1016/j.immuni.2008.12.020.
[136] C. P. Ferreira *et al.*, “LFA-1 Mediates Cytotoxicity and Tissue Migration of Specific CD8+ T Cells after Heterologous Prime-Boost Vaccination against Trypanosoma cruzi Infection,” *Front. Immunol.*, vol. 8, 2017, Accessed: Apr. 27,

2023. [Online]. Available: https://www.frontiersin.org/articles/10.3389/fimmu.2017.01291
[137] T. Capece *et al.*, “A novel intracellular pool of LFA-1 is critical for asymmetric CD8+ T cell activation and differentiation,” *J. Cell Biol.*, vol. 216, no. 11, pp. 3817–3829, Nov. 2017, doi: 10.1083/jcb.201609072.
[138] E. Galkina, J. Thatte, V. Dabak, M. B. Williams, K. Ley, and T. J. Braciale, “Preferential migration of effector CD8+ T cells into the interstitium of the normal lung,” Dec. 01, 2005. https://www.jci.org/articles/view/24482/pdf (accessed Apr. 27, 2023).
[139] C. Lu, M. Shimaoka, M. Ferzly, C. Oxvig, J. Takagi, and T. A. Springer, “An isolated, surface-expressed I domain of the integrin αLβ2 is sufficient for strong adhesive function when locked in the open conformation with a disulfide bond,” *Proc. Natl. Acad. Sci.*, vol. 98, no. 5, pp. 2387–2392, Feb. 2001, doi: 10.1073/pnas.041606398.
[140] S. Li *et al.*, “Efalizumab binding to the LFA-1 αL I domain blocks ICAM-1 binding via steric hindrance,” *Proc. Natl. Acad. Sci. U. S. A.*, vol. 106, no. 11, pp. 4349–4354, Mar. 2009, doi: 10.1073/pnas.0810844106.
[141] E. O. Major, “Progressive Multifocal Leukoencephalopathy in Patients on Immunomodulatory Therapies*,” Feb. 2010, doi: 10.1146/annurev.med.080708.082655.
[142] B. J. G. Baaten, C.-R. Li, and L. M. Bradley, “Multifaceted regulation of T cells by CD44,” *Commun. Integr. Biol.*, vol. 3, no. 6, pp. 508–512, Nov. 2010, doi: 10.4161/cib.3.6.13495.
[143] H. C. DeGrendele, P. Estess, and M. H. Siegelman, “Requirement for CD44 in Activated T Cell Extravasation into an Inflammatory Site,” *Science*, vol. 278, no. 5338, pp. 672–675, Oct. 1997, doi: 10.1126/science.278.5338.672.
[144] J. D. Klement *et al.*, “An osteopontin/CD44 immune checkpoint controls CD8+ T cell activation and tumor immune evasion,” *J. Clin. Invest.*, vol. 128, no. 12, pp. 5549–5560, Nov. 2018, doi: 10.1172/JCI123360.
[145] P. Mrass, I. Kinjyo, L. G. Ng, S. L. Reiner, E. Puré, and W. Weninger, “CD44 Mediates Successful Interstitial Navigation by Killer T Cells and Enables Efficient Antitumor Immunity,” *Immunity*, vol. 29, no. 6, pp. 971–985, Dec. 2008, doi: 10.1016/j.immuni.2008.10.015.
[146] C. Ernst and B. R. Christie, “Isolectin-IB4 as a vascular stain for the study of adult neurogenesis,” *J. Neurosci. Methods*, vol. 150, no. 1, pp. 138–142, Jan. 2006, doi: 10.1016/j.jneumeth.2005.06.018.
[147] F. Boscia, C. L. Esposito, A. Casamassa, V. de Franciscis, L. Annunziato, and L. Cerchia, “The isolectin IB4 binds RET receptor tyrosine kinase in microglia,” *J. Neurochem.*, vol. 126, no. 4, pp. 428–436, Aug. 2013, doi: 10.1111/jnc.12209.
[148] C. M. Bishop, *Pattern recognition and machine learning*. in Information science and statistics. New York: Springer, 2006.
[149] K. I. Jankowska *et al.*, “Integrins Modulate T Cell Receptor Signaling by Constraining Actin Flow at the Immunological Synapse,” *Front. Immunol.*, vol. 9,

2018, Accessed: Jul. 04, 2023. [Online]. Available: https://www.frontiersin.org/articles/10.3389/fimmu.2018.00025
[150] S. N. Lawson, “Chapter 8 - The Peripheral Sensory Nervous System: Dorsal Root Ganglion Neurons,” in *Peripheral Neuropathy (Fourth Edition)*, P. J. Dyck and P. K. Thomas, Eds., Philadelphia: W.B. Saunders, 2005, pp. 163–202. doi: 10.1016/B978-0-7216-9491-7.50011-9.
[151] V. Mayya *et al.*, “Durable Interactions of T Cells with T Cell Receptor Stimuli in the Absence of a Stable Immunological Synapse,” *Cell Rep.*, vol. 22, no. 2, pp. 340–349, Jan. 2018, doi: 10.1016/j.celrep.2017.12.052.
[152] R. Basu *et al.*, “Cytotoxic T cells use mechanical force to potentiate target cell killing,” *Cell*, vol. 165, no. 1, pp. 100–110, Mar. 2016, doi: 10.1016/j.cell.2016.01.021.
[153] M. H. W. Chin, M. D. A. Norman, E. Gentleman, M.-O. Coppens, and R. M. Day, “A Hydrogel-Integrated Culture Device to Interrogate T Cell Activation with Physicochemical Cues,” *ACS Appl. Mater. Interfaces*, vol. 12, no. 42, pp. 47355–47367, Oct. 2020, doi: 10.1021/acsami.0c16478.